Precipitation of dispersoids containing Mn and/or Cr in Al-Mg-Si-alloys

by Lars Lodgaard

A thesis submitted to
The Norwegian University of Science and Technology (NTNU)
in partial fulfilment for the requirements for the degree of

Doktor Ingeniør

Trondheim
May 2000

Preface

This thesis is divided into five main parts, reflecting the different subjects. Parts III and IV consist of three papers which have been submitted to Material Science & Engineering A (Part IIIa), Materials Science and Technology (Part IIIb) and Aluminum Transactions (Part IV). Several changes were introduced in order to make the papers more suitable for presentation in this thesis. Figure and equation numbering, alloy designation and symbols have been changed. The reference list has been retained without changes. Consequently each paper includes a separate reference list while Parts I, II and V have one common reference list.

List of publications

Parts of this work have been published, or have been submitted for publication.

L. Lodgaard and N. Ryum. Accepted for publication in: *Material Science & Engineering A*. The submitted manuscript is identical to **Part IIIa**

L. Lodgaard and N. Ryum. Submitted to: *Materials Science and Technology.* The submitted manuscript is identical to **Part IIIb**

L. Lodgaard and N. Ryum. Submitted to: *Aluminum Transactions.* The submitted manuscript is identical to **Part IV**

L. Lodgaard and N. Ryum. Submitted to: ICAA-7.

L. Lodgaard and N. Ryum: in Proc. Conf. 5th European Conference on Advanced Materials and Processes and Application, April 1997, Netherlands Society for Material Science, 4/69.

Acknowledgements

This doctoral thesis is based upon work carried out at the Department of Materials Technology and Electrochemistry, The Norwegian University of Science and Technology (NTNU). Professor Nils Ryum has been my supervisor throughout the work, and I would like to take this opportunity to thank Nils for his excellent guidance. He has always had time for help and discussions and encouraged me forward when needed.

Special thanks are given to Dr O. Reiso and Dr U. Tundal, Hydro Aluminium R&D Centre Sunndalsøra for their participation and valuable discussions during the project.

Others have also contributed to this work, and I would like to extend my thanks to all of them:

- Professor Jan Kjetil Solberg, for helpful discussions during my TEM work.
- Dr Sigmund Andersen, for helpful discussions during my TEM work.
- Ms. Anne Lise Dons, who has contributed to many discussions.
- Ms. Unn Ese, who prepared a great deal of my specimens for light microscope investigation.
- Ms. Tone Anzjøen and Ms Birgitte Karlsen, who have prepared some of my TEM-specimens.
- Dr Asgeir Bardal, for helpful discussions of the use of EELS.
- Mr. Amund Slettan and Mr. Thomas Hagen, who contributed to the present work by their diploma works.
- Ms Ingrid Page, Dr Bjørn Rønning and my father, Svein Sandvik, who have helped me to prepare the manuscript.

Moreover, many thanks are due to NTNU which granted my scholarship and to Hydro Aluminium for materials and finical support.

Finally. I would like tothank my wife, Eirin, and our two children, Oda and Ane, for their support, and patience during this doctoral work

Contents

Abstract

The present work is an investigation of Mn- and/or Cr-containing dispersoids in Al-Mg-Si alloys. Special emphasis has been placed on precipitation, distribution and density of the dispersoids. A comprehensive study of the effect of different heat treatment procedures on these parameters has been carried out. The experimental techniques used were electrical resistivity measurements and light-, scanning electron- and transmission electron microscopy.

For alloys containing Mn and Mn+Cr it has been shown that during the heating of the as-cast alloys to 580 °C (which is a typical homogenisation temperature in the industry) and at a heating rate of 3 K/min, an intermediate phase, referred to as the "u-phase" nucleated on the β'-Mg_2Si needles. This phase has a hexagonal unit cell with a = 0.670 nm, c = 0.808. The precipitates were rod-shaped and lined up in the [100] directions in the Al lattice. With continued annealing, α-Al(MnFe)Si or α-Al(MnCrFe)Si dispersoids nucleates heterogeneously on the "u-phase" precipitates.

During heating of an alloy containing Cr, small α-Al(CrFe)Si particles nucleate at the surface of the primary β-AlFeSi particles at approx. 460 °C and after additional heating to a higher temperature the α- particles grow and the β-particles dissolve. If the content of Cr is high (~ 0.3 wt.% Cr) both α-Al(CrFe)Si- and α'-AlCrSi dispersoids are discovered in the matrix during heating while only α-Al(CrFe)Si dispersoids are present when the Cr-content is low (~ 0.15 wt.% Cr). The nucleation mechanisms are not fully discoverd but most likely the dispersoids containing Cr also nucleate by means of the "u-phase" precipitates.

In order to measure the distribution of the dispersoids in a specimen, the Kontron KS 300 image analysing technique was used. A parameter which gives the fraction of an area empty of dispersoids A_e was introduced. To determine A_e, a macro (computer program) which carries out the measurements automatically was developed.

A tendency towards a nonuniform distribution of dispersoids was related to the nucleation mechanisms of dispersoids and the microsegregation of the alloying elements after solidification. It was demonstrated that a prerequisite for a homogeneous distribution of dispersoids is a heat treatment procedure that produce an abundant density of β'-Mg_2Si - needle in a temperature range between 250 °C to 350 °C.

Dispersoids coarsening is a process in which the number of particles per unit volume of the system decrease with time at elevated temperatures. The dispersoids density decreases considerably during annealing and the effect increases with increasing temperatures. The coarsening of α-Al(MnFe)Si dispersoids is particularly fast while the α-Al(CrFe)Si dispersoids coarsen much more slowly. Since the elements Mn and Cr have lower diffusion rates than the other elements in the dispersoids (Fe and Si) diffusion of Mn and Cr is the rate limiting step in the coarsening process. Consequently the difference in the rate of coarsening between α-Al(MnFe)Si- and α-Al(CrFe)Si dispersoids is due to the difference in the rate of diffusion of Mn and Cr in Al.

Part I

Theoretical background and earlier work

1. Diffusion

A collective movement of atoms, or diffusion, is divided into interstitial and substitutional diffusion. Interstitial diffusion is the movement of smaller atoms from or to positions that are not part of the main lattice. The small atoms migrate between the ordinary larger atoms. Subtitutional diffusion means replacement of atoms of different type in the main lattice. This process requires lattice vacancies, which function as temporary sites for jumping atoms. The treatment of both diffusion processes is a question of statistical probability.

The simplest type of diffusion is takes place when a steady state exists, i.e. when the concentration at every point does not change with time. Fick assumed that the diffusion is proportional to the concentration gradient in the material. If the diffusion occurs in only one direction, the equation known as *Fick's first law of diffusion* has the form

$$J_B = D_B \frac{\partial C_B}{\partial x} \qquad \text{(I-1)}$$

where J_B is the flux of B-atoms, D_B is the diffusion constant and C_B is the concentration of B-atoms.

In most real situations, steady state conditions are not established, i.e. the concentration varies with both distance and time, and Fick's first law can therefore no longer be used. By allowing for no steady state *Fick's second law for diffusion* is deduced from equation I-1. If variation of D_B with the concentration can be ignored the equation can be simplified to

$$\frac{\partial C_B}{\partial t} = D_B \frac{\partial^2 C_B}{\partial x^2} \qquad \text{(I-2)}$$

There are several solutions to this equation. One solution, which is encountered in homogenisation heat treatment, will be considered later in chapter 4.5.1.

2. Nucleation in solids

2.1. Homogeneous nucleation

Vollmer and Weber [1925] as well as Becker and Döring [1935] are the "fathers" of the classic theory of nucleation. The theory was derived for the formation of liquid from gases. Nucleation phenomena in solids are more complex than in liquids and gases due to the multitude of crystallographic relationships between matrix and nucleus, the possibility of supporting shear stress and the existence of lattice defects. Nevertheless nucleation in solids could basically be treated by application of the classic nucleation theory.

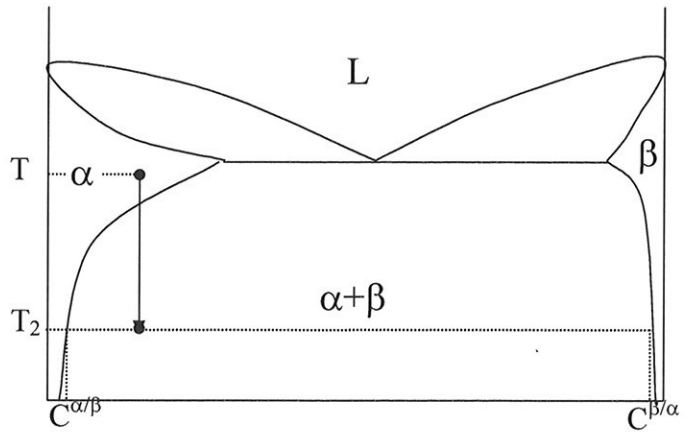

Figure I-1 *Quenching of an alloy in order to obtain a metastable supersaturated matrix.*

In order to obtain a supersaturated α matrix, the alloy with a concentration C_0 is quenched from T_1 to T_2 (Figure I-1). From the α matrix the new phase β precipitates. When β precipitates, B-atoms within the α matrix must first diffuse together to form a small volume with a concentration $C^{\beta/\alpha}$. If needed, the atoms must rearrange themselves into the β crystal structure. The free energy changes associated with the nucleation process will have the following three contributions.

$$\Delta G = -V\Delta G_v + A\gamma + V\Delta G_s \qquad \text{(I-3)}$$

V is the volume of β, ΔG_v is the free energy reduction per unit volume of β, A is the area of the interface between α and β, γ is the α/β interface energy and

ΔG_s is the misfit strain energy per unit volume of β. If we ignore the variation of γ with the interface orientation and assume that the nucleus is spherical with a radius of curvature r, equation I-3 becomes

$$\Delta G = -\frac{4}{3}\pi r^3(\Delta G_v - \Delta G_s) + 4\pi r^2\gamma \qquad \text{(I-4)}$$

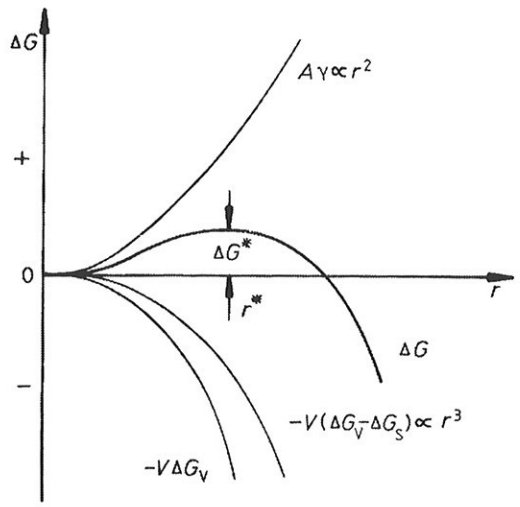

Figure I-2 *The variation of ΔG with r for a homogeneous nucleus. There is an activation energy barrier ΔG^* [Porter and Easterling 1981].*

Figure I-2 shows the variation of ΔG with r for a homogeneous nucleus. The critical nucleus size and activation energy for the nucleation is obtained after differentiation of equation I-4 with respect to r.

$$\frac{d(\Delta G)}{dr} = 0 \qquad \text{(I-5)}$$

$$r^* = \frac{2\gamma}{(\Delta G_v - \Delta G_s)} \qquad \text{(I-6)}$$

$$\Delta G^* = \frac{16\pi\gamma^3}{3(\Delta G_v - \Delta G_s)^2} \qquad \text{(I-7)}$$

The concentration of critical-sized nuclei X^* is given by

$$X^* = X_0 \exp\left(-\frac{\Delta G^*}{kT}\right) \qquad \text{(I-8)}$$

Here X_0 is the number of atoms per unit volume in the β phase, k is the Boltzman constant and T the absolute temperature. If each nucleus can be made supercritical at a rate of f the homogeneous nucleation rate is given by

$$N_{\text{hom}} = fX^* \qquad \text{(I-9)}$$

Becker [1948] and Turnbull and Fisher [1949] treated the rate of nucleation by introducing the activation energy of diffusion Q into the exponent of equation I-9. f depends on how frequently a critical nucleus can receive an atom from the α matrix. This will depend on the surface area of the nucleus and the rate at which diffusion can occur. The nucleation rate will therefore be of the form

$$N_{\text{hom}} = \omega X_0 \exp\left(-\frac{Q + \Delta G^*}{kT}\right) \qquad \text{(I-10)}$$

Here ω is a factor that includes the vibration frequency of the atoms and the area of the critical nucleus.

Incoherent nuclei have such a high value of γ that incoherent homogeneous nucleation is virtually impossible. If, however, the nucleus has an orientation relationship to matrix, and coherent interface are formed, ΔG^* is greatly reduced and homogeneous nucleation becomes feasible.

2.2 Heterogeneous nucleation

If the creation of a nucleus results in the destruction of defects such as grain boundaries, dislocation and vacancies, some free energy (ΔG_d) will be, thereby reducing the activation energy barrier. The equivalent to Equation I-3 for heterogeneous nucleation is

$$\Delta G = -V(\Delta G_v - \Delta G_s) + A\gamma + V\Delta G_d \qquad \text{(I-11)}$$

Experimental evidence has indicated that when the theory is modified for solids (equation I-11), the nucleation behaviour in most supersaturated solid solutions, with all thermodynamic data available, can not be predicted even quantitatively [Hornbogen 1969]. In alloys, such as binary aluminium, which has been most frequently investigated, it is still not possible to predict the precipitation behaviour. The reason is that additional factors affect the nucleation.

2.3. Factors affecting nucleation

There are three main factors which affect nucleation in solids

a) Crystallographic possibilities

The structures of interface between the matrix and the nucleus can be quite different. Usually the structure of the interface can be divided into three categories.

Coherent nucleation:	The crystal structure and the atomic distance of matrix and nucleus are the same (Figure I-3a).
Semicoherent nucleation:	The crystal structure and the atomic distance of matrix and nucleus have a relationship (Figure I-3b).
Incoherent nucleation:	The atomic configuration in the matrix and the nucleus is very different (Figure I-3c).

The minimum possible surface energy can be expected in the case of coherent nucleation, (the minimum activation barrier is obtained when there is no misfit between matrix and nucleus, case 1, Figure I-3a) while the surface energy for incoherent nucleation will be highest.

b) Strain energy

In general, the transformed volume will not fit perfectly into the space originally occupied by the matrix and this gives rise to a misfit strain energy. The origin of a misfit between matrix and nucleus can be difference of lattice parameters or different symmetry of the crystal lattice.

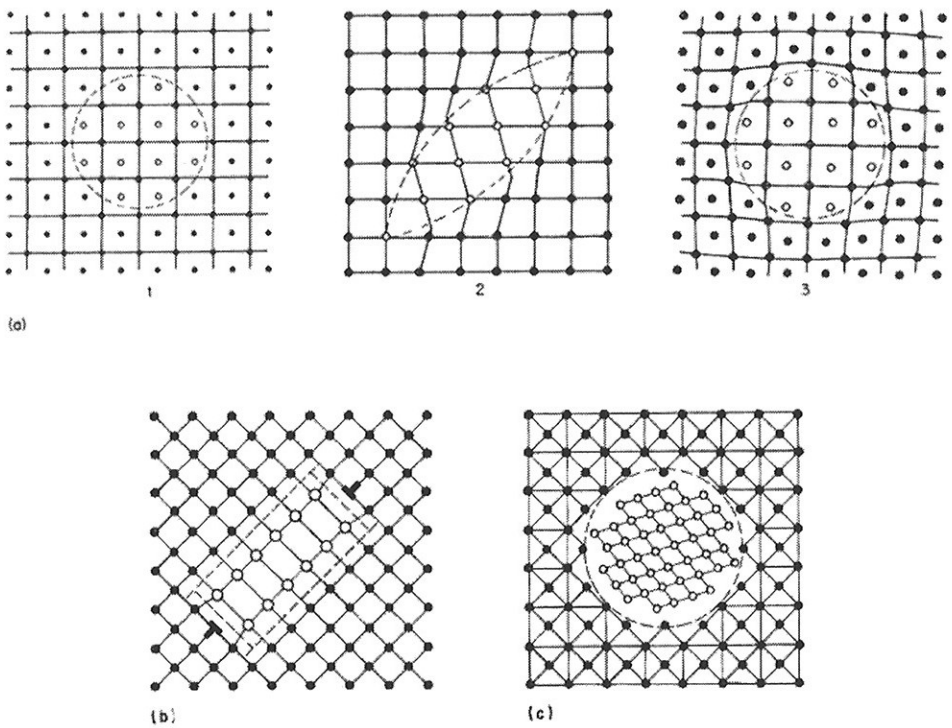

Figure I-3 *Three types of nuclei in solids: a) coherent nucleus, 1. without misfit, 2. distortion by stress, 3. distortion by stress due to volume change; b) semicoherent nucleus – the interface consists partially of dislocations (dislocation ring); c) noncoherent nucleus – the interface is similar to that of a high-angle grain boundary [Hornbogen 1969].*

c) Lattice defects

In supersaturated solid solutions, the following types of lattice defects can be expected:

2-dimensional defects –	grain boundaries, twin boundaries, stacking faults, antiphase domain boundaries
1-dimensional defects-	dislocations
0-dimensional defects-	vacancies.

A combination of the two factors, crystallographic relationship and lattice defects, is proposed as a way to bring order to a large number of nucleation phenomena. The combination of the most common defects in the matrix and the crystallographic relationships are given in Table I-1.

Table I-1 ΔG^* decreases in direction of the arrows. [Hornbogen 1969]

Defect / Cryst. relationship between α and β	B = Grain boundary		D = Dislocation		V = Vacancy		H = Homogeneous nucleation in a perfect lattice
c = coherent	Bc	→	Dc	→	Vc	≈	Hc
	↓		↓		↑		↑
s = semichoerent	Bs	→	Ds	←	Vs	←	Hs
	↓		↑		↑		↑
n =incoherent	Bn	←	Dn	←	Vn	←	Hn

From table I-1, four types of nucleation with a minimum value of ΔG^* are evident: incoherent nucleation at grain boundary (Bn), semicoherent nucleation at dislocation (Ds), coherent nucleation at vacancies (Vc) and coherent homogeneous nucleation (Hc).

3. Particle coarsening

When the precipitate growth is finished and the concentration in the matrix has reached the equilibrium concentration, the particle coarsening begins. In this process the small particles shrink and disappear while large particles grow. The driving force is provided by the reduction in the total interface free energy of the material. Since smaller particles in a solution have a higher surface area/volume-fraction than larger particles, smaller particles are less stable than larger particles of the same material. An increase in the mean particle radius $\bar{r}$ will reduce the total free energy of the system and this reduction in energy is the driving force in the coarsening reaction. The theoretical description of coarsening is based on the Gibbs-Thomson-equation and is given in the following form:

$$C_B^{\alpha/\beta}(r) = C_{eq}^{\alpha/\beta} \exp\left[\frac{2\gamma V_m^{\beta}}{RTr}\right] \qquad \text{(I-12)}$$

$C_B^{\alpha/\beta}(r)$ is the solubility of a particle B of radius r and $C_{eq}^{\alpha/\beta}$ is the solubility of a particle B of infinite radius. V_m^{β} is the molar volume of the β-phase, γ is the interface energy, and is constant and independent of the radius of the particle *r*. This equation assumes a dilute - ideal binary α(A-B)-solution and that the β-phase is nearly pure B. As pointed out, the coarsening process is the last stage in the decomposition of a supersaturated solution, which implies that the supersaturation is largely eliminated and $C_B^{\alpha/\beta}(r) \approx C_{eq}^{\alpha/\beta}$ for all particles in the system. Equation I-12 can thus be linearized:

$$C_B^{\alpha/\beta}(r) = C_{eq}^{\alpha/\beta}\left[1 + \frac{2\gamma V_m^{\beta}}{RTr}\right] \qquad \text{(I-13)}$$

Equation I-13 is an acceptable approximation when $2\gamma V_m^{\beta}/RT \leq 0.3$ which means that the average particle radius must be larger than $\sim 3 \cdot 10^{-9}$m.

Equation I-13 shows that the solute concentration in the matrix adjacent to a particle will increase as the radius of curvature decreases. Thus, the system will contain concentration gradients and the system is not at its lowest free energy state. It can move in the direction of lower energy by reducing the magnitude of the concentration gradients. This can be obtained by moving material from the smaller particles and depositing it at the larger ones. The smaller particles will thus decrease in size while the larger particles will grow, Figure I-4. The overall results are that the total number of particles decreases and the mean radius ($\bar{r}$) increases with time.
Lifshiz and Slyozov [1961] and Wagner [1961] have developed the theoretical relationship between mean particle radius and coarsening time (t). When long-range diffusion through the lattice is the rate limiting for the coarsening the relationship has to be of the form

$$\bar{r}^3 - \bar{r}_0^3 = Kt \qquad \text{(I-14)}$$

where

$$K = \frac{8}{9}\frac{D\gamma V_m^{\beta} C_{eq}^{\alpha/\beta}}{RT}$$

$\bar{r}_0$ is the mean radius of the particles at $t = 0$ and D is the diffusion coefficient. Since D and $C_{eq}^{\alpha/\beta}$ increase exponentially with temperature, the coarsening rate will increase rapidly with increasing temperature.

When short-range diffusion across the interface boundary is the rate limiting for the coarsening, the relationship has to be of the form

$$r^2 - \bar{r}_0^2 = K_1 t \qquad \text{(I-15)}$$

where

$$K_1 = \left(\frac{8}{9}\right)^2 \frac{\gamma V_m^{\beta} C_{eq}^{\alpha/\beta} \nu}{RT(C_B^{\alpha} - C_{eq}^{\alpha/\beta})}$$

Here ν is the velocity of the interface.

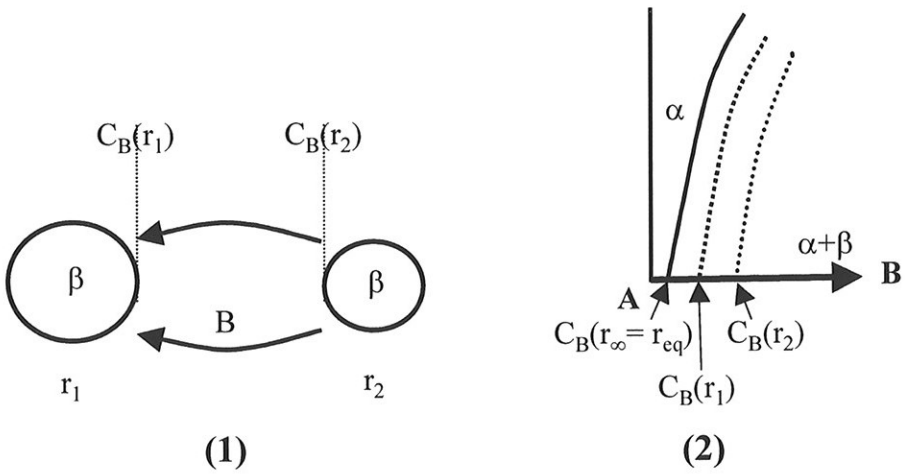

Figure I-4. *(1) Due to the Gibbs – Thomson effect, the concentration of solute is highest outside the smallest particle. (2) A sketch of the A-corner of the A-B phase diagram which shows solid solution of α outside the two particles. B atoms will diffuse from the high concentration $C_B(r_2)$ (small particle) in the direction of the low concentration $C_B(r_1)$ (largest particle) until the small particles have disappeared.*

4. The Al-Mg-Si system

4.1 Generally

Alloys in the 6xxx series contain silicon and magnesium approximately in the proportion required for formation of Mg_2Si, thus making these alloys heat-treatable. Although the strength is not as high as for most of the 2xxx and 7xxx alloys, the 6xxx series alloys have good formability, good machinability, high corrosion resistance and medium strength. These heat-treatable alloys may be formed in the T4 temper (solution heat-treated but not precipitation heat-treated) and strengthened after forming to full T6 properties by precipitation heat treatment. The 6xxx series are the dominating alloys in the aluminium extrusion industry [Reiso 1992]. Uses include architectural applications, bicycle frames, transportation equipment, bridge railings and welded structures. From year to year the use of aluminium alloys in automotive applications has increased and there is an increasing demand for medium and high strength alloys of the 6xxx series with good ductility and formability.

4.2 The ternary Al-Mg-Si phase diagram [Phillips 1959]

The ternary Al-Mg-Si liquids surface, the limit of solubility and the solidus are shown in Figure I-5. Aluminium and the binary constituent Mg_2Si form a quasi-binary system dividing the ternary system into two parts. In the quasi-binary system the constituents form a eutectic at 595 °C. There is an appreciable solid solubility in aluminium reaching 0.85 wt.% Mg and 1.10 wt.% Si at the eutectic temperature. Aluminium, silicon and Mg_2Si form a ternary eutectic containing 4.97 wt.% Mg and 12.95 wt.% Si. This eutectic freezes at 555 °C. Knowledge of the limits of solid solubility in this alloy system is of great importance. The wide range of solubility along the quasi-binary line, and the marked decrease in solid solubility with temperature makes these alloys sensitive to heat treatment.

4.3 The process route in the production of aluminium extrusions

The different process stages for an extruded section are shown in Figure I-6. Since every stage affects the quality of the final product, each of the main stages will be discussed. Casting, ageing, extrusion and recrystallization are only studied briefly, while homogenisation is studied more thoroughly and with special emphasis on the dispersoids.

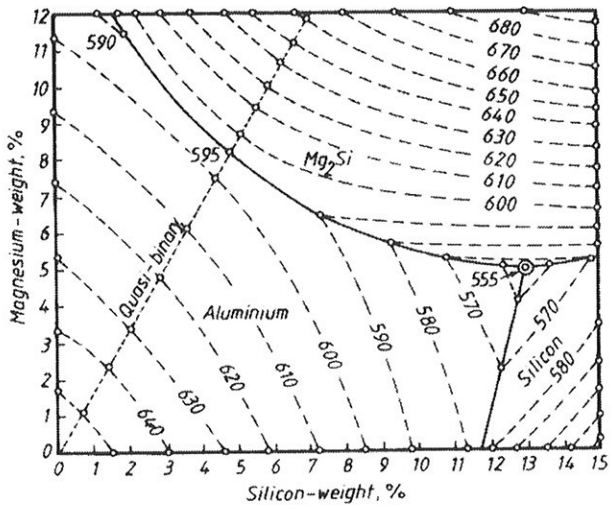

Figure I-5a Al-Mg-Si liquids [Phillips 1959]

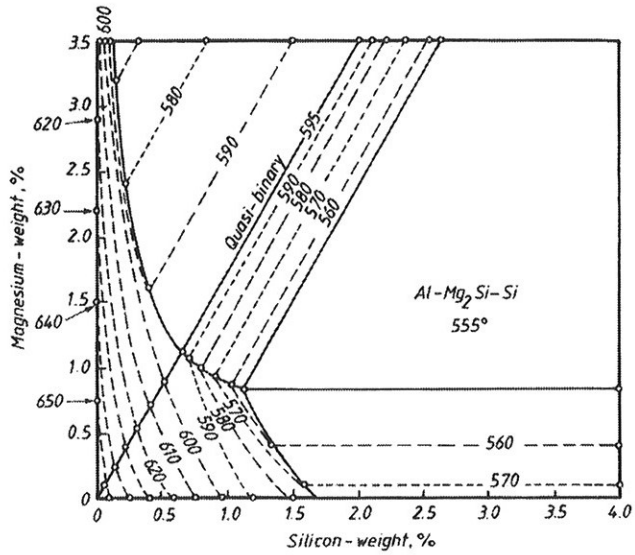

Figure I-5b Al-Mg-Si solubility [Phillips 1959]

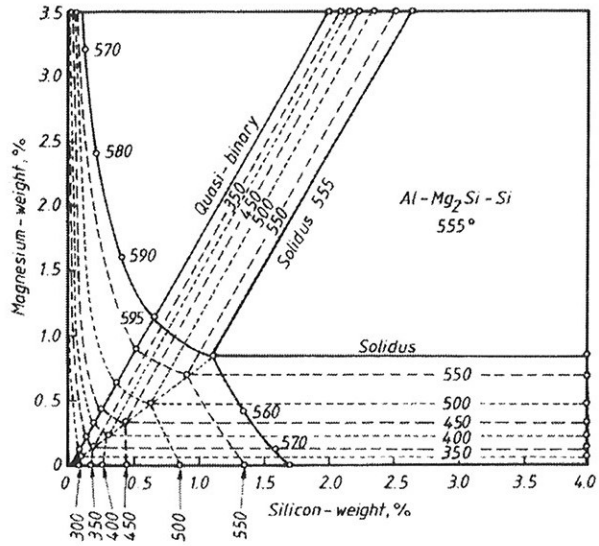

Figure I-5c Al-Mg-Si solidus [Phillips 1959]

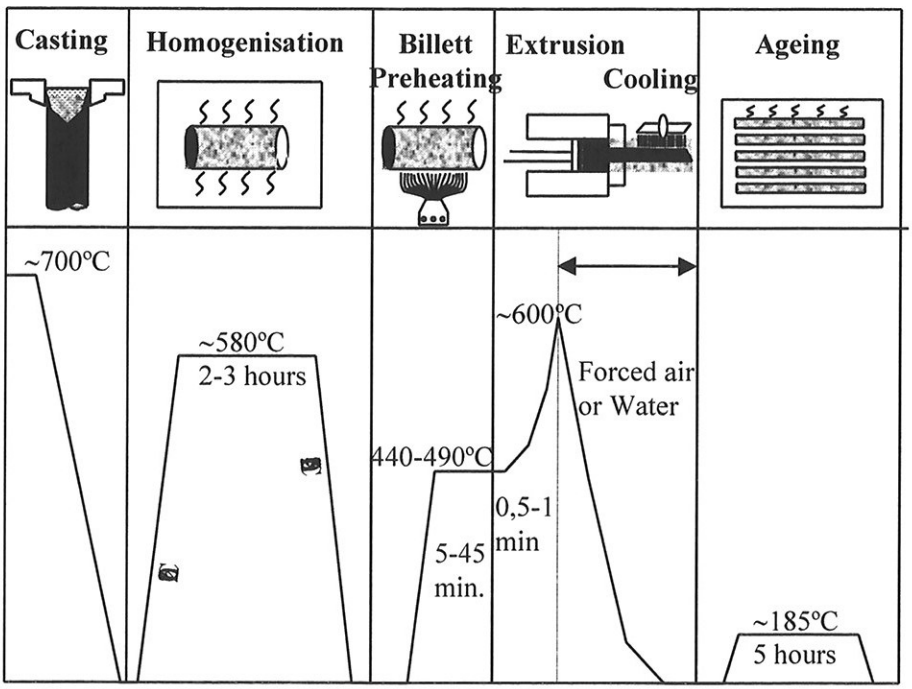

Figure I-6 Sketch of the process route in production of Al-Mg-Si extrusions. Typical temperatures and times for each operation are indicated. [Reiso 1992]

4.4 Casting

To produce the cylindrical extrusion billets the direct-chill (DC) casting method is used i.e. liquid metal is solidified continuous through vertical casting in water-cooled lined moulds, followed by direct water spray, see Figure I-6.

4.5 Homogenisation

The term homogenisation is used for a heat treatment operation of the as cast material in order to improve the workability of the material and the properties of the final product. The main effects of the homogenisation treatment on the microstructure in Al-Mg-Si alloys are:

- Level out microsegregation.
- Control the precipitation of dispersoid particles from dispersoid forming elements such as Mn and Cr.
- Transform non-equilibrium phases to stable phases (e.g. transformation of β-AlFeSi particles to α-Al(MnCrFe)Si particles).
- Dissolve low melting point eutectics in the material (e.g. Mg_2Si)
- Spheroidize insoluble phase particles.

4.5.1. Microsegregation

In all commercial aluminium alloys produced in normal casting processes, solute is redistributed during solidification. On a microscale this phenomenon can be observed as a dendritic segregation pattern. It has to be realized that in all castings the alloying elements and the impurities are unevenly distributed on a microscale as well as on a macroscale. In practice, it is not possible to smooth out concentration differences over a long distances by diffusion processes, so we have to accept the macro-segregation. On a microscale, i.e. over distances of some few hundreds of μm, which is usually a longer distance then the dendrite arm spacing (DAS) much can be done. The microsegregation remaining after solidification and cooling is often reduced during homogenisation. In this process the material is heated to a temperature between 450 - 600 °C and held at this temperature for a given time. During the homogenisation, the concentration differences even out by diffusion.

The rate of diffusion is individual for each element and element combination. The temperature dependent diffusion coefficient or the diffusivity, is usually given as

$$D = D_0 \exp\left(-\frac{Q}{RT}\right) \qquad \text{(I-16)}$$

Where D_0 is the pre-exponential term [cm^2/s], Q is the activation energy [kJ/mol], R is the gas constant and T is the absolute temperature. The activation energy represents an energy barrier the atom must defeat in order to move to a new position. A list of some of the published diffusion data for the elements Mg, Si, Fe, Mn and Cr is given in Table I-2.

Table I-2 Literature data for the diffusion coefficient.

Element	D_0 [cm^2/s]	Q [kJ/mole]	$D_{580\,°C}$	Reference
Si	0.90	133	$6.5 \cdot 10^{-9}$	Altenpohl 1965
	2.02	136	$9.5 \cdot 10^{-9}$	Fujikawa 1978
	2.48	137	$1.1 \cdot 10^{-8}$	Smithells 1983
Mn	$2.2 \cdot 10^{9}$	330	$1.4 \cdot 10^{-11}$	Altenpohl 1965
	104	211	$1.2 \cdot 10^{-11}$	Mehrer 1992
Fe	$4.1\ 10^{-9}$	57,8	$1.2 \cdot 10^{-12}$	Altenpohl 1965
	135	192	$2.4 \cdot 10^{-10}$	Alexander 1970
	$1.1 \cdot 10^{4}$	222	$2.8 \cdot 10^{-10}$	Mantl 1983
Mg	0.0623	115	$5.8 \cdot 10^{-9}$	Smithell 1983
Cr	$1.85*10^{3}$	253	$5.8 \cdot 10^{13}$	Mehrer 1992

From the data in Table I-2 it is obvious that the diffusion rate for the "fast moving" elements Mg and Si is at least one order of magnitude higher than the "immobile"elements Mn and Cr (and Fe).

First we consider only elimination of microsegregations and assume that the diffusion rate of each element is the rate determining factor. Furthermore, if we assume that the solute distribution is a one-dimensional problem, the distribution can be described by a sinusoidal function. This simple model is shown in Figure 1-7.

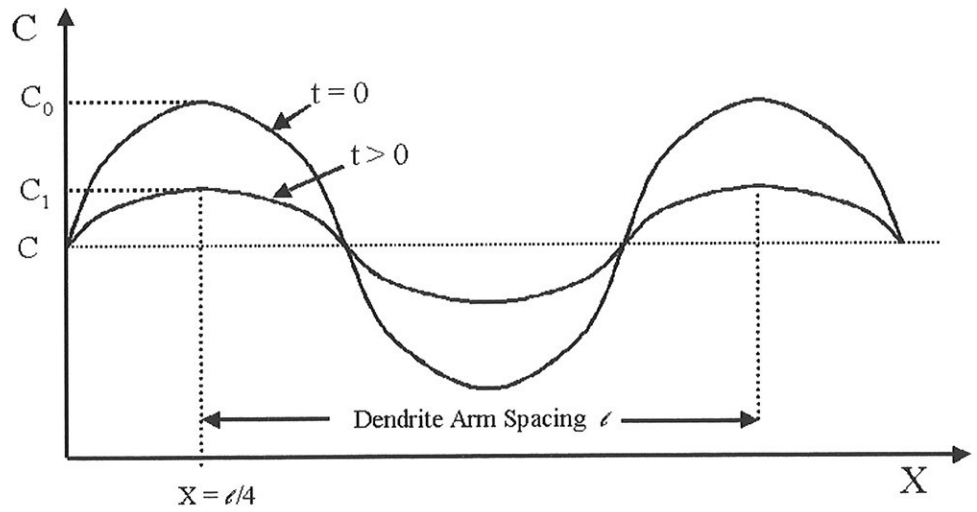

Figure 1-7 The microsegregation pattern can be represented approximately by a sine-function. The wavelength of this function is equal to the dendrite arm spacing.

A solution of Fick's second law (equation I-2) of this diffusion problem can be written as:

$$C = \overline{C} + (C_0 - \overline{C})\sin\left(\frac{2\pi x}{DAS}\right)\exp\left(-\frac{4\pi Dt}{DAS^2}\right) \quad \text{(I-17)}$$

The formula expresses the degree of segregation where t is the time, ℓ is the dendrite arm spacing and D is the diffusion constant. The relationship between degree of segregation after heat treatment and the original degree of segregation is is given by the coefficient δ_i:

$$\delta_i = \frac{C - \overline{C}}{C_0 - \overline{C}} \quad \text{(I-18)}$$

At x = DAS/4. Inserting this value together with Equation I-17 into Equation I-18:

$$\delta_i = \exp\left(-\frac{4\pi Dt}{DAS^2}\right) \quad \text{(I-19)}$$

Substituting Equation I-16 into Equation. (I-19) gives for constant teperature:

$$\delta_i = \exp - \left(\frac{4\pi t D_0 \exp\left(-\frac{Q}{RT} \right)}{DAS^2} \right) \qquad \text{(I-20)}$$

If the temperature is not constant during homogenisation the solution to the diffusivity problem is more complex. A solution can be deduced when the heating rate or cooling rate θ [K/s] is constant.

$$D = D_0 \int_0^t \exp\left(-\frac{Q}{RT(t)} \right) dt \qquad \text{(I-21)}$$

$$\frac{dT}{dt} = \theta \qquad \Rightarrow \qquad dt = \frac{dT}{\theta} \qquad \text{(I-22)}$$

Substituting Eq. (I-22) into Eq. (I-21) gives:

$$D = \frac{D_0}{\theta} \int_{T_1}^{T_2} \exp\left(-\frac{Q}{RT} \right) dT \qquad \text{(I-23)}$$

4.5.2 Dispersoids

Small amounts of Mn and/or Cr have for a long time been used in order to modify the microstructure and thus improve the properties of the alloys. During high temperature annealing (400 - 580 °C) different types of precipitates containing Mn and/or Cr are formed with various crystallographic structures and chemical compositions. These types of precipitates, which have a rather small direct effect on the mechanical properties, are usually referred to as dispersoids. Due to their fairly high density and high thermal stability they can, however, have a strong effect to prevent recovery, recrystallization and grain growth.

Dispersoids are found to be either the α-Al(MnCrFe)Si phase [Dons 1985, Reiso 1994, Westengen 1980,] or the α-AlCrSi phase [Reiso 1994]. The formation of such dispersoids has been investigated for many years, but is still not completely understood. The dispersoids have a rather complex structure and the interface between the dispersoids and the Al-matrix is incoherent. Thus homogeneous nucleation seems to be unlikely. Several sites

for heterogeneous nucleation have been suggested. Hirasawa [1975] gave, based on an electron microscopy observation, some evidence that the strengthening particles β- and β- Mg_2Si needles formed during the heating up period can act as nucleation site for the dispersoids containing Mn during high temperature annealing. Even β - plates have been suggested as nucleation sites. In 1980 Westengen et al [1980] investigated the formation of dispersoids in both Mn- and Cr-containing 6000 series alloys by means of electrical resistivity measurement and TEM metallography. In alloys containing Mn a relatively large variation in the electrical resistivity was observed during the high temperature annealing. Much less variation was found during a similar heat treatment of the alloys containing Cr. The examination in TEM showed dispersoids in both alloys after the heat treatment.

One very important observation, made by Conte [1996] and Westengen et al. [1980], is the tendency of the dispersoids to be very nonuniformly distributed in the material. Observations indicate that a slow heating rate promotes a uniform distribution of dispersoids [Westengen 1980]. Kolby et al [1994] reported that the presence of silicon in AlMn-alloys dramatically enhances the precipitation kinetics. Thus, a nonuniform distribution of silicon after solidification may be responsible for the nonuniform distribution of the dispersoids.

Due to the diffusion rate, the number of dispersoids increases with decreasing homogenisation temperature. But a low homogenisation temperature can result in a low redistribution of solute and a low degree of spheroidization of primary particles. The spheroidization of primary particles decreases the deformation resistance of the material, resulting in a better extrudability [Zajac et al. 1994]. A homogenisation at high temperatures gives a high degree of spheroidization, but at the same time it gives a rather small number of dispersoids, resulting in a material with a low recrystallization resistance.

4.5.3 α-Al(MnCrFe)Si dispersoids

In 1950, Phragmen presented a metallographic investigation of several ternary and quaternary aluminium alloy systems. This study included the Al-Mn-Si, Al-Fe-Si and the Al-Mn-Fe-Si systems. In this investigation he found one similar type of particle all systems. X-ray investigation of this type of particle in the Al-Mn-Fe-Si system showed that the structure was cubic with a lattice parameter a = 1.263 nm. This value agrees well with the corresponding value for the cubic α-AlMnSi (a = 1.2625 nm) and the cubic α-AlFeSi (a = 1.2523 nm). This indicates the existence of a phase with a homogeneity range from AlMnSi to AlFeSi as shown in Figure I-8. The phase with chemical

composition between α-AlMnSi and α-AlFeSi was designated α-Al(FeMn)Si. Several authors have found the same phase but with slight modifications [Copper 1967, Donnaieu 1992, Dons 1984[1], Dons 1984[2], Dons 1985, Munson 1967, Nes 1972, Ping 1987, Reiso 1994, Westengen et.al. 1980, Westengen 1982]. Munson reported that in pure Al-Fe-Si alloys the α-AlFeSi phase has a hexagonal structure (a = 1.23 nm c =2.62 nm). The cubic structure was formed only when some other transition metals (Cr, Mn, V, Cu, Mo or W) were present above a critical concentration. He also suggested that when the Mn/Fe ration increases, the sequence of phases are: hexagonal α-AlFeSi → bcc α-Al(FeMn)Si → simple cubic (sc) α-AlMnSi.

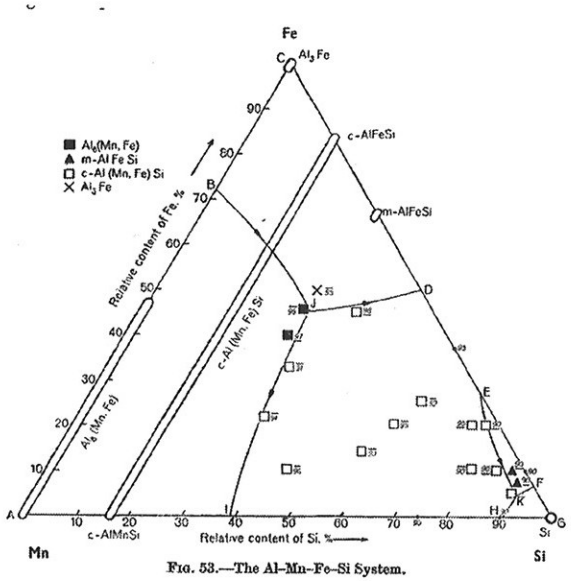

FIG. 53.—The Al–Mn–Fe–Si System.

Figure 1-8 The Al-Mn-Fe-Si system. The relative amount of alloying elements form the co-ordinates in the diagram. α-AlFeSi and α-AlMnSi are linked together by a homogeneity range in the composition [Phragmen 1950].

Dons [1984[1], 1984[2], 1985] also investigated α-Al(FeMn/Cr)Si particles. Some DC-cast alloys with 1.0 wt.% Si - 0.6wt.% Mg - 0.2 wt.% Fe with addition of 0.2 wt.% Cr or 0.5 wt.% Mn (ÅSV 2018) were investigated. Series of different heat treatments of the alloy were carried out. During this heat treatment small secondary α-Al(FeMn/Cr)Si particles (dispersoids) were found to nucleate. In the alloy containing Mn all the primary particles formed during solidification were found to belong to the α - Al(FeMn)Si phase. In the alloy containing Cr, β-AlFeSi (monoclinic) with traces of Cr occurred as well. The primary α-particles were found to have a bcc structure and to

contain more Fe than Mn or Cr. The secondary α-Al(FeMn/Cr)Si particles probably had a simple cubic structure and contained more Mn or Cr than Fe. In the as cast material the particles were large and had a Fe/Mn ratio of about 1.2. The secondary α-Al(FeMn)Si particles were Mn-rich, but after extensive annealing the composition of the two set of particles approached each other as shown in Figure I-9. Equilibrium was not reached even after 26 days, but it

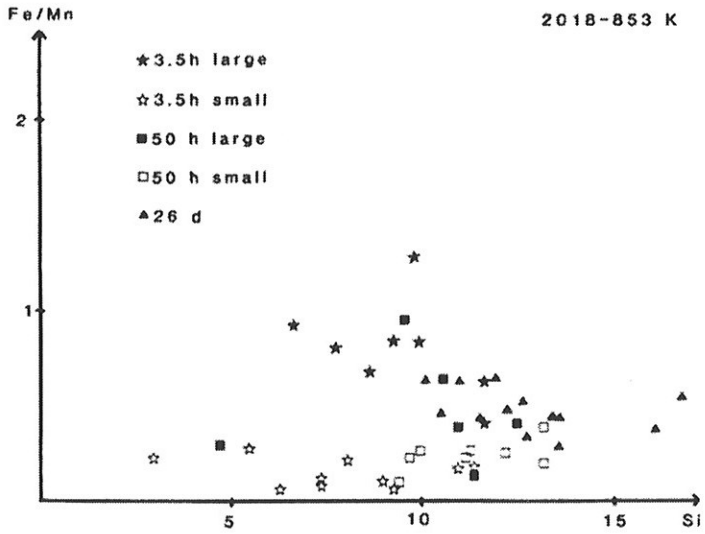

Figure I-9 *The diagram shows how the Fe/Mn-ratios in the particles in ÅSV 2018 alloy changed during the heat treatment at 580°C. The Fe/Mn-ratios have been plotted as a function of at-% Si. Small, Mn-rich dispersoids formed at an early stage. As time went on, both the dispersoids and the Fe-richer primary particles grew, and approached each other in composition. After 26 days there were still variations from one particle to another [Dons 1984[2]].*

seems that the Fe/Mn ratio stabilised at about 0.45 at 580 °C. In the DC-cast ÅSV 2018 alloy it appeared that the composition of α-Al(FeMn/Cr)Si particles may vary somewhat, but it is assumed that $Al_{13}(FeMn)_3Si_2$ is a good approximation.

Ping [1987] also observed a superlattice in the bcc α-AlFeSi structure. The superlattice was found to be rhombohedral. The strong reflection in the SAED pattern (TEM investigation) came from the bcc primary lattice while the weaker reflections were due to the superlattice. Other authors believe that the weaker reflections are due to the transformation from bcc to sc.

4.5.4 α' - AlCrSi dispersoids

In addition to α-Al(CrFe)Si dispersoids, α-AlCrSi dispersoids can precipitate in an Al-Mg-Si alloy containing Cr [Reiso 1994]. The α-AlCrSi particles have a face centred cubic unit cell (FCC) with lattice parameter a = 1.092 nm [Robinson 1953].

4.5.5 Transformation of β-AlFeSi to α-Al(MnCrFe)Si

After casting of AlMgSi alloys with small amount of Cr and/or Mn, the primary β-AlFeSi phase particles will be present [Mulazimoglu et al. 1996, Størkersen et al. 1980]. These particles have a monoclinic unit cell with lattice parameters a = 0.616, b = 0.618, c= 2.08 nm and β = 90.4° [Rømming et al. 1994, Størkersen et.al 1980]. In several reports [Mondolfo 1976, Mulazimoglu et al. 1996, Zajac et.al. 1994] it has been claimed that the hard eutectic β-AlFeSi particle severely restricts hot workability and to a large extent is responsible for the occurrence of pickup during extrusion, which leads to a poor surface finish. During homogenisation, which is designed to reduce the microsegregation of Mg and Si, the majority of the β-AlFeSi particles transforms to α-Al(MnCrFe)Si particles. The α-Al(MnCrFe)Si particles have a more globular morphology which improves the ductility and extrudability of the alloy and entails improved properties and surface finish of the final product.

4.6 Extrusion

A gas heater or an induction heater preheats the billet before extrusion. The billet is then placed inside a pre-heated extrusion container and a ram presses the material through a die with the same geometry as the final section, see Figure I-6. The extrusion speed is a measure of the productivity. One of the factors affecting extrusion speed is the flow stress of the material, which decreases with increasing temperature. An increased amount of elements in solid solution increase the flow stress. On the other hand, the presence of low melting point phases such as Mg_2Si can result in incipient melting during extrusion. If the extrusion speed is too high, the incipient melting can result in tearing. Reiso [1992] suggested that the extrudability of Al-Mg-Si alloys is controlled by the concentration of Mg and Si in solid solution and the occurrence of incipient melting in the material.

4.7 Quench sensitivity

If the strength of the material after ageing decreases with decreasing cooling rate from solution temperature, the material is said to be quench sensitive When the cooling rate is low, a substantial amount of Mg and Si may precipitate on heterogeneities such as grain boundaries and primary particles. The vacancy supersaturation is also reduced. Both factors reduce the nucleation potential of β"-Mg_2Si in the neighbourhood of such sites. Addition of Mn and/or Cr are found to increase the quench sensitivity [Dorward 1992, Kovacs-Csetenyi et al. 1987[1], Kovacs-Csetenyi et al.1987[2], Lim and Shercliff 1993, Lohne and Dons 1983, Merchant et al. 1988, Musulin and Celliers 1991]. The reason for this is that Mn/Cr bearing dispersoids are good nucleation sites for the non hardening β' - Mg_2Si particles during slow cooling, which leads to a lower supersaturation of solutes and lower β``precipitation hardening during subsequent ageing [Kovacs-Csetenyi et al.1987[1], Kovacs-Csetenyi et al 1987[2], Lohne and Dons 1983,]. The dispersoid size, density and distribution are a function of alloying elements, heating rate to homogenisation temperature and homogenisation temperature and time. Increasing contents of Mn/Cr produce more dispersoids and therefore additional nucleation sites which increase the quench sensitivity [Dorward 1992, Kovacs-Csetenyi et al.1987[1], Kovacs-Csetenyi et al 1987[2], Lim and Shercliff 1993, Musulin and Celliers 1991].

4.8 Recrystallization

In order to obtain high strength in a 6xxx alloy after extrusion, the material must be fully unrecrystallized. Small dispersoids effectively retard recrystallization due to pinning of the moving reaction front by the particles. The time before cooling after extrusion clearly influences the recrystallization. Water quenching of the material after extrusion gives a considerably thinner recrystallized surface layer of the extruded section than air-cooling does.

5 Electrical resistivity [Hatch 1984]

Electrical resistivity is one of the most sensitive properties of aluminium, as it is particularly responsive to changes in alloying elements. Fortunately, resistivity is readily measured with high precision. All known metallic additions to aluminium increases the electrical resistivity. Elements in solid

solution elevate the resistivity to a greater extent than when out of solution (Table I-3). As the amount of elements in solid solution increases, the resulting rapid increase in resistivity is in marked contrast to much slower increase in resistivity as the concentration of these elements exceeds its solid solubility limit. A summary of the maximum solubilities and effect on electrical resistivity of various elements in aluminium is shown in Table I-3.

Table I-3. Effect of elements in and out of solid solution on the resistivity of aluminium. [Hatch 1984]

Element	Maximum solubility in Al, %	Average increase in resistivity per wt%, μΩ·cm	
		In solution	Out of solution(a)
Chromium	0.77	4.00	0.18
Copper	5.65	0.344	0.030
Iron	0.052	2.56	0.058
Lithium	4.0	3.31	0.68
Magnesium	14.9	0.54(b)	0.22(b)
Manganese	1.82	2.94	0.34
Nickel	0.05	0.81	0.061
Silicon	1.65	1.02	0.088
Titanium	1.0	2.88	0.12
Vanadium	0.5	3.58	0.28
Zinc	82.8	0.094(c)	0.023(c)
Zirconium	0.28	1.74	0.044

Note: Add above increase to the base resistivity for high-purity aluminum, 2.65 μΩ·cm at 20 °C (68 °F) or 2.71 μΩ·cm at 25 °C (77 °F).
(a) Limited to about twice the concentration given for the maximum solid solubility, except as noted. (b) Limited to approximately 10%. (c) Limited to approximately 20%.
Source: L.A. Willey, Alcoa Research Laboratories.

The effect of two or more additions on the resistivity of aluminium depends on the interaction between the elements. In general, if the elements individually go into solid solution in aluminium, their effects on resistivity are additive.

Part II

The material

1. Experimental procedure

1.1 Casting and chemical composition

At the start of this project, six Al-Mg-Si alloys with various contents of Cr and Mn were produced. A pilot scale casting equipment at Hydro Aluminium Sunndalsøra was used to produce the alloys. Billets Ø95 in diameter were DC-cast using the hot-top technology. During the course of the investigation it turned out that a comparative investigation of an alloy with a somewhat higher Cr content than 0.15 wt.% would be valuable. Alloy Y with about 0.35 wt.% Cr was made by remelting alloy A, and adding Cr to the melt. In order to have a reference alloy, which was cast in a similar way to alloy Y but without Cr, alloy X was made. Alloy X was made by simply remelting alloy A and cast it in a copper mould. After the casting the chemical composition of the billets was determined by spectrographic analysis at Hydro Aluminium Sunndalsøra. The measured concentrations are given in Table II-1.

Table II-1. The measured chemical composition [wt.%]

Alloy	Mg	Si	Fe	Cr	Mn
A	0.589	0.936	0.214	0.002	0.007
B	0.617	0.936	0.214	0.002	0.267
C	0.605	0.944	0.215	0.002	0.535
D	0.594	0.920	0.219	0.149	0.011
E	0.628	0.933	0.224	0.144	0.547
F	0.609	0.918	0.216	0.145	0.285
X	0.569	0.934	0.190	0.002	0.005
Y	0.559	0.910	0.189	0.316	0.005

1.2 Microstructure

1.2.1 Grain size and secondary dendrite arm spacing (DAS)

The location from which the samples for all experimental investigations in this work was taken is shown in Figure II-1. Cubes of 15 · 15 · 15 mm were produced from discs cut approximately 100 mm from the top of the billets. Material from the centre and at the outer edge of the billets was ignored due to experience of some inhomogeneity in these areas. Grain size and the dendrite arm spacing (DAS) were measured in the as-cast material. The

samples were mechanically ground by means of grinding paper with a fineness 80 to 2400 grit. Then the samples were polished in two steps starting with cloth and 3 μm and 1 μm. Finally the samples were anodised in 40 ml HBF_4 and 760 ml water.

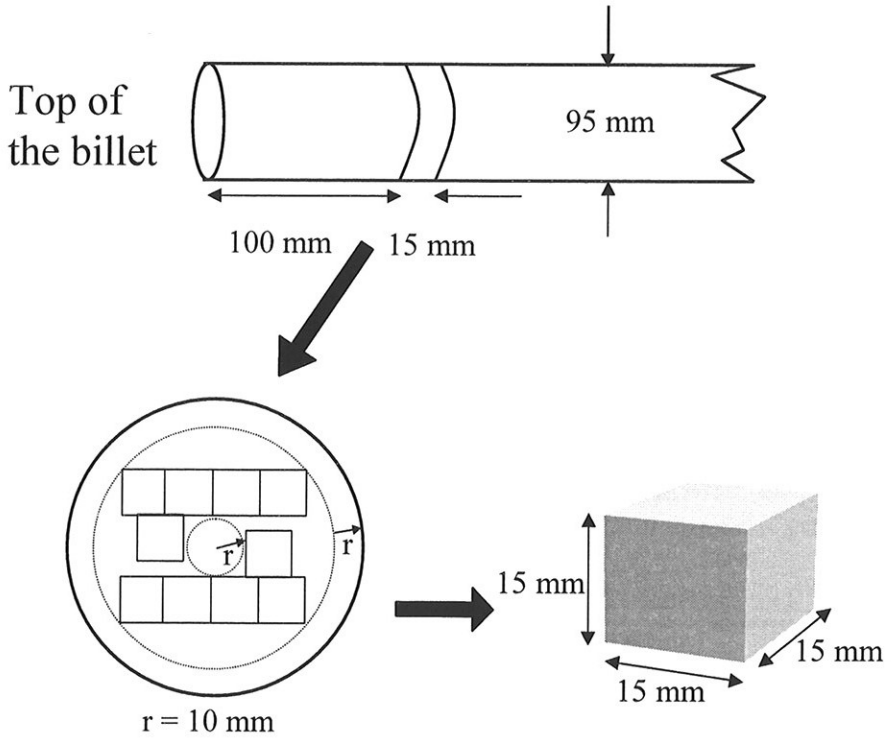

Figure II-1 Location and size of samples which were used in the experimental investigation.

The samples were investigated in polarised light in a Reichert MeF3A microscope. The grain size and the DAS were measured using the linear intercept method. The grain size measured by the linear intercept method is given by:

$$D_G = \frac{L_D}{n_D - 1} \qquad \text{(II-1)}$$

where D_G is the grain size, n_D is the number of intercepts and L_D is the distance between the first and last intercept. For each sample at least 100 intercepts were counted for both grain size and DAS measurements. The selected line for L_D was random when the grain size was measured, while the

selected line for L_D was placed out off the largest grains when the DAS was measured.

1.2.2 Microsegregations

The microsegregations in the as-cast alloys were investigated by means of a JEOL JKA-8900R microanalyser (only alloys A-F were investigated). The microanalyser was equipped with both wavelength dispersive spectrometers (WDS) and energy dispersive spectrometers (EDS). The specimen was ground and polished as described in Section 1.2. The applied acceleration voltage was 15 kV. The electron beam was moved along a line in steps and measurements were carried out every 2 μm

1.2.3 Primary particles

In order to obtain a general overview of the casting microstructure, all the alloys were investigated in a Scanning Electron Microscope (SEM). In Al-Mg-Si alloys with or without Mn and/or Cr, Mg_2Si, α-Al(MnCrFe)Si and β-AlFeSi phases are the three main primary particles [Bäckerud et al. 1986]. α-AlFeSi and π-AlMgSiFe phases may also form during casting [Bäckerud et al.1986, Mondolfo 1976]. In addition several metastable phases can exist [Mondolfo 1976]. In order to determine the primary particles, the chemical composition was determined by EDS point analysis. The specimens were ground and polished as described in chapter 1.2.1. The investigation was carried out by means of a SEM JEOL JMS-840 with EDS Link eXL

2. Results and discussion

2.1 Grain size and secondary dendrite arm spacing

Figure II-2 shows the microstructures of the alloys. For alloys A – F the grain size varies between 69 μm and 96 μm and has a tendency to increase with the concentration of alloying elements (Table II-2). Cr seems to have the most pronounced effect on grain size.. In samples with a low alloying-concentration, the grains are small and the grain size distribution is uniform. In samples with a high alloying concentration, some very large grains are observed together with the smaller grains (Figure II-2e). The variation in DAS is very small, but the measurements were only carried out in the areas out off the large grains. In alloy X and Y the measurements show that the values for the grain size and the DAS are higher than in alloys A - F. Due to

different casting techniques the solidification rate of the alloys is different. The DC-cast alloys A - F have a higher solidification rate than alloys X and Y, which are cast in the laboratory.

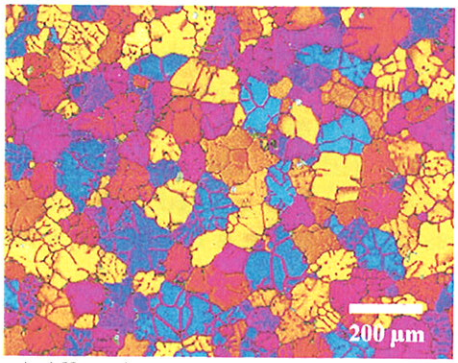

a) Alloy A

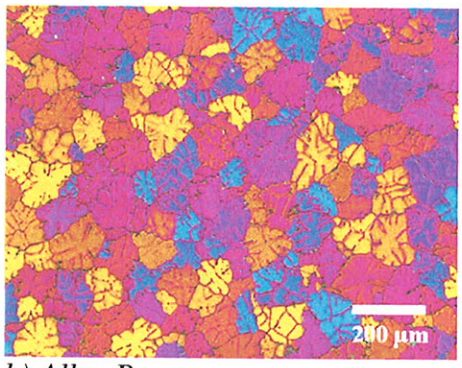

b) Alloy B

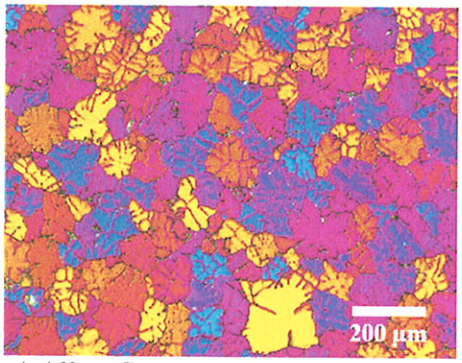

c) Alloy C

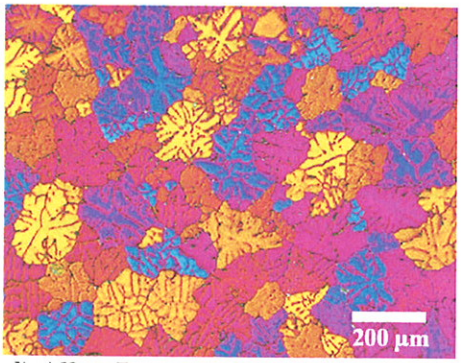

d) Alloy D

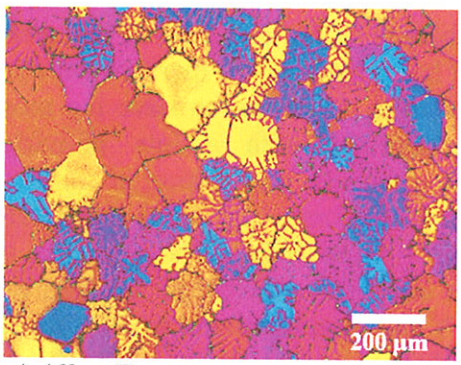

e) Alloy E

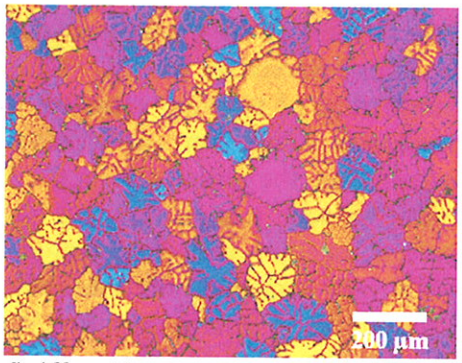

f) Alloy F

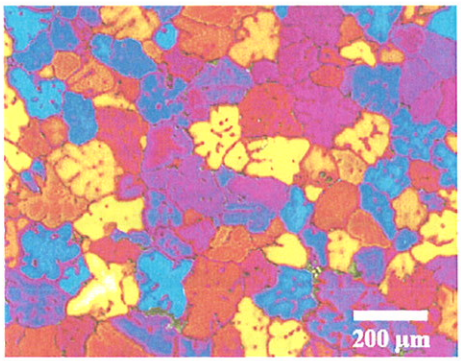

g) Alloy X

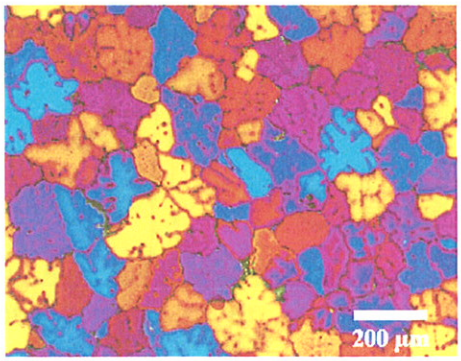

h) Alloy Y

Figure II-2 Microstructure in the as-cast material.

Table II-2. Grain size (D_G) and secondary dendrite arm spacing (DAS).

Alloy	D_G [µm]	DAS [µm]
A	70	25
B	69	25
C	75	23
D	95	25
E	96	26
F	82	24
X	110	37
Y	114	38

2.2 Microsegregations

The results of the microprobe analyses of alloys A - F as-cast, are shown in Figure II-3. The measured elements were Si, Mg, Fe, Mn and Cr. As shown, Mn and Cr in solid solution are roughly uniformly distributed within the grains interior, while Mg and Si show a marked tendency to segregation with a wavelength of approximately 25 µm, which is equal to the secondary dendrite arm spacing. The solid solubility of Fe in Al after solidification is less than 0.05%, which is at the limit of the resolution of the X-ray microanalyser. The variation in Fe concentration within the grains is thus uncertain.

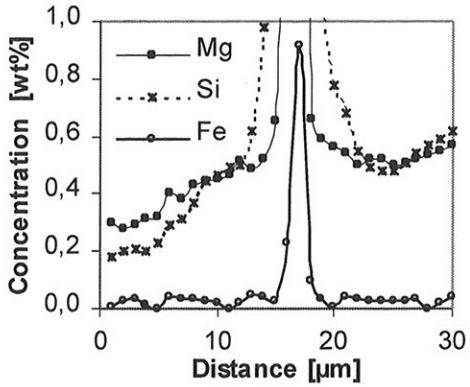

a) Alloy A

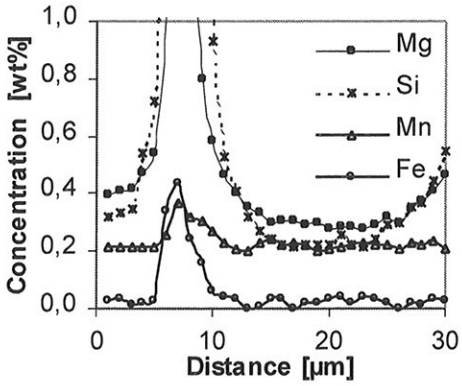

b) Alloy B

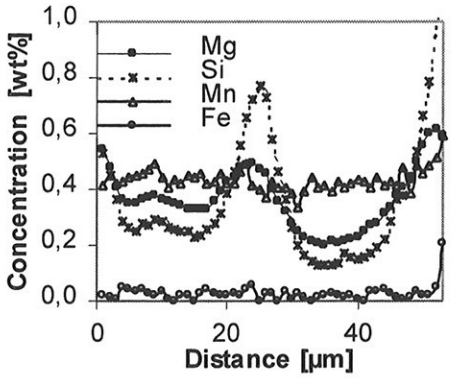

c) Alloy C

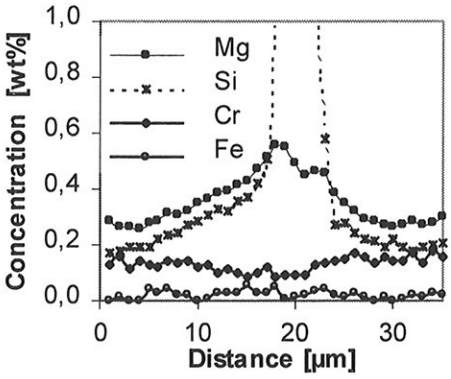

d) Alloy D

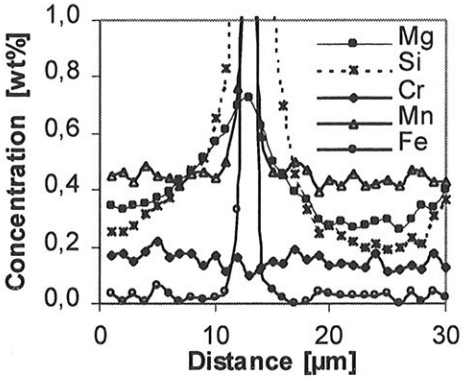

e) Alloy E

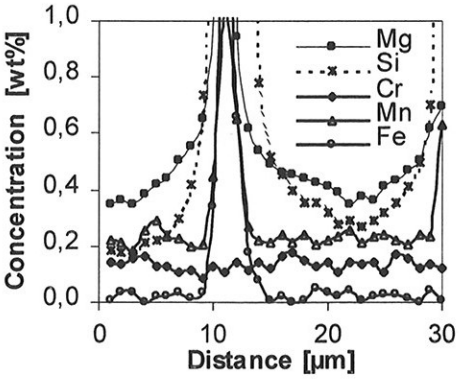

f) Alloy F

Figure II-3 Microsegregation in as cast material.

2.3 Primary particles

Three different primary particles were observed after casting, Mg2Si, β-AlFeSi and α-Al(XFe)Si. X means Mn, Cr or Mn and Cr depending on which elements the alloy contains. SEM micrographs of all the alloys are shown in Figure II-4.

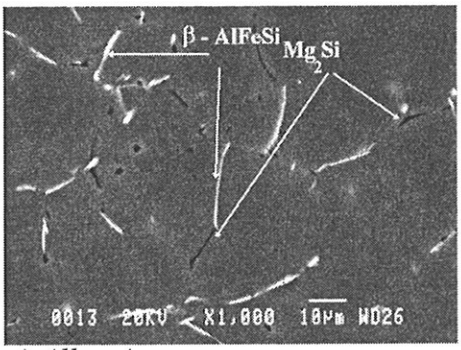

a) Alloy A

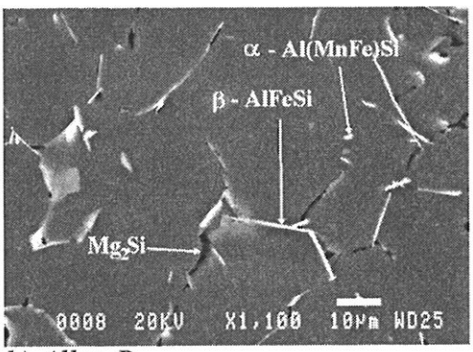

b) Alloy B

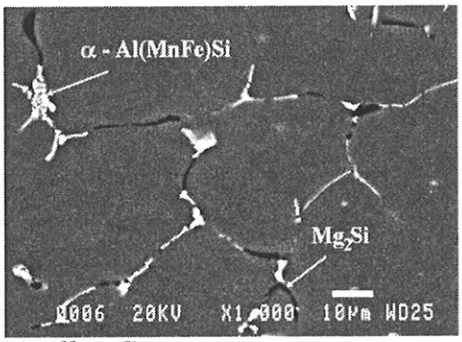

c) Alloy C

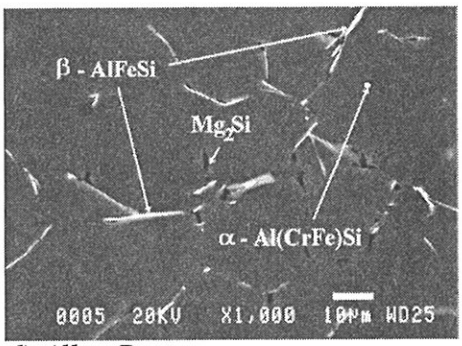

d) Alloy D

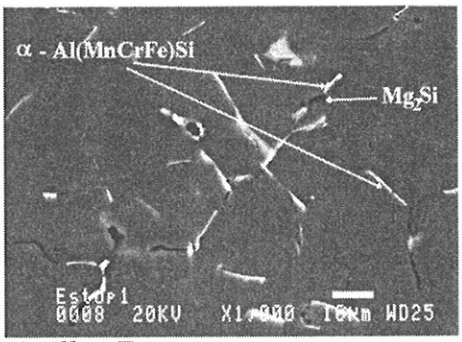

e) Alloy E

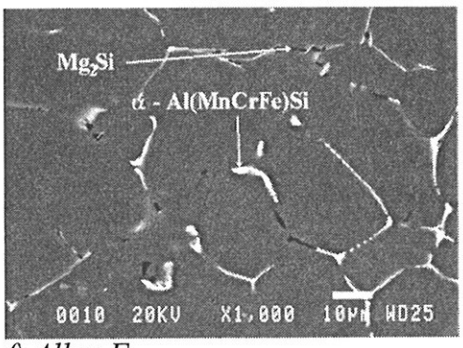

f) Alloy F

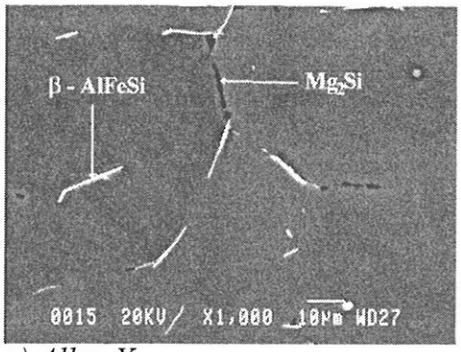

g) Alloy X

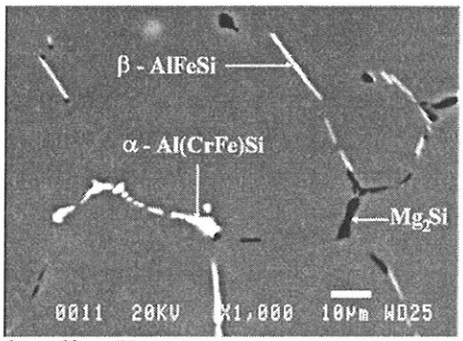

h) Alloy Y

Figure II-4 The primary particles

Only platelike β-AlFeSi particles and dark Mg_2Si particles on the cell boundary were observed in the alloys without Mn and Cr. When Mn and/or Cr were added, α-Al(XFe)Si particles could also be observed. With an increasing amount of Cr and/or Mn, the content of α-Al(XFe)Si particles increased while the content of β-AlFeSi particles decreased. In alloys C, E and F no β-AlFeSi particles were observed. Due to the larger grain size and DAS in alloys X and Y, the primary particles were larger and the number of particles was smaller than in the other alloys.

Part III

Precipitation of dispersoids

Part IIIa
Precipitation of dispersoids containing Mn and/or Cr in Al-Mg-Si alloys

Lars Lodgaard and Nils Ryum
Department of Materials Technology and Electrochemistry
Norwegian University of Science and Technology
N- 7491 Trondheim, Norway

1. Abstract

The formation of dispersoids containing Mn and/or Cr in Al-Mg-Si alloys was studied metallographically and by means of electrical resistivity measurements. Special emphasis was placed on the nucleation mechanisms. For alloys containing Mn and/or Cr it was shown that during the heating of the as-cast alloys to 580 °C (which is a typical homogenization temperature) and at a heating rate of 3 K/min, an intermediate phase, referred to as the "u-phase" nucleated on the β'-Mg_2Si needles. The phase has a hexagonal unit cell with a = 0.670 nm, c = 0.808 nm. The precipitates were rod-shaped and were lined up in the [100] directions in the Al lattice. The phase was found to be rich in Mn and/or Cr. With continued annealing, dispersoids containing Mn and Mn+Cr nucleated heterogeneously on the "u-phase" precipitates before these precipitates dissolved. The nucleation sites for the dispersoids with Cr were not conclusively identified.

2. Introduction

Al-Mg-Si alloys (6000-series) are widely used for medium strength structural applications and architectural sections. There is also an increasing demand for this type of alloys in the automotive industry. They are mostly produced as extrusions, although they are also available in sheets and plates. In addition, small amounts of Mn and/or Cr have for a long time been used in order to modify the microstructure and thus improve the properties of the alloys. During high temperature annealing (400 °C - 550 °C) different types of precipitates containing Mn and/or Cr are formed with various crystallographic structures and chemical compositions. These types of precipitates, which a have rather limited direct effect on the mechanical properties, are usually referred to as dispersoids. Due to their fairly high density and high thermal stability they can, however, have a strong effect on the recovery, recrystallization, grain growth processes and may even act as nucleation sites for the precipitation of the strengthening precipitates [1,2]. The

crystallographic nature of such dispersoids in aluminium alloys has been investigated for a long time. In alloys containing Mn and/or Cr, the dispersoids are referred to as the α-Al(Mn/CrFe)Si phase precipitates [3-13]. This phase has a cubic unit cell with a in the range 1.25 to 1.27 nm. There is on-going discussion whether the structure is simple cubic (SC) or body centred cubic (BCC). There are strong indications that the unit cell is SC when the Fe/Mn-ratio is low and becomes BCC when the Fe/Mn ratio becomes higher [6,7,11]. When only Cr is present an α-AlCrSi phase with an FCC unit cell with a = 10.9 nm is found in addition to the α-Al(CrFe)Si [14]. The manner in which such dispersoids are formed has been investigated for many years, but is still not completely understood. They have all rather complex structures with an incoherent interface to the Al-matrix and homogeneous nucleation thus seems to be excluded. Several sites for heterogeneous nucleation have been suggested. Using electron microscopy observation Hirasawa [15] provided some evidence that the strengthening particles β''- and β'-Mg_2Si needles that were formed during the heating period can act as nucleation sites for the dispersoids containing Mn during high temperature annealing. Even β-Mg_2Si plates have been suggested as nucleation sites. Westengen et al. [8] investigated the formation of dispersoids in 6000 series alloys containing both Mn and Cr by means of electrical resistivity measurement and transmission electron microscope (TEM). In the alloys containing Mn, a relatively large variation in the electrical resistivity was observed during the high temperature annealing. Much less variation was found during a similar heat treatment of the alloys containing Cr. TEM examination revealed dispersoids in both alloys after the heat treatment. One very important observation, made by several researchers [14,16], is the tendency for the dispersoids to have a higly nonuniform distribution in the alloy. This tendency is also found to be strongly dependent on the details in the annealing procedure. Observations indicate that a slow heating rate promotes a uniform distribution of dispersoids [14]. Colby et al. [17] reported that the presence of silicon in AlMn-alloys dramatically enhances the precipitation kinetics. Thus a nonuniform distribution of silicon after solidification may be responsible for the nonuniform distribution of the dispersoids [16].

The aim of the present investigation is to study the formation of dispersoids in AlMgSi alloys containing Mn and/or Cr with special emphasis on the nucleation mechanisms and the reason for the tendency towards nonuniform distribution of dispersoids.

3. Experimental

Six Al-Mg-Si alloys with varying amounts of Mn and Cr contents were directly chill cast as cylindrical billets (95 mm in diameter) in pilot plant

casting equipment at the Research & Development Laboratories, Hydro Aluminium A/S, Sunndalsøra. Traditional grain refinement with Al-Ti-B grain refiner was used. The chemical compositions of the alloys are shown in Table IIIa-1. In order to investigate the microsegregation in the as-cast alloys

Table IIIa-1 Chemical composition [wt.%] mean grain size D_G [μm], and dendrite arm spacing DAS [μm] of specimens

Alloy	Mg	Si	Fe	Cr	Mn	D_G	DAS
A	0.589	0.936	0.214	0.002	0.007	70	25
B	0.617	0.936	0.214	0.002	0.267	69	25
C	0.605	0.944	0.215	0.002	0.535	75	23
D	0.594	0.92	0.219	0.149	0.011	95	25
E	0.628	0.933	0.224	0.144	0.547	96	26
F	0.609	0.918	0.216	0.145	0.285	82	24

a JEOL JKA-8900R microanalyser was used. This was equipped with both wavelength- (WDS) and energy dispersive spectrometers (EDS). The metallographic preparation of the x-ray microanalysis was carried out in a standard way, and the microsegregation was determined by quantitative line analyses with a step size of 2 μm. The grain size and dendrite arm spacing (DAS) were measured in light microscope and determined by the line intercept method. Specimens with dimension 15 mm · 15 mm · 15 mm were heat treated in air in a furnace at constant heating rate of 3 K/min from room temperature to 580 °C. Samples were removed from the furnace at selected temperatures and quenched in water. Immediately after quenching the electrical resistivity was measured at 21 °C ± 1 °C. The measurements were carried out using a Förster Sigmatest D2.068. In order to establish the nucleation mechanisms of the dispersoids more accurately an additional heat treatment, as shown in Figure IIIa-1, was carried out. The specimens of the C-

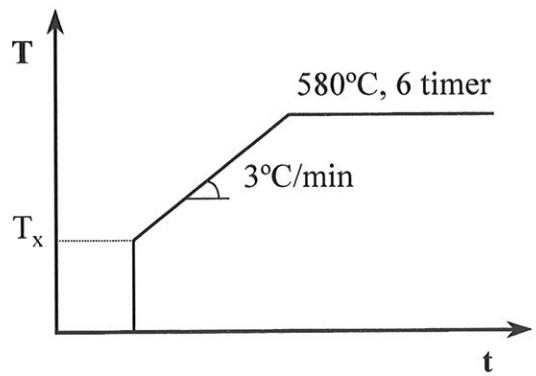

Figure IIIa-1 Outline of the additional heat treatment of alloys C and D.

and D- alloys of the same size as those used above were up-quenched in a salt bath furnace to temperature T_x and were then immediately transferred to an air furnace. The temperature was increased further at a rate of 3 °C/min to 580 °C. This heat treatment procedure was completed with an isothermal annealing for 6 hours at 580°C, and then quenching in water. The metallographic preparation was done in a standard way. In order to investigate the distribution of the dispersoids in the light microscope the samples were etched in 20 % sulphuric acid at 70 °C for 1-2 min. Thin foils for TEM were prepared in a Tenupol automatic jet electropolisher in a standard way. The electrolyte contained 2 parts methanol and 1 part nitric acid. Thinning was performed at 20 V at - 20 °C. The TEM investigation was performed in a JEOL 2010 transmission microscope and the chemical analysis was determined by EDS point analysis.

4. Results

The mean grain size (D_G) and the secondary dendrite arm spacing (DAS) are given in Table 1.There was a slight increase in the mean grain size following the addition of Mn and/or Cr. Also, while the grain size distribution was uniform in alloy A, the addition of the dispersoid forming elements induced a fraction of larger grains in between the smaller ones. The DAS was not affected by the additionof Mn and/or Cr. The results of the microsegregation in the as-cast condition of alloy C are shown in Figure IIIa-2. As can be seen, in solid solution the

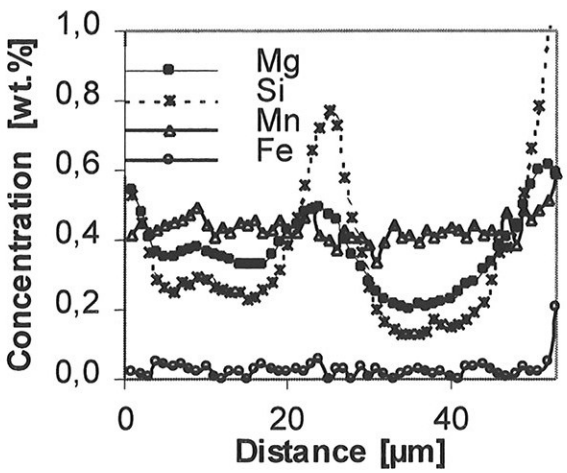

Figure IIIa-2 Microsegregation in the as-cast alloy C.

Mn is roughly uniformly distributed within the grains, while Mg and Si show a marked tendency towards segregation with a wavelength of approximately 25 μm, which is equal to the secondary dendrite arm spacing. The solid solubility of Fe in Al after solidification is less than 0.05 wt.%, which is at the resolution limit of the X-ray microanalysis. The variation of the Fe concentration within the grains is thus uncertain. Very similar results were obtained in the other alloys. In the alloy containing Cr, in solid solution the Cr is uniformly distributed within the grain.

Figure IIIa-3 shows the microstructure in alloy C after the heat treatment procedure shown in Figure IIIa-1. When T_x = 580 °C, a very inhomogeneous distribution of dispersoids is observed, with high density between the dendrite arms and nearly empty regions in the centre of the dendrite arms, Figure IIIa-3a. With decreasing value of T_x the density of the dispersoids is homogenized and when $T_x \leq 250$ °C a nearly uniform distribution is obtained, Figure IIIa-3b. Similar results were obtained in the other alloys containing Mn and/or Cr. The observations demonstrate that the nucleation of the dispersoids is strongly affected by the slow heating from $T_x \approx 250$ °C to the homogenization temperature, 580 °C.

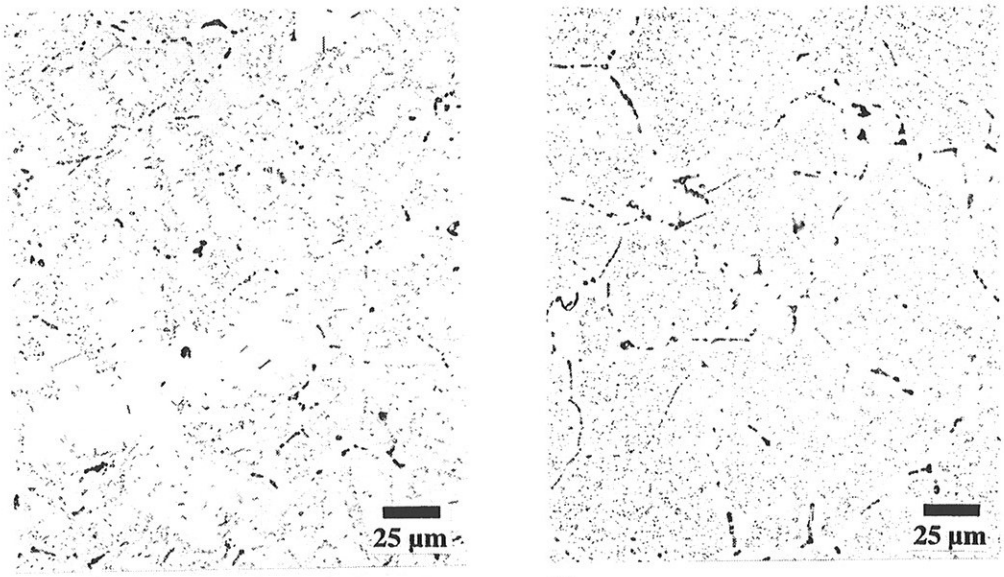

a) *b)*

Figure IIIa-3 a) Dispersoid distribution in alloy C when T_x = 580 °C. b) Dispersoid distribution in alloy C when T_x = 250 °C.

The reactions, which take place during heating from room temperature to 580 °C, were investigated in greater detail by electrical resistivity

complex variation in the electrical resistivity. The start of the precipitation is at approximately 490 °C and it is not completed until T ~ 580 °C. The electrical resistivity measurements thus demonstrate that the precipitation of particles containing Cr is much more sluggish than particles containing Mn and Mn+Cr.

The precipitates formed during continuous heating were investigated by a TEM. In alloy C (0.5 wt.% Mn) after continuous heating to 340 °C and 370 °C only β'-precipitates were observed. They are rod-shaped with a hexagonal unit cell with a = 0.705 nm; c = 0.405 nm [20]. These precipitates are semicoherent with the Al matrix with the c-axis parallel to direction [001] in the Al-lattice. After continuous heating to 400 °C, small (5-10 nm) apparently equiaxed dispersoids were observed. They were lined up in the [100] direction of the Al lattice as shown in Figure IIIa-5. Due to their small size at this stage their unit cell could not be determined. In addition to the dispersoids an additional type of precipitates was observed and will be referred to in the following as the "u-phase" precipitates. These "u-phase" precipitates are also seen in Figure IIIa-5. As can be seen, the "u-phase" precipitates are rod-shaped with their long dimension in the [100] directions in the Al lattice. After continuous heating to 430 °C the dispersoids had reached a size of 10-20 nm. The unit cell of the dispersoids could now be determined and was found to be either simple cubic (SC) or body centred cubic (BCC) with a = 1.26 nm. These dispersoids are thus identical to the α-Al(MnFe)Si phase [3-13]. After heating to 460 °C, all the dispersoids investigated had the SC unit cell.

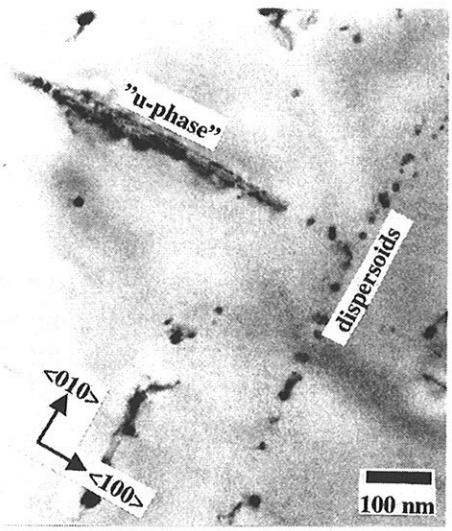

Figure IIIa-5 TEM bright-field micrograph of a "u-phase" particle and dispersoids after continuous heating to 400 °C (alloy C).

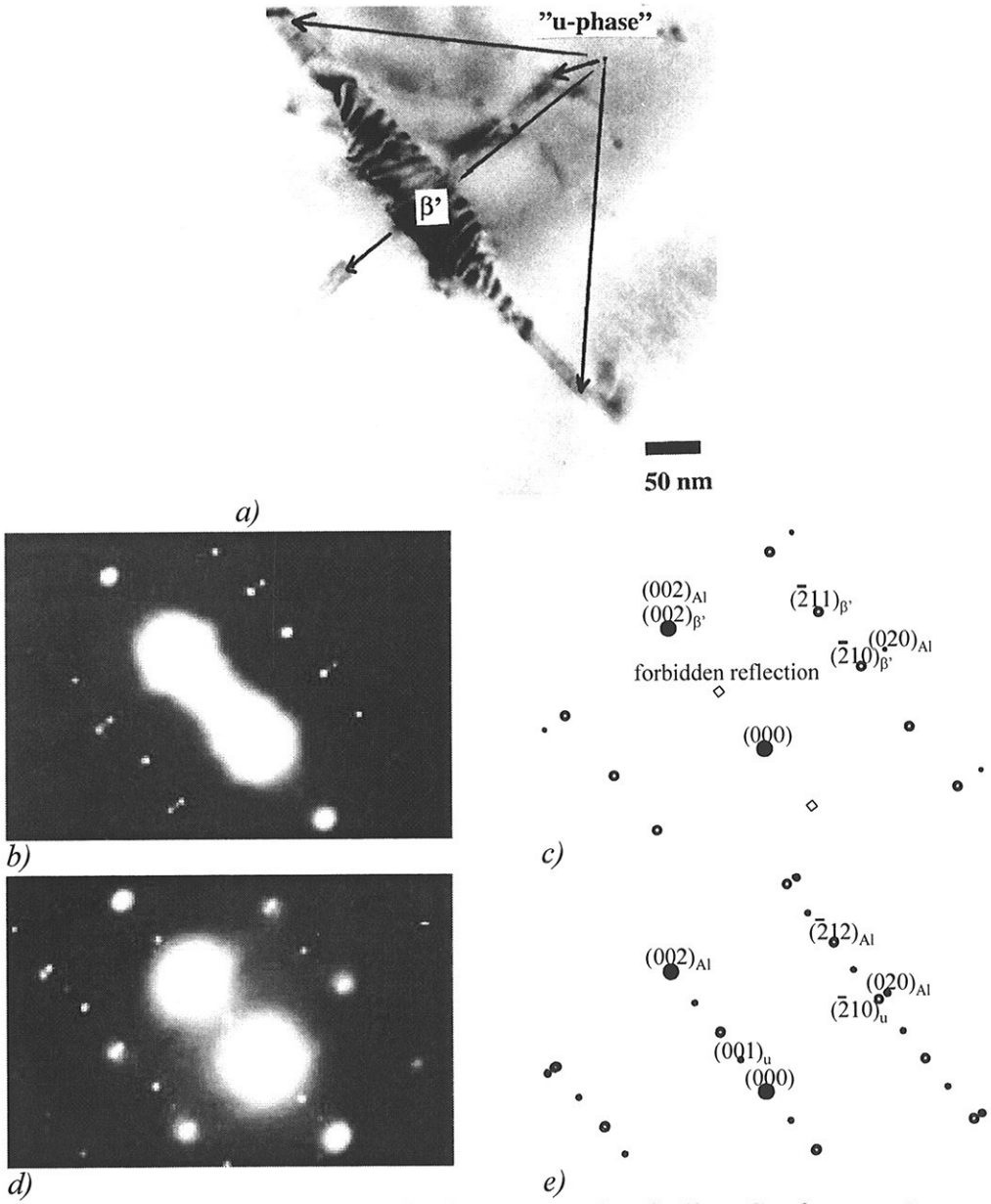

Figure IIIa-6 *a) TEM bright-field micrograph of alloy C after continuous heating to 350 °C and subsequent annealing at this temperature for two hours. The composite particle shown is composed of the β' and the "u-phase". b) Electron diffraction pattern from the β' precipitate taken along the [120]$_{\beta'}$ direction. c) Indexing of the diffraction pattern shown in (b). d) Electron diffraction pattern from the "u-phase" precipitate taken along the [120]$_{\text{"u-phase"}}$ direction. e) Indexing of the diffraction pattern shown in (d).*

In an effort to investigate if there was any relationship between the β' precipitates, the α - dispersoids and the "u-phase" precipitates, one specimen was continuously heated to 350 °C, then kept at this temperature for two hours before being quenched in water. After this heat treatment all the three types of particles described above were found to be present. In addition, a composite particle, made up of the β' precipitate and the "u-phase" precipitate was frequently observed. A micrograph showing a typical example of one such composite particle is shown in Figure IIIa-6a. The diffraction patterns from the area of β' and "u-phase" are shown in Figures IIIa-6b – IIIa-6e. The unit cell of the "u-phase" could now be determined. It was found to be hexagonal with a = 0.670 nm and c = 0.808 nm. The c-axis is thus very close to twice the length of the cube length of aluminium (a_{Al} = 4.04 nm). All the composite particles were aligned perfectly in the [100] directions in Al lattice. The orientation relationship between the "u-phase" precipitate and the Al lattice was found to be (Figure IIIa-7):

$$[001]_{\text{"u-phase"}} \parallel [100]_{Al}$$
$$[010]_{\text{"u-phase"}} \parallel [\bar{1}10]_{Al}$$

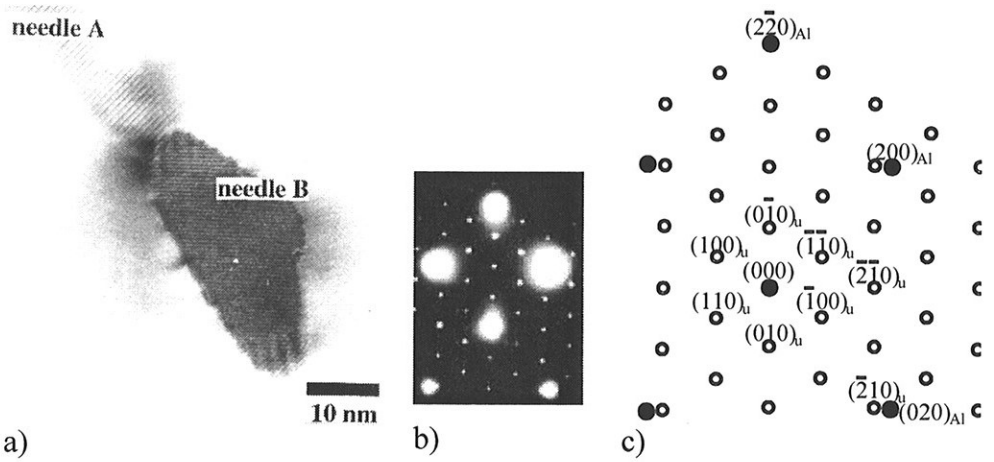

Figure IIIa-7 a) HRTEM micrograph of alloy C after continuous heating to 350 °C and subsequent annealing at this temperature for two hours. The particles are two "u-phase" needles, where needle A is oriented along the $[010]_{Al}$ direction while needle B is oriented along the $[001]_{Al}$ direction. b) Electron diffraction pattern from needle B taken along the $[001]_{Al}$- and $[001]_{\text{"u-phase"}}$ direction. c) Indexing of the diffraction pattern shown in (d).

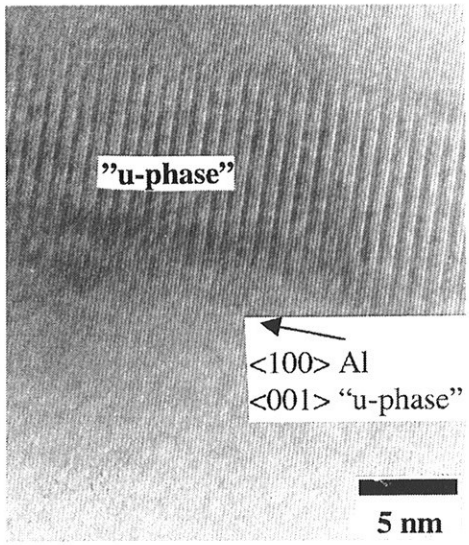

Figure IIIa-8 HRTEM micrograph of the "u-phase" precipitate in alloy C after continuous heating to 350 °C and subsequent annealing at this temperature for two hours.

The "u-phase" precipitates are thus semi-coherent with the Al lattice in one [100] Al direction as shown from the HRTEM image in Figure IIIa-8. The chemical analysis done by the EDS technique showed that the "u-phase" contained Mg, Si, Mn, Fe and also probably some Al, see Figure IIIa-9. This phase has been found previously by Reiso et al. [21] in an aluminium alloy with a slightly different chemical composition and after a completely different heat treatment

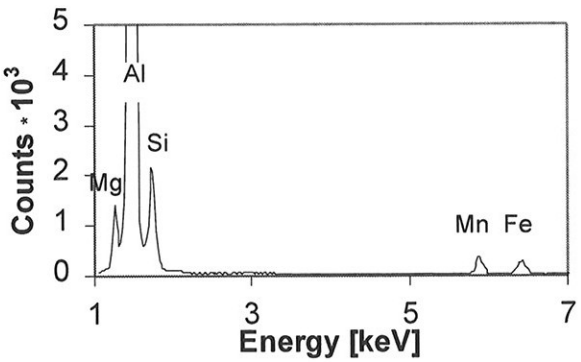

Figure IIIa-9 The chemical analysis of the "u-phase". The EDS spectrum from the "u-phase" precipitates showing the presence of Mg, Si, Mn and Fe.

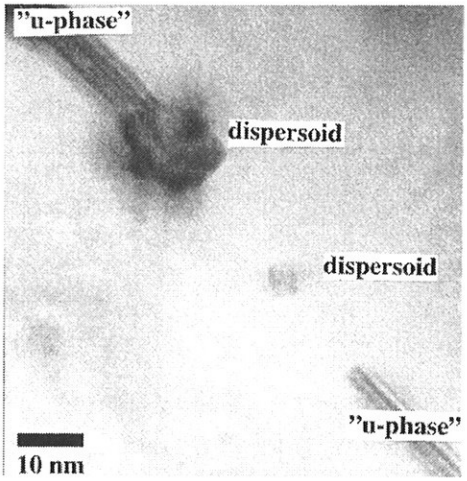

Figure IIIa-10 TEM bright-field micrograph of a dispersoids nucleated on the surface of the "u-phase" precipitate in alloy C after continuous heating to 350 °C and subsequent annealing at this temperature for two hours.

procedure. The particles found by Reiso et. al. were approximately equiaxed and of smaller size (10-30 nm).

Dispersoids nucleated on the surface of the "u-phase" were also observed, as shown in Figure IIIa-10. Due to the small size of the dispersoids at this stage their unit cell could not be determined. It is important to note that none of the dispersoids were observed on the surface or in the vicinity of the β' precipitates. This demonstrates that only the "u-phase" precipitates act as a nucleation site for the dispersoids.

The effect of a reduced Mn concentration on the mode of precipitation during continuous heating was investigated in alloy B. As pointed out above the reduction in electrical resistivity started at about 400 °C, which is roughly the same temperature as the one found in alloy C. The maximum reduction in electrical resistivity was reached at about 520 °C - 550 °C, which is slightly lower than the corresponding temperature found for alloy C The reduction was 3 to 4 times smaller. The metallographic investigation of this alloy gave results which were very similar to those found in alloy C. After continuous heating to 460 °C the dispersoids were of the α-Al(MnFe)Si type mostly with an SC unit cell.

A combination of Cr and Mn is often industrially used in such alloys. In alloys E and F, 0.15 wt.% Cr was added to the alloys containing 0.25 wt.% and 0.5 wt.% Mn. The electrical resistivity showed a variation after annealing that was rather similar to the variation observed in the alloy without Cr. This indicates that Cr precipitates in the same temperature range as Mn. This was also confirmed by metallographic investigation. After continuous heating to 460 °C, dispersoids of the same type and similar arrangement as in alloy C were observed as shown in Figure IIIa-11. The unit cell was always SC, see Figure IIIa-12. Also the investigation of the chemical composition of the dispersoids revealed that they contained considerably more Mn than Cr, see Figure IIIa-13. No dispersoids were found that only contained only Cr. This demonstrates that Cr precipitates together with Mn as α-Al(MnCrFe)Si dispersoids.

The precipitation of Cr in the alloys without Mn was subsequently investigated in alloy D, which contained 0.15 wt.% Cr. The variation in electrical resistivity during annealing indicated that the precipitation of dispersoids containing Cr is much more sluggish than when Mn is not present in the alloy. The metallographic investigation showed that the dispersoids containing Cr which appeared after continuous heating to 520 °C were of the α-Al(CrFe)Si type. The unit cell was either SC or BCC with a = 1.26 nm. We found no tendency towards the alignment of these dispersoids in specific crystallographic directions. In addition no α-AlCrSi phase dispersoids were found

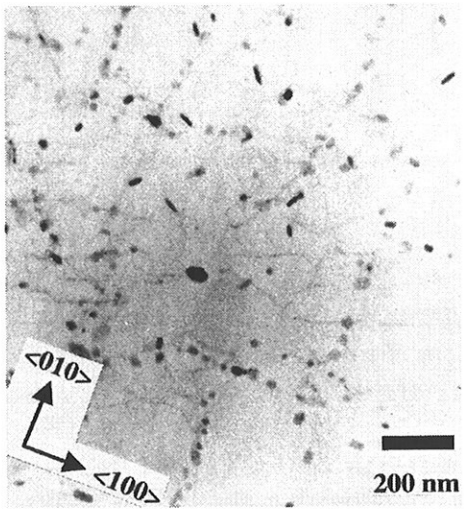

Figure IIIa-11 TEM bright-field micrograph of dispersoids aligned parallel to the $[100]_{Al}$- and $[010]_{Al}$ direction after continuous heating to 460 °C in alloy C.

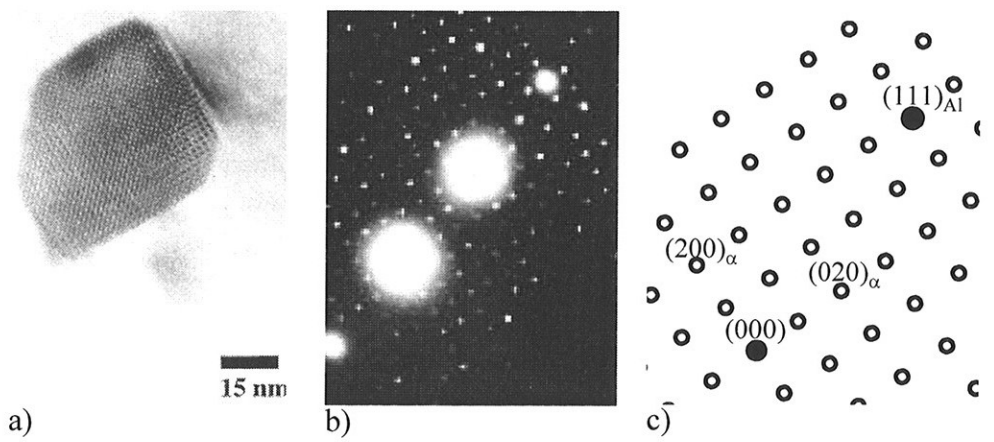

Figure IIIa-12 a) HRTEM micrograph of an α-Al(MnCrFe)Si dispersoid in alloy E after continuous heating to 460 °C. b) Electron diffraction pattern from the α-Al(MnCrFe)Si dispersoid taken along $[001]_{Al(MnCrFe)Si}$ direction . c) Indexing of the diffraction pattern shown in (b).

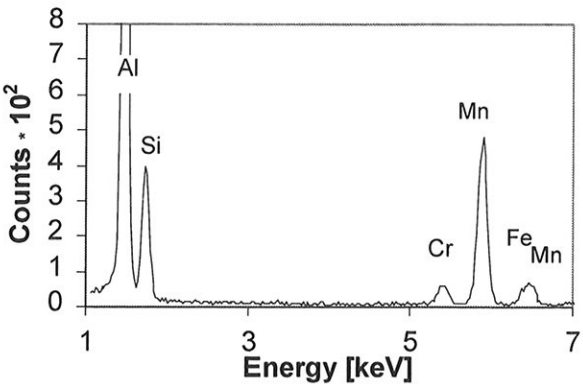

Figure IIIa-13 The chemical analysis of the α-Al(MnCrFe)Si dispersoid shown in Figure IIIa-12a. The EDS spectrum shows the presence of Si, Cr, Mn and Fe.

5. Discussion and conclusion

In many precipitation strengthening aluminium alloys, the nucleation of the precipitates (mostly semi - coherent), has been shown to be heterogeneous, even though the precipitate density is quite high (10^{12} - 10^{16}/cm^3), and the precipitate distribution apparently uniform [22-31]. Determining of the nature of the nucleation sites has turned out to be particularly difficult and in spite of

extensive experimental effort, only indirect information is available. In most cases the sites are formed during the quenching or up-quenching operations.

In the present investigation, the dispersoids formed during high temperature annealing have an incoherent interface to the aluminium matrix and the homogeneous nucleation rates are practically nil, according to the classical theory of nucleation. However, even in this case the dispersoid density is fairly high (typical $10^{14}/cm^3$) and, after suitable heat treatment, nearly uniform. The sites cannot be formed during quenching because the quenching rate (during solidification) is too low (dT/dt ~ 1 K/sek). However, the present investigation has clearly demonstrated that a rather intricate type of consecutive nucleation takes place.

During continuous heating, the β' precipitates first nucleate homogeneously with subsequent growth, then there is coarsening and partial dissolution with increasing temperature. These reactions take place within the temperature range of ~100 °C - 350 °C. The driving force for the formation of β' precipitates is the supersaturation of Mg and Si. When reaching ~ 350°C, the "u-phase" precipitates are formed heterogeneously on the dissolving β' precipitates as shown in Figure IIIa-6a.

The chemical analysis showed that the "u-phase" contained dispersoids-forming elements (Figure IIIa-9). The driving force for the formation of this phase is most likely the supersaturation of Mn. The "u-phase" is thus an intermediate phase with respect to the α-Al(MnFe)Si equilibrium phase, which cannot be formed homogeneously due to its incoherent interface with the Al-matrix. This nucleation event is fairly easy, due to the structural similarity between the β' and the "u-phase" and between the "u-phase" and the aluminium matrix (Figure IIIa-8). During a further increase in the temperature, the β' precipitates dissolve completely. The α-Al(MnFe)Si dispersoids are heterogeneously nucleated on the "u-phase" precipitates and finally consume the "u-phase" completely. Several dispersoids are nucleated on every single "u-phase" precipitate. Thus the final result is a breaking up of the original β' precipitate into a chain of α-Al(MnFe)Si dispersoids, as shown in Figures IIIa-5 and IIIa-11. This precipitation sequence is schematically presented in Figure IIIa-14. This model describes quite well the reaction in alloys B and C which both contain Mn. When Cr is also present in the alloys, the Cr atoms are included in the "u-phase" and in the dispersoids, which can now be written as α-Al(MnCrFe)Si dispersoids. Thus with this modification the model, shown in Figure IIIa-14, is also valid for alloys E and F. When only Cr is present as dispersoid-forming elements, which is the case for alloy D, the nucleation of the dispersoids is found to be much more sluggish, as can be seen from Figure IIIa-4. The decrease in electrical resistivity starts at a temperature that is nearly 100 °C higher than for the alloys containing Mn.

The "u-phase" precipitates have not been found and the nucleation sites for the dispersoids have not been identified so far.

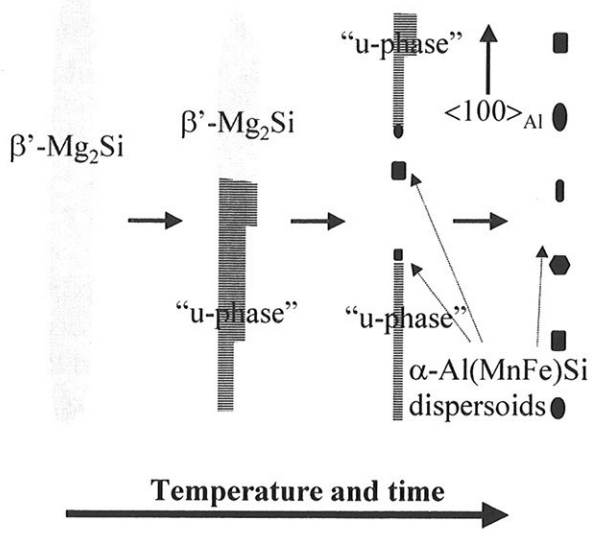

Figure IIIa-14 A model of the precipitation of the dispersoids.

On the basis of this model a qualitative explanation of the observed heterogeneous distribution of the α-dispersoids can also be given, as shown in Figures IIIa-3a and IIIa-3b. In the as-cast condition, the β'-forming elements, Mg and Si, have segregated towards the dendrite boundaries, as seen in Figure IIIa-2. The nucleation of the β' precipitates, which are the prerequisite for the "u-phase" precipitates will thus occur more easily within these regions where the supersaturation is high and much more slowly or not at all in the dendrite centres. Also, the α-dispersoids contain Si-atoms thus a critical Si-concentration is probably necessary for the α-dispersoids to nucleate. A tendency towards a heterogeneous distribution of the dispersoids will thus always be present.

As shown in Fig. IIIa-3a and IIIa-3b, the dispersoid distribution is strongly affected by the heating procedure. In order to obtain a uniform dispersoid distribution it is necessary to heat with a low heating rate from a fairly low temperature (T_x < 250 °C) to the annealing temperature. During such slow heating (dT/dt ~ 3 K/min) a large number of β'-precipitates are formed which is a prerequisite for a high density of nucleation sites for the α-dispersoids. If the heating is more rapid (dT/dt ~ 500 K/sek), for instance upon up-quenching in a salt bath, the density of the dispersoids decreases and they become less uniform.

6. Acknowledgements
The authors would like to thank Hydro Aluminium AS. Sunndalsøra for financial support and the provision of the necessary materials and chemical analyses. Special thanks are given to Dr O. Reiso and Dr U. Tundal, Hydro Aluminium R&D Centre Sunndalsøra and Dr S. Andersen, SINTEF Applied Physics for helpful discussions.

7. References

[1] H. D. Merchant, J. Crane, E. H. Chia, Homogenization and Annealing of Aluminium and Copper Alloys, 1988, pp. 183.

[2] O. Lohne, A.L.Dons, Scand. J. Met. 12 (1983) 34.

[3] G. Phragmen, J. Inst. Metals. 77 (1950) 489.

[4] D. Munson, J. Inst. Metals. 95 (1967) 217.

[5] A.L.Dons, Z. Metallkde. 75 (1984) 170.

[6] A.L.Dons, Scand. J. Met. 13 (1984) 137.

[7] A.L.Dons, Z. Metallkde. 76(1985) 151.

[8] H. Westengen, O. Reiso, L. Auran, Aluminium, 56 (1980) 768.

[9] H. Westengen, Z. Metallkde. 73 (1982) 360.

[10] M. Copper, Acta Cryst. 23 (1967) 1106.

[11] P. Donnadieu, G. Lapasset, B. Thanaboonsombut, T. H. Sanders, Proceedings of the 4th Int. Conf. on Aluminium Alloys, Atlanta, USA, Sept. 11-16, 1994, Georgia Institute of Technology, School of Materials Science and Engineering, Atlanta, p. 668.

[12] E. Nes, S. E. Naess, R. Hoier, Z. Metallkde. 63 (1972) 248.

[13] L. Ping, Development of microstructure in cast and rapidly solidified Aluminium alloys, doctoral thesis, Department of Physics, Chalmers University of Technology, Sweden, 1987.

[14] O. Reiso, Hydro Aluminium A/S, Sunndalsøra, private communication, 1980.

[15] H. Hirasawa, Scripta Met. 9 (1975) 955.

[16] Conte and T. H. Sanders, Proceedings of the 5th Int. Conf. on Aluminium Alloys, Grenoble, France, 1996, Transtec Publication Ltd, Switzerland, p. 119.

[17] P.Colby, C. Sigli and C. J. Simensen, Proceedings of The 4th Int. Conf. on Aluminium Alloys, Atlanta, USA, Sep 11-16, 1994, Georgia

Institute of Technology School of Materials Science and Engineering, Atlanta, p. 508.

[18] John E. Hatch: Aluminum: Properties and Physical Metallurgy, 3nd ed., AMS., USA, 1988, p. 205.

[19] H. J. Wollenberger,in: R.W. Cahn and P. Haasen (Eds), Physical Metallurgy, 3nd ed., North-Holland Physics Publishing, The Netherlands, 1983, p. 1140.

[20] M. H. Jacobs, Phil.Mag. 26 (1972) 1.

[21] O.Reiso, U Tundal, S. Andersen, Proceedings of 6th International Aluminum Extrusion Technology Seminar. Vol. I, Chicago, USA, May 14-17, Aluminum Extruders Council, USA, 1996, p. 141.

[22] H.S.Rosenbaun, D.Turnbull, Acta Met. 6 (1958) 653.

[23] E.Ozawa, H.Kimura, Acta Met. 18 (1970) 995.

[24] E.Ozawa, H.Kimura, Mat. Sci. Eng. 8 (1971) 327.

[25] M.Beller, Z. Metallkde. 63 (1972) 663.

[26] M.Beller, Z. Metallkde. 64 (1973) 189.

[27] M.Beller, Z. Metallkde. 64 (1973) 387.

[28] N.Ryum, Z. Metallkde. 63 (1972) 338.

[29] N.Ryum, Z. Metallkde. 66 (1975) 344.

[30] N.Ryum, Z. Metallkde. 66 (1975) 377.

[31] H.Westengen, N.Ryum, Z. Metallkde. 70 (1979) 528.

Part IIIb

Precipitation of disperoids containing Cr in Al-Mg-Si alloys

Is not included due to copyright

Part IV
Distrubution of disperoids

Is not included due to copyright

Part V

Microstructural changes during homogenisation

1. Experimental

1.1. Isothermal heat treatment

Two Al-Mg-Si alloys, one containing 0.5 wt.% Mn (alloy C), the other containing 0.15 wt.% Cr (alloy D) were included in this investigation. In addition, an alloy without Mn and Cr was used as a reference alloy (Table II-1 –see page 27). The size of the samples and their positions in the billet are described in Part II, chapter 1.2.1. Isothermal heat treatments were carried out in a salt bath furnace at various temperatures. In order to reach the annealing temperature rapidly, the samples were heavily stirred in the salt bath for 30 seconds. The samples were annealed at different temperatures for different times and subsequently quenched in water. Immediately after quenching the electrical resistivity was measured at 21 °C ± 1 °C. The measurements were carried out using a Förster Sigmatest D2.068. The annealing temperatures were 350 °C, 400 °C, 460 °C, 520 °C and 580 °C and the annealing times varied between 30 seconds and 28 days. Samples annealed for 20 hours were also investigated in the light microscope. The samples were mechanically ground on grinding papers with a fineness from 80 to 2400 grit, followed by polishing in two steps 3 μm and 1 μm. The polishing was completed with a chemical polishing suspension (Struers OP-S) with a weak etching effect that minimized the roughness of the specimens. In order to increase the contrast in the light microscope the specimens were etched in 20% sulphuric acid at 70 °C for 2 minutes.

1.2. Continuous heat treatment

Samples from alloys A – F were heated in an air circulation furnace at a heating rate of 3 K/min from room temperature to 520 °C, 550 °C or 580 °C, followed by annealing at these temperatures for different length of times. All specimens were quenched in water. The annealing times are shown in Table V-1.

1.2.1. The amount of alloying elements in solid solution

In order to investigate the precipitation of alloying elements from solid solution the electrical resistivity was measured. Immediately after quenching

Table V-1. Investigation of samples after annealing.

time Temp → ↓ Alloy →	520 °C					
	A	B	C	D	E	F
0 min	e	e	edEs	ed	edE	e
10 min	e	e	ed	ed	ed	e
30 min	e	e	edlS	edl	ed	e
60 min	e	e	ed	ed	ed	e
180 min	e	e	eds	ed	ed	e
360 min	e	e	edlS	edl	ed	e
600 min	e	e	ed	ed	ed	e
1200 min	e	e	ed	ed	ed	e
3000 min	e	e	edlSsE	edl	edE	e
time Temp → ↓ Alloy →	550 °C					
	A	B	C	D	E	F
0 min	e	e	ed	ed	ed	e
10 min	e	e	ed	ed	ed	e
30 min	e	e	ed	ed	ed	e
60 min	e	e	ed	ed	ed	e
180 min	e	e	ed	ed	ed	e
360 min	e	e	ed	ed	ed	e
600 min	e	e	ed	ed	ed	e
1200 min	e	e	ed	ed	ed	e
3000 min	e	e	ed	ed	ed	e
time Temp → ↓ Alloy →	580 °C					
	A	B	C	D	E	F
0 min	e	e	edEs	ed	edE	e
10 min	e	e	edc	ed	ed	e
30 min	e	e	edlS	edl	ed	e
60 min	e	e	edc	ed	ed	e
180 min	e	e	edcs	ed	ed	e
360 min	e	e	edlS	edl	ed	e
600 min	e	e	edc	ed	ed	e
1200 min	e	e	ed	ed	ed	e
3000 min	e	e	edlSsEc	edl	edE	e

e = electrical resistivity, d = dispersoid density, l = light microscope,
S = SEM, s = dispersoid size, E = EDS analysis, c = chemical analysis

the measurements were carried out at 21 °C ± 1 °C. It is well-known from the literature that the resistivity increases with increasing concentration of alloying elements in solid solution.

The concentration of alloying elements in solid solution was also analysed by an alternative method developed by Simensen et al. [1984] at SINTEF and is referred to as the Butanol method. The specimens are dissolved in distilled 1-butanol and the intermetallic particles are removed from the solution by filtration. The amount of the elements Mg, Mn, Fe and Si in the solution was then analysed by ICP-AES (inductively coupled plasma-atomic emission spectroscopy) or by AAS (atomic absorption spectroscopy). The Butanol method is a rather costly method and only a limited number of specimens were analysed. These specimens were taken from alloy C and were annealed at 580 °C for different length of times.

1.2.2. Light microscope and SEM

The main purpose of this investigation was to observe the change in morphology and size of the primary particles and the dispersoids during annealing. Samples from alloy C and D which were annealed for 30 min., 360 min. and 3000 min. at selected temperatures were subjected to light microscope investigation. The samples from alloy C were also investigated in SEM. The samples were ground, polished and etched as described in Part II (chapter 1.2.1), The etching procedure was omitted for the samples studied in SEM. The light microscope and SEM investigation were carried out in a Reichert MeF3A and on a JEOL JSM-840, respectively.

1.2.3. Dispersoid size

The morphology of the dispersoids varied considerably. Some dispersoids were globular, some rod shaped and other plate shaped. Due to this difference in morphology it was not possible to give a precise size distribution of the dispersoids. Nevertheless, based on some assumptions (see below), the size distribution in alloy C after annealing at 520 °C and 580 °C for different times was determined. TEM investigation was necessary in order to observe the dispersoids and several TEM micrographs were made from each heat treatment. Thin foils for TEM were prepared in a Tenupol automatic jet electropolisher in a standard way. The electrolyte contained 2 parts methanol and 1 part nitric acid. Thinning was performed at 20 V at - 20 °C. The TEM investigation was performed in a JEOL 2010. The size of the dispersoids were measured interactively using the image analysis computer program Kontron KS 300 on enlarged TEM images. The contours of the dispersoids were drawn by means of a cursor and the program determined the maximum

diameter d_{max} and minimum diameter d_{min}. The size of the dispersoids were expressed by the radius r given by the formula:

$$r = \frac{d_{max} + d_{\min}}{4} \qquad \text{(V-1)}$$

1.2.4. Dispersoid density

The change in dispersoid density in alloys C, D and E during annealing was determined. The density measurements were carried out in TEM. Thin foils were prepared in a standard way as described above. The TEM investigation was performed in a JEOL 2010 or Phillips CM 30 with an accelerating voltage of 150 kV. When using TEM for measuring the dispersoid density, it is necessary to know the foil thickness. Several methods for measuring the foil thickness exist [Bardal 1999], but almost all of them are time-consuming and not suitable when a large number of measurements are necessary. A fast method was developed based on the electron energy loss spectroscopy (EELS).

EELS [Bardal 1999, Egerton 1986]
The EELS method for measuring foil thickness is based on the simple relationship between the intensity distribution in the EELS spectrum and the ratio between the foil thickness and the mean free path for inelastic scattering of electrons. This method is much faster than the alternatives. The real benefit is gained when many thickness measurements are needed. An estimate of the thickness can be established from the low-energy region of the energy loss spectrum. The simple procedure involves the measurements of the area of the low-loss peaks. The zero loss intensity I_0 (represented by the area under the zero-loss peak) is given by:

$$I_0 = I_t \exp(-\frac{l}{\lambda}) \qquad \text{(V-2)}$$

I_t is the total intensity reaching the spectrometer (represented by the area under the whole spectrum) measured up to some suitable energy loss Δ (see Figure V-1). l is the foil thickness and λ is a mean free path for the energy losses less than Δ. From equation (V-2), it is found that the foil thickness is given by

$$l = \lambda \ln(\frac{I_0}{I_t}) \qquad \text{(V-3)}$$

This is a simple way to measure the relative foil thickness (l/λ) or the absolute thickness if λ is known.

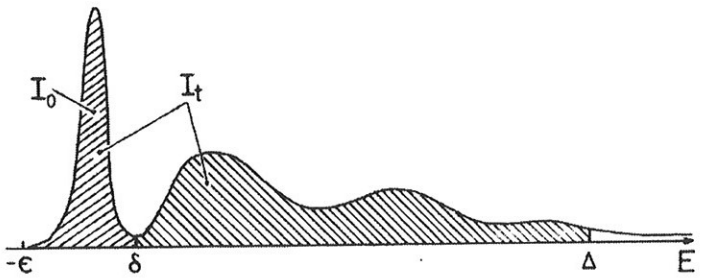

Figure V-1 The integrals and energies involved in measuring the low energy regions of loss spectrum. [Egerton 1986]

By means of convergent beam electron diffraction (CBED) the foil thickness can be determined with good accuracy. By combining EELS and CBED measurements λ can be determined. Bardal and Lie. [Bardal 1999] carried out both EELS and CBED measurements in combinations in order to determine λ in four different aluminium alloys. In the case when no calibration of λ has been made, they concluded that a value of λ = 120 nm ± 10 nm can be used for most 1xxx, 2xxx, 3xxx, 5xxx, 6xxx and 7xxx series alloy (at 150 KV), irrespective of alloy temper.

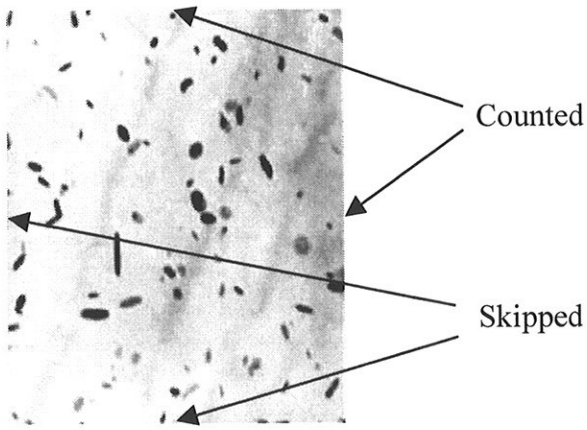

Figure V-2 Dispersoids observed partly on the edges of the photo were counted on two sides and skipped on the two other sides.

The measurements

10 TEM micrographs from each heat treatment (two samples) were recorded at a distance approximately 5 μm from the interdendritic regions and the dispersoids were counted. The number of dispersoids in each heat treatment varied between 300 and 1000. Only dispersoids lying on two of the edges of the micrograph were counted. Dispersoids lying on the other two edges were not couted, see Figure V-2. There is a possibility that the dispersoids in the thin foil surface fell out during preparation (V-3). If all dispersoids that touches the surface fall out, the thickness of the foil should be reduced by a distance that is equal to the mean diameter of the dispersoids. On the other

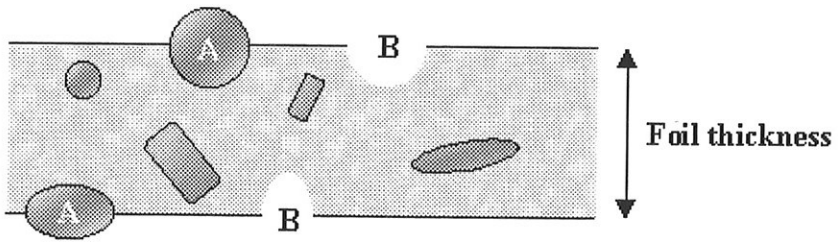

Figure V-3 Outline of the thin foils.

hand, if all the dispersoids that touches the surface are retained, the thickness of the foil should be increased by a distance equal to the mean diameter of the dispersoids. Finally, if only half of these dispersoids fall out, the thickness of the foil, measured by the method describe above, should be used.

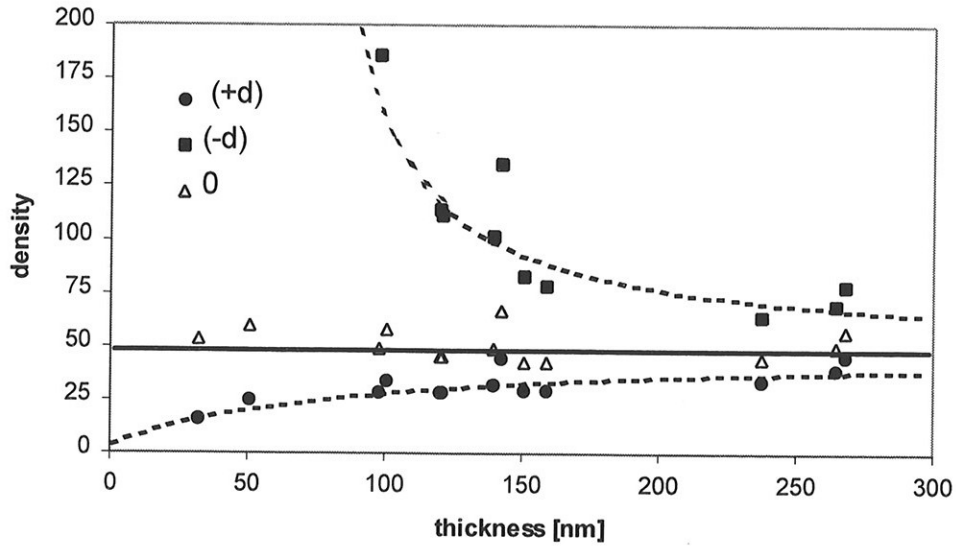

Figure V-4 The dispersoids density as a function of the foil thickness.

The effect of varying the foil thickness with the mean diameter of the dispersoids on the dispersoids density was investigated in a thin foil from alloy C heated (3 K/min) to 580 °C and quenched. Several dispersoid density measurements were recorded from areas with different foil thicknesses. The results are shown in Figure V-4. The dispersoid density is unchanged when no correction of the foil thickness is made, while an increase or a decrease in dispersoid density with increasing foil thickness is observed when a correction is made. Thus, no correction of the foil thickness was made when the dispersoids density was determined.

Because the dispersoids are incoherent with the matrix and because there is no preferred orientation between the matrix and the dispersoids, the dispersoids have varying contrast. If a small particle with a low contrast is located below a big particle with a high contrast the small particle will be invisible. On the other hand, if the small particle has a high contrast and the big particle has a low contrast both particles are visible (Figure V-5). Since the foil thickness is relatively small and the volume fraction of dispersoids is low, this error is negligible.

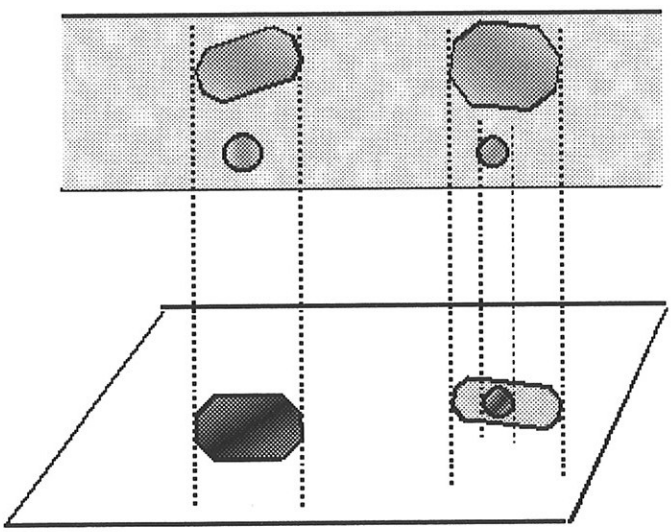

Figure V-5 Two particles observed as one or two depend on the contrast of each of them.

1.2.5. Variation in composition of the α-Al(MnCrFe)Si and α-Al(MnFe)Si particles during anneling

This investigation has two main purposes: To confirm previous results by [Dons 1984[2]] who showed that the Mn/Fe ratio in the dispersoids and the α-

primary particles change during annealing, and to investigate whether the difference in the rate of diffusion of Cr and Mn in Al affect the composition of α-Al(MnCrFe)Si dispersoids.

In alloys C and E the primary particles and the dispersoids were of the α-Al(MnFe)Si and α-Al(MnCrFe)Si type respectively. Samples from these alloys in the as-cast condition and after annealing for 0 min. and 3000 min. at 520 °C and 580 °C were investigated in TEM. The chemical analysis of the dispersoids and the primary particles were determined quantitatively by the EDS point analysis technique. Thin foils for TEM were prepared in the way described above. The analysed dispersoids were located minimum 5 μm from the primary particles. In alloy C dispersoids in the vicinity of the primary particles were also analysed.

2. Results and discussion

2.1. Isothermal heat treatment

2.1.1. Electrical resistivity

The reactions taking place during heat treatment were investigated in great detail by electrical resistivity measurements. The resistivity after annealing at a temperature T and time t is to the first approximation given by the following expression:

$$\rho(T,t) = \rho_{Al} + \sum K_i C_i \qquad \text{(V-3)}$$

Here ρ_{Al} is the electrical resistivity of pure aluminium, C_i is the concentration of elements in solid solution at T, and K_i is a proportional constant. During heating of alloy A, the variation in $\rho_{Al}\ (T,t)$ is thus due to the precipitation and/or dissolution of precipitates containing Mg and Si. The expression

$$\Delta\rho(T,t) = \rho_A(T,t) - \rho_A(RT) \qquad \text{(V-4)}$$

is a measure of the concentration of Mg and Si in solid solution after continuous annealing to a temperature T compared to the same concentrations in the as-cast condition. In the alloys containing Mn and/or Cr, dispersoids containing these elements will also form during heating. The difference

$$\Delta\rho_{C-A} = \Delta\rho_C - \Delta\rho_A \qquad \text{(V-5)}$$

is thus a measure of the concentration of Mn in solid solution in alloy C after continuous heating to temperature T, compared with the concentration of Mn in this alloy in the as-cast condition. This approach assumes that the precipitation of the precipitates containing Mg and Si and the dispersoids containing Mn and/or Cr occurs independently.

Figure V-6 shows the variation in electrical resistivity in alloy A and alloy C during annealing at 460 °C. The curve C-A describes the precipitation of Mn. Figure V-7 and V-8 show the variations in electrical resistivity with

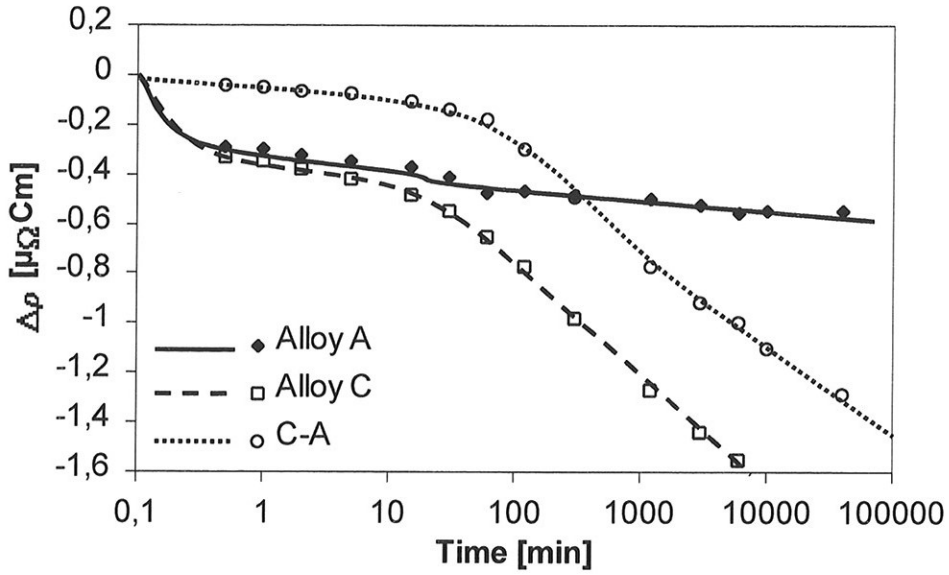

Figure V-6 Variation in electrical resistivity in alloy A and C during isothermal annealing at 460 °C.

annealing time at different temperatures in alloy C and D respectively. The decrease in resistivity in alloy C is due to the precipitation of Mn and the decrease in alloy D is due to the precipitation of Cr. The precipitation rate of both Mn and Cr increases with increasing annealing temperature. Since the rate of diffusion of Mn in Al is higher than Cr in Al at the same temperature the precipitation is faster in alloy C than in alloy D. Even after an annealing of 9000 min. at 350 °C no variation in electrical resistivity was observed in alloy D. On the other hand, the resistivity has decreased considerably in alloy C after the same heat treatment. After sufficient annealing time the alloys will establish equilibrium. The electrical resistivity will decrease with increasing annealing time and gradually level out. However, even after annealing at 580 °C for a rather long time equilibrium was not established in any of the alloys. But after annealing at 580 °C for approximately 1000 min. the electrical resistivity in alloy D decreased insignificantly with additional annealing and probably approached the equilibrium. On the other hand, the electrical resistivity in alloy C still decreased substantially. This means that the equilibrium was established earlier in alloy D than in alloy C. This observation was unexpected, since the diffusion rate of Mn in Al is higher than the diffusion rate of Cr in Al.

In alloy C the primary particles and the dispersoids are both of the α-Al(MnFe)Si type. The primary particles were found to contain more Fe than Mn while the dispersoids contained more Mn than Fe. After extensive

annealing the composition of the two sets of particles approached each other [Dons 1984[2]]. Due to this exchange of Fe and Mn, extensive annealing is probably needed to establish equilibrium.

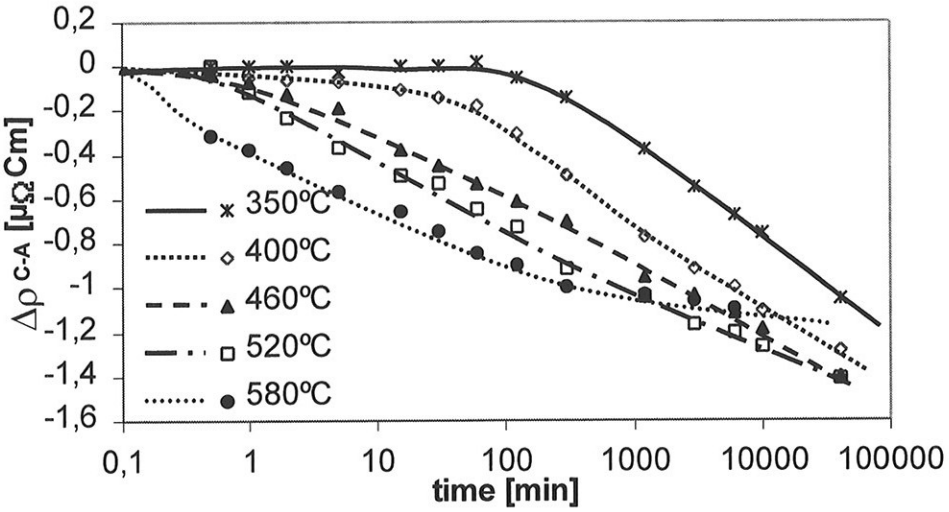

Figure V-7 Variation in electrical resistivity due to the precipitation of Mn in alloy C after annealing at different temperatures.

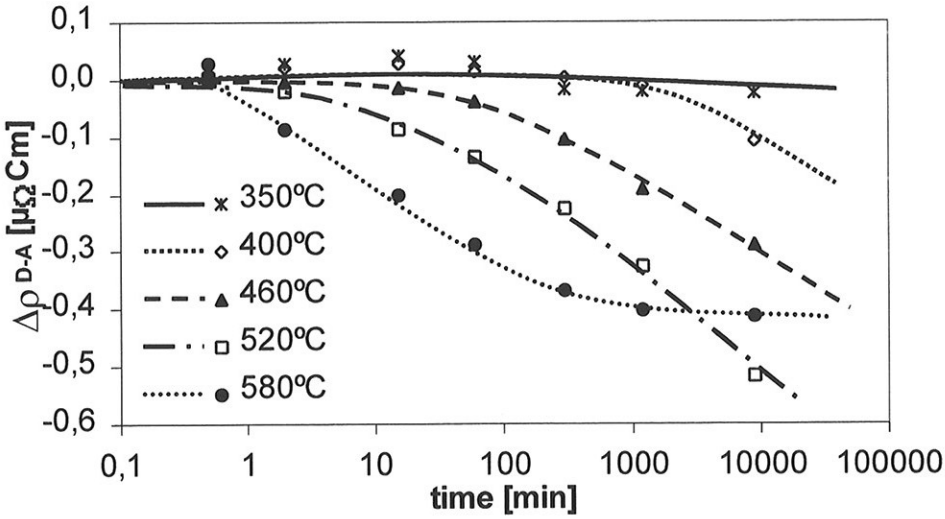

Figure V-8 Variation in electrical resistivity due to the precipitation of Cr in alloy D after annealing at different temperatures.

Since Mn diffuses faster in Al than Cr does, the exchange of elements between the primary particles and the dispersoids is slower in alloy D than in alloy C. This difference in rate of transmission may be the cause for the small decrease in resistivity in alloy D after extensive annealing at 580 °C compared with the more evident dip for alloy C.

The different decrease in resistivity can also be explained by the presence of different primary particles in alloys C and D. Most of the primary particles in alloy D are of the β-AlFeSi phase. During heating to the annealing temperature, the α-Al(CrFe)Si particles nucleate on the interface between primary β-AlFeSi particles and the aluminium matrix. After additional annealing the α-Al(CrFe)Si particles grow and the β-AlFeSi particles dissolve. The α-Al(CrFe)Si particles which are nucleated on the primary β-AlFeSi particles have approximately the same content of Cr and Fe as the α-Al(CrFe)Si dispersoids which nucleated in the matrix. Thus it will not be exchange of Fe and Cr, and consequently the annealing time to establish equilibrium will be shorter.

2.1.2. Light microscope

Figure V-9 shows the microstructure of alloys C and D after 20 hours annealing at different temperatures. The primary particles in alloy C are either the β-Mg_2Si- or the α-Al(MnFe)Si phase. With increasing annealing temperature, the β-Mg_2Si particles dissolve partially and according to the phase diagram they will be completely dissolved at approximately 500 °C.

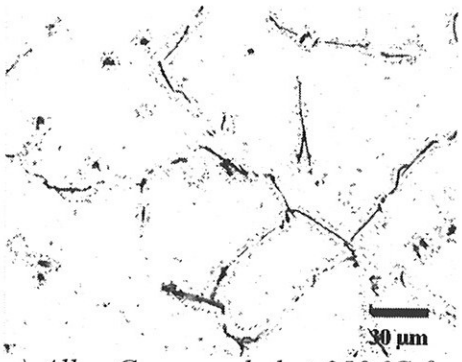

a) Alloy C - annealed at 350 °C for 20 hours.

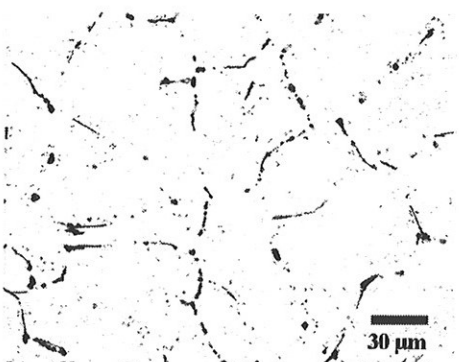

b) Alloy C - annealed at 400 °C for 20 hours.

Figure V-9 Continue next page.

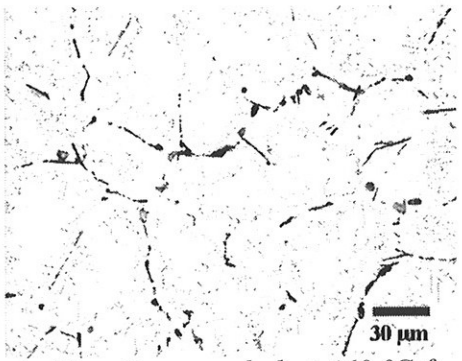

c) Alloy C - annealed at 460 °C for 20 hours.

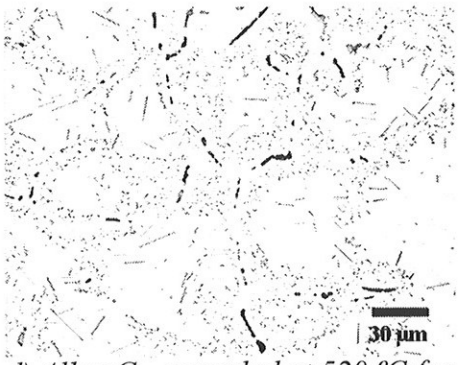

d) Alloy C - annealed at 520 °C for 20 hours.

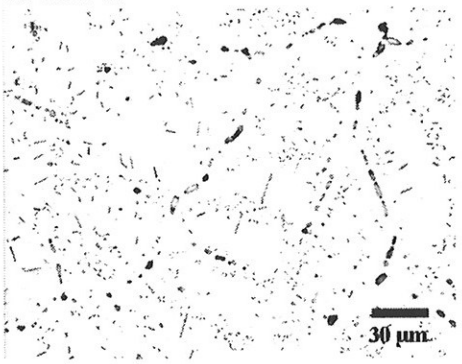

e) Alloy C - annealed at 580 °C for 20 hours.

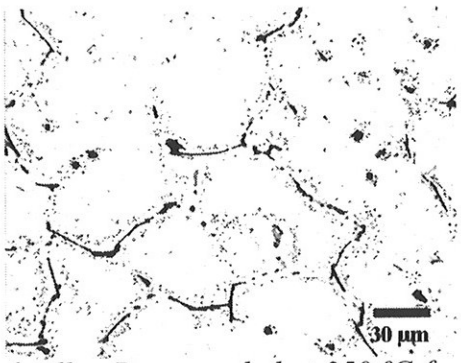

f) Alloy D - annealed at 350 °C for 20 hours.

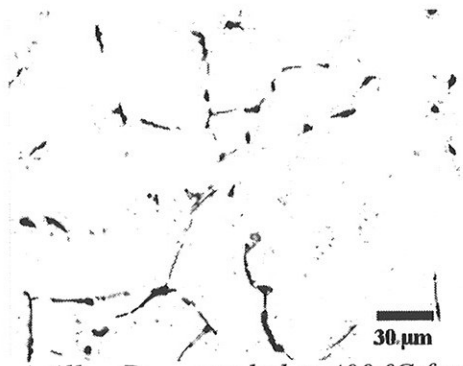

g) Alloy D - annealed at 400 °C for 20 hours.

Figure V-9 Continue overleaf.

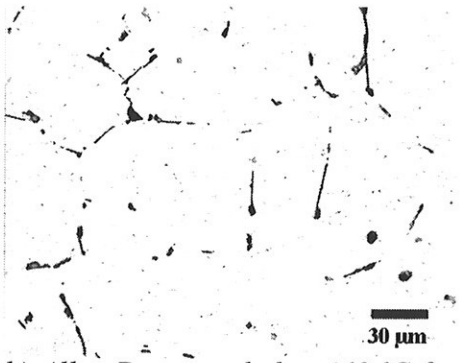

h) Alloy D - annealed at 460 °C for 20 hours.

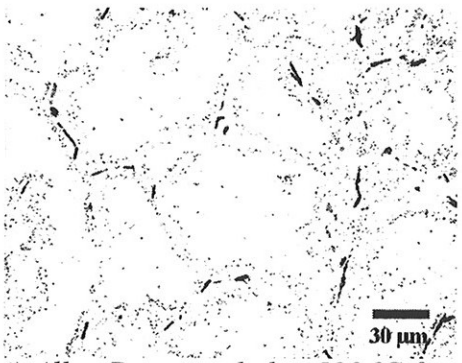

i) Alloy D - annealed at 520 °C for 20 hours.

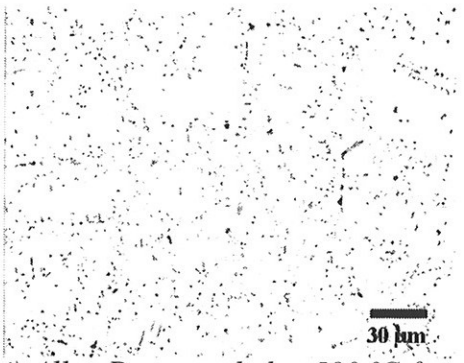

j) Alloy D - annealed at 580 °C for 20 hours

Figure V-9 Light micrographs of alloys C and D after isothermal heat treatment. The annealing temperature was changed between 350 °C and 580 °C, while the duration of the annealing was 20 hours.

The α-Al(MnFe) particles spherodize during annealing and the spehrodization increases with increasing annealing temperature. In alloy D the primary particles are the β-Mg_2Si-, the β-AlFeSi- or the α-Al(CrFe)Si particles. During annealing the β-Mg_2Si- and the α-Al(CrFe)Si particles undergo the same changes as those described above for alloy C. As described earlier, the α-Al(CrFe)Si particles nucleate on the surface of the β-AlFeSi particles and during continued annealing the α-Al(CrFe)Si particles grow and the β-AlFeSi particles dissolve. The extent of this exchange increases with increasing temperature.

After annealing at 350 °C some particles are observed in the vicinity of the primary particles (in areas with a high content of alloying elements) in both alloys. As seen in Figures V-7 and V-8 some Mn has precipitated in

alloy C after 20 hours annealing while no Cr has precipitated in alloy D. The observed particles in alloy C are thus mainly small β-Mg_2Si particles and in addition some α-Al(MnFe)Si dispersoids. When the annealing temperature increases to 400 °C a different microstructure is observed. In alloy C some particles are still present while all the particles in alloy D have disappeared. In both alloys, the small precipitated β-Mg_2Si particles are dissolved, absorbed by the big primary β-Mg_2Si particles or coarsened to fewer and bigger particles. According to Figure V-7 and V-8 considerable amounts of Mn has precipitated in alloy C and thus α-Al(MnFe)Si dispersoids are present while no Cr has still precipitated in alloy D. When the annealing temperature increases to 460 °C α-Al(CrFe)Si precipitates are also observed in alloy D. The α precipitates in both alloys become bigger and more visible when the annealing temperatures are increased to 520 °C and 580 °C. The reason for the empty regions of α particles in the centre of the dendrites is discussed in Part IV.

2.2. Continuous heat treatment

2.2.1. The amount of alloying elements in solid solution

As shown in Figure V-10, the variation in electrical resistivity is considerable during heating for all of the alloys, except for alloy D. This observation is explained in Part III. These drops in resistivity are due to the precipitation of Mn or Mn+Cr and the drops increase with increasing amounts of alloying elements. The alloys were heated at a constant heating rate to three different annealing temperatures (520 °C, 550 °C and 580 °C) followed by isothermal annealing at these temperatures for different times.

At all temperatures the resistivity decreases somewhat during the isothermal annealing, and still after 3000 min. (50 hours) the equilibrium is not attained in any of the alloys (Figures V-11a, V-11b and V-11c).

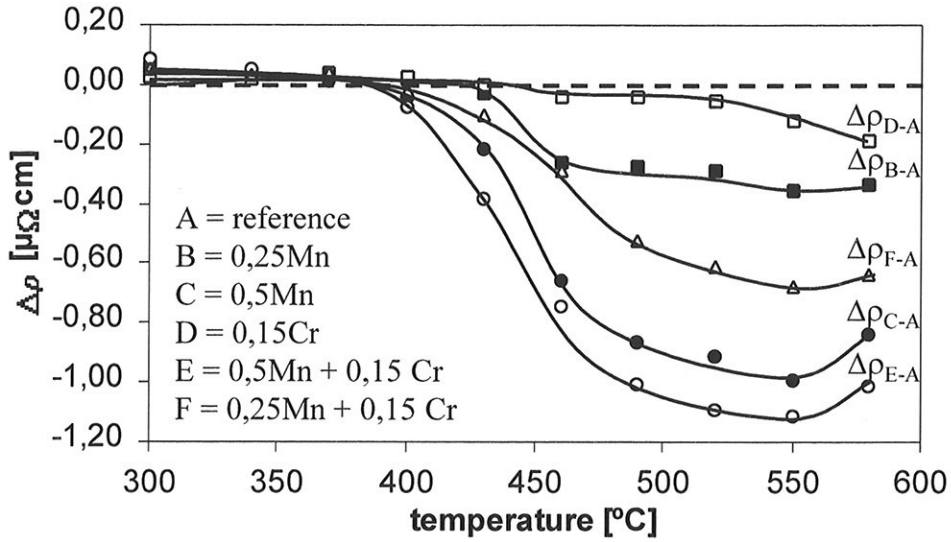

Figure V-10 Variation in electrical resistivity due to the precipitation of Mn and/or Cr in the alloys after heating (heating rate = 3 K/min) to different temperatures.

The resistivity versus times curves for alloys B and C which contain only Mn have nearly a constant slope in a semi- logarithmic diagram. When the alloy contains Cr or Cr + Mn (alloys D, E and F) the resistivity makesa drop before

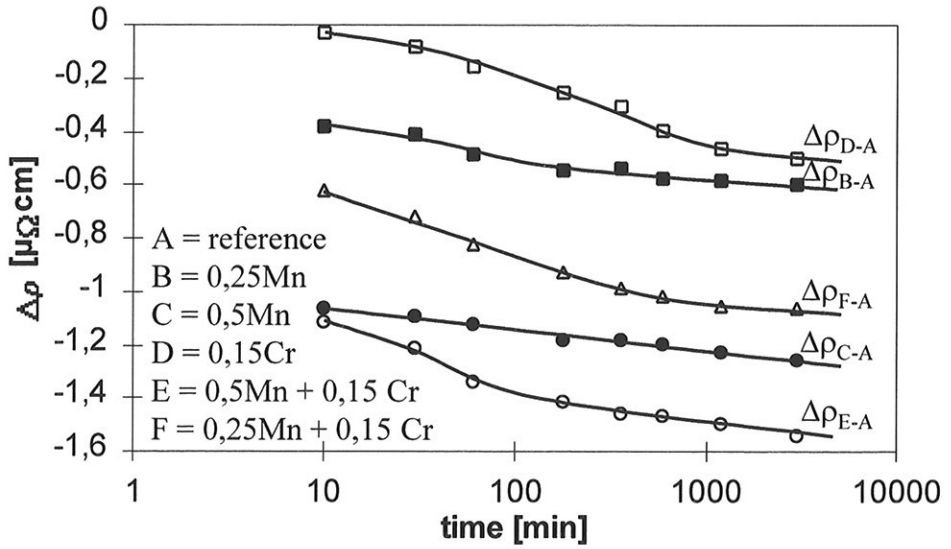

a) Annealing at 520 °C

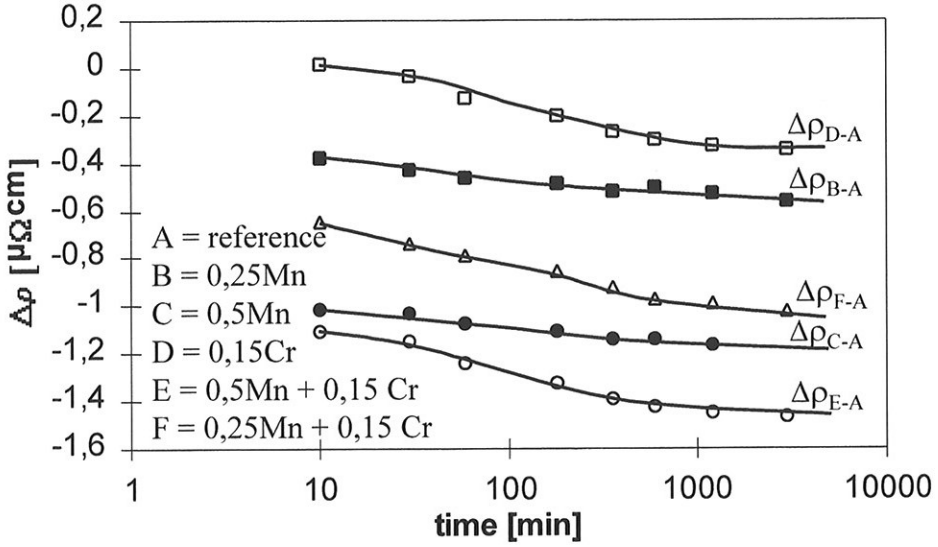

b) Annealing at 550 °C

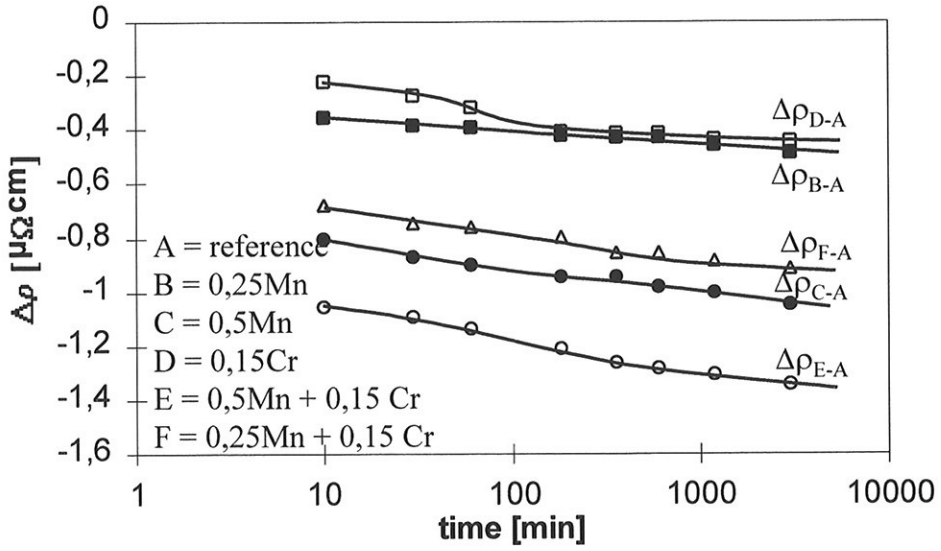

c) Annealing at 580 °C

Figure V-11 Variation in electrical resistivity during annealing in all the alloys. The samples have been heated with a constant heating rate of 3 K/min to the annealing temperature.

the resistivity curves level out, and decrease with a constant slope. This drop becomes smaller as the annealing temperature increases and at 580 °C the

resistivity curve of alloy F has almost a constant slope during the complete annealing.

Which elements is removed from solid solution and the size of the removal is not possible to determine by resistivity measurements. In order to measure the amount of elements in solid solution in alloy C after annealing at 580 °C, the samples were dissolved in Butanol and the primary particles and the dispersoids were separated from the aluminium containing solution. Since the content of Fe in solid solution was low and close to the limit of detection, the Fe measurements were not carried out. The results of the measurements of Mg, Mn and Si contents are shown in Table V-2. The content of all the elements in solid solution decreases during annealing. The decrease in Mn and Si is, however, greater than the decrease in Mg.

Table V-2. The amount of solid solution in alloy C during annealing at 580 °C.

Time [min]	Element		
	Mg [wt.%]	Mn [wt.%]	Si [wt.%]
10	0.568	0.165	0.88
60	0.494	0.126	0.89
180	0.557	0.138	0.85
600	0.547	0.126	0.85
3000	0.535	0.118	0.73

In order to evaluate the results from the chemical analysis, calculation of the electrical resistivity was carried out. The relationship between the electrical resistivity and the amount of elements in solid solution is described by Hatch [1984] and Trømborg [1994]. According to Trømborg the relationship can be described by the following equation:

$$\rho = 0{,}0267 + 0{,}033 Mn_{SS} + 0{,}0068 Si_{SS} + 0{,}0057 Mg_{SS} \qquad \text{(V-6)}$$

while Hatch gives the following relationship:

$$\rho = 0{,}0265 + 0{,}0294 Mn_{SS} + 0{,}0102 Si_{SS} + 0{,}0053 Mg_{SS} \qquad \text{(V-7)}$$

Where ρ is the electrical resistivity and Mn_{SS}, Si_{SS} and Mg_{SS} are the concentration in wt.% of manganese, silicon and magnesium in solid solution, respectively. The results from the calculations and the electrical resistivity measurements are shown in Figure V-12. The results of the calculated resistivity deviate somewhat from the measured ones. Hatch's

equation gives a too high resistivity while Trømborgs equation gives lower values than the measured ones. Nevertheless, the gradient of the resistivity curve is nearly the same for the calculated and the measured resistivity.

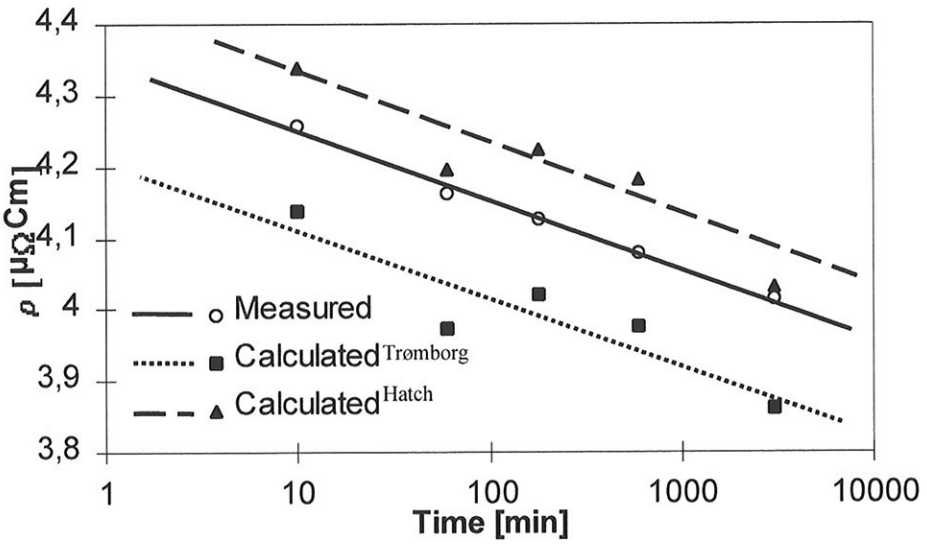

Figure V-12 The measured and the calculated electrical resistivity during annealing at 580 °C.

2.2.2. Light microscope and SEM

The homogenisation annealing causes the microstructure to shift toward the equilibrium condition.. The SEM and light microscope micrographs from alloy C, taken after different annealing procedures, are shown in Figures V-13 and V-14, respectively. The main effect of annealing, visible in SEM and in light microscope, is spheroidizing of primary particles and coarsening of dispersoids. The microstructure after annealing for 30 min. at 520 °C have approximately the same appearance as the microstructure in the as-cast material (Part II). The long primary particles are mainly located on the grain boundaries, while the smaller primary particles are located mainly inside the grain, probably in the interdendritic regions. During annealing the long primary particles will be broken up into a necklace structure of much smaller, more rounded particles. This effect is more pronounced when the temperature is increased from 520 °C to 580 °C.

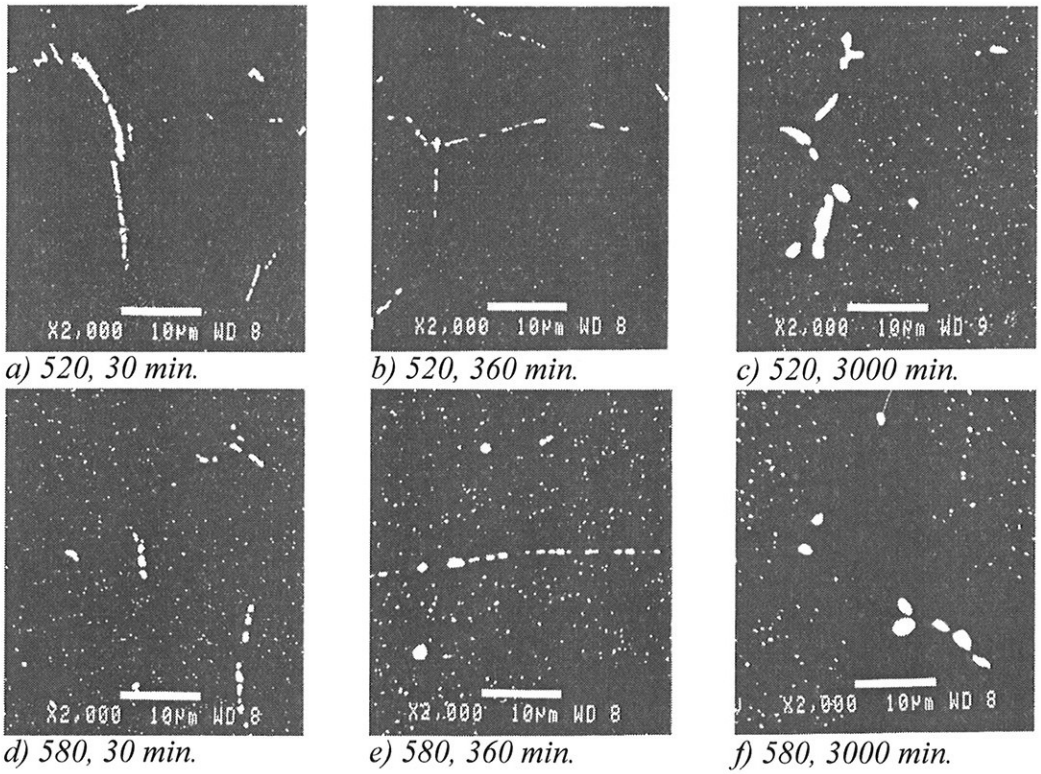

a) 520, 30 min. *b) 520, 360 min.* *c) 520, 3000 min.*

d) 580, 30 min. *e) 580, 360 min.* *f) 580, 3000 min.*

Figure V-13 SEM micrographs show the alterations in microstructure of alloy C during annealing at 520 °C and 580 °C.

As will be demonstrated later in this investigation, the dispersoids are present after 30 min. annealing at 520 °C. Due to the small size of the dispersoids at this stage it was not possible to observe them clearly in either the SEM or the light microscope.

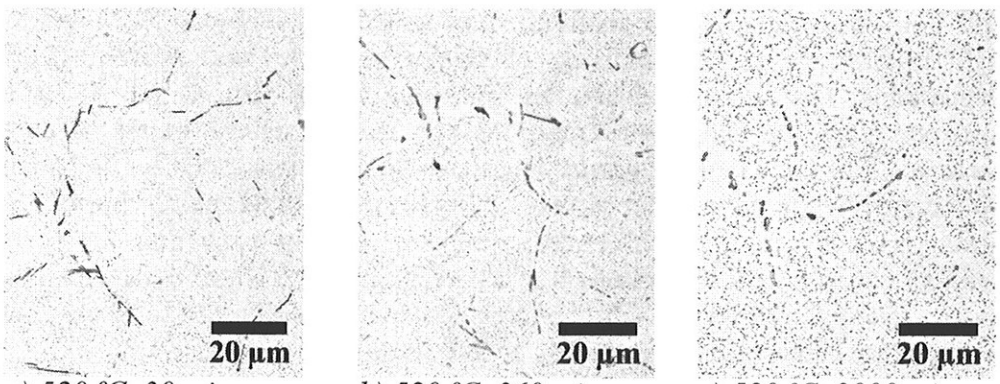

a) 520 °C, 30 min. *b) 520 °C, 360 min.* *c) 520 °C, 3000 min*

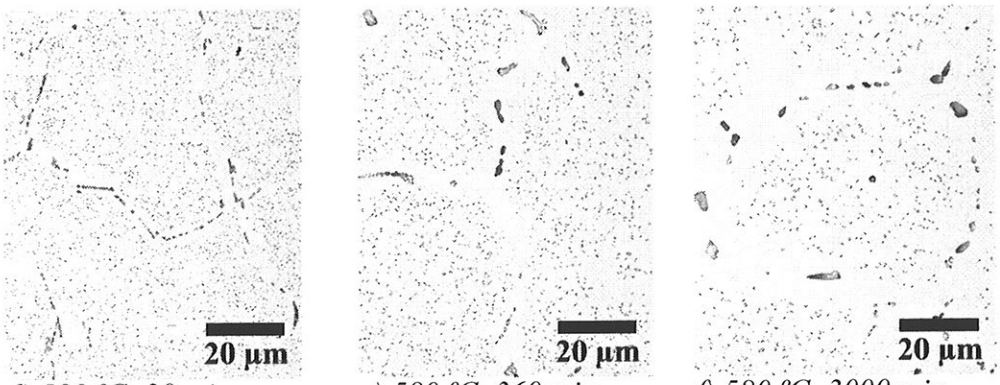

d) 580 °C, 30 min. *e) 580 °C, 360 min.* *f) 580 °C, 3000 min.*

Figure V-14 Light microscope micrographs from alloy C. The alterations of microstructure during annealing at 520 °C and 580 °C.

In alloy C, which contains 0.5 wt.% Mn, primary α-Al(MnFe)Si particles will always be present and no change of this phase occurs during annealing. In alloy D, which contains 0.15 wt.% Cr, brittle primary β-AlFeSi particles are present in addition to some primary α-Al(CrFe)Si phase particles. During annealing, transformation of the β-AlFeSi phase to a more rounded α-Al(CrFe)Si phase occurs. As seen in Figure V-15a, platelike β-AlFeSi particles cover the grain boundaries, and during annealing the particles transform (nucleation of the α-Al(CrFe)Si phase and dissolution of the β-AlFeSi phase) into small, spherical α-Al(CrFe)Si particles. The nucleation of the dispersoids was probably not finished after 30 min. annealing at 520 °C, and the dispersoids which are present are too small to be seen in the light microscope. Even after 360 min. annealing at this temperature, only large dispersoids in the vicinity of the interdendritic regions are visible.

The amount of primary particles after annealing is considerably larger in alloy C than in alloy D. During annealing the primary particles in alloy D are nearly completely dissolved while a appreciable density is still present in alloy C. One important observation is the presence of dispersoid-depleted zones (DDZ) between the dendrites. At the start of the annealing the DDZ is narrow, but increases continuously with the annealing time, and most strongly in alloy C.

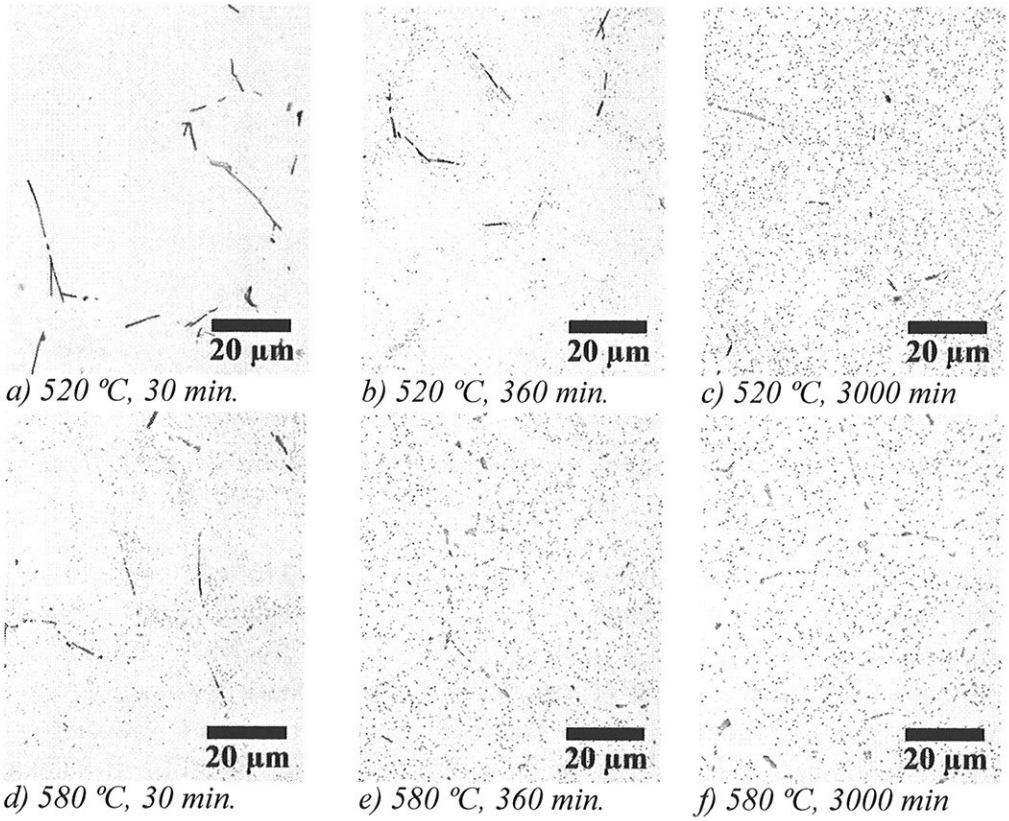

a) 520 °C, 30 min. *b) 520 °C, 360 min.* *c) 520 °C, 3000 min*

d) 580 °C, 30 min. *e) 580 °C, 360 min.* *f) 580 °C, 3000 min*

Figure V-15 Light microscope micrographs from alloy D. The alteration of microstructure during annealing at 520 °C and 580 °C.

Two effects contribute to this DDZ. Firstly, the microprobe measurements (Part II), showed that the concentration of Mn and Cr was nearly constant within the material, but a detailed evaluation of the solidification path by means of the Alstruc microstructure solidification model [Dons et al. 1999] demonstrates that a significant drop in the concentration of these elements occurs towards the end of the solidification process (Part III). However, the extent of this drop is too narrow to be detected in the microprobe. As a consequence of this drop a corresponding drop in the density of the dispersoids will also be present. Secondly, during annealing the primary particles will grow at the expense of the neighbouring dispersoids and DDZ between the dendrites will develop.

The drop in the concentration towards the end of solidification is narrow and contributes only to a smaller part of the DDZ after extensive annealing. Hence, the major variation in the width of the depleted zones between the alloys is due to the different growth rate of the primary particles that grow at the expense of the neighbouring dispersoids. In alloy C both the

primary particles and the dispersoids are of the α-Al(MnFe)Si-type. The element Mn belongs to the slowly diffusing impurities in aluminium, and since the α-phase contains this element the rate of growth and coarsening of this phase is determined by the rate of diffusion of Mn in aluminium. In alloy D the growth of DDZ is more intricate, because the primary particles belong to the β-AlFeSi phase and the dispersoids belong to the α-Al(CrFe)Si phase. During annealing α-Al(CrMn)Si particles nucleate at the surface of the primary β-AlFeSi particles and after continued annealing the α-Al(CrFe)Si particles grow while the β-AlFeSi particles dissolve. When this transformation is completed the bigger α-Al(CrFe)Si precipitates (which has been precipitated on the β-surface) grow at the expense of the smaller neighbouring dispersoids. This growth of the DDZ is expected to be slower in alloy D than in alloy C since the diffusion of Mn in Al is higher than the diffusion of Cr in Al at the same temperature. The transformation from β to α and the slow growth rate of primary α-particles containing Cr thus make the DDZ narrower in alloy D than in alloy C.

2.2.3 Dispersoid size distribution

Particle coarsening is due to a higher solubility of small particles compared with larger ones. The small particles tend to dissolve while larger particles tend to grow. The driving force is provided by the reduction of total interfacial energy. The mean particle size will thus increase during annealing. The particle size distribution can be expressed as the frequency of particles in a given scaled size interval as a function of the scaled particle size $r/\bar{r}$, where r is the radius of the particles and $\bar{r}$ is the mean particle radius. Figure V-16 shows the influence of annealing at 520 °C on the particle size distribution. The mean particles radius increase from 15 nm at the start of the annealing to 79 nm after 3000 min. annealing.

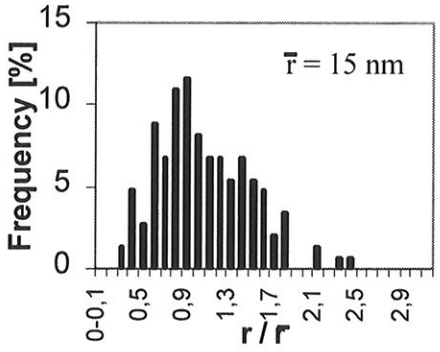

a) 520 °C, 0 min.

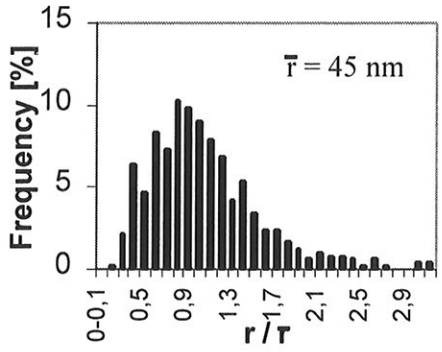

b) 520 °C, 180 min.

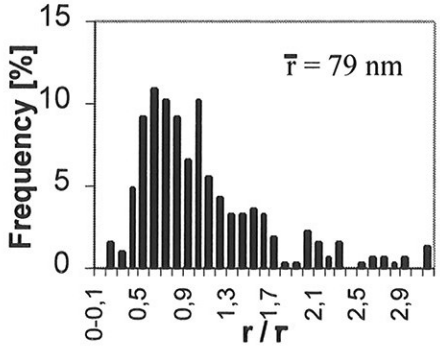

c) 520 °C, 3000 min.

Figure V-16 The influence of annealing at 520 °C on particle size distribution. a)-c) Quasi-stationary distribution profiles,

Figure V-17 shows the influence of annealing at 580 °C on the particle size distribution . The mean particle radius increases from 36 nm after 0 min. annealing to 130 nm after 3000 min. annealing.

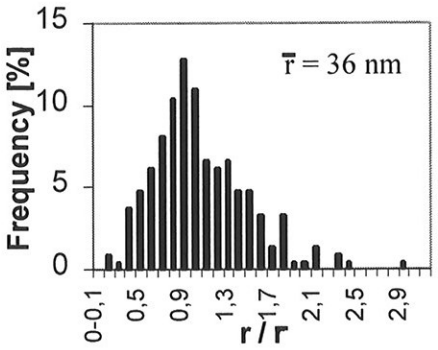

a) 580 °C, 0 min.

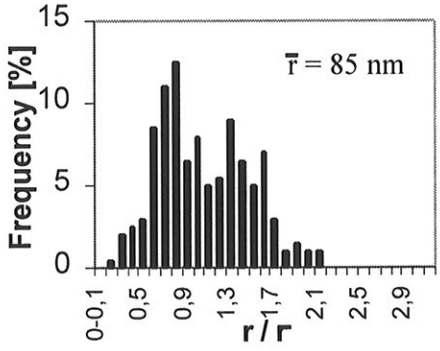

b) 580 °C, 180 min.

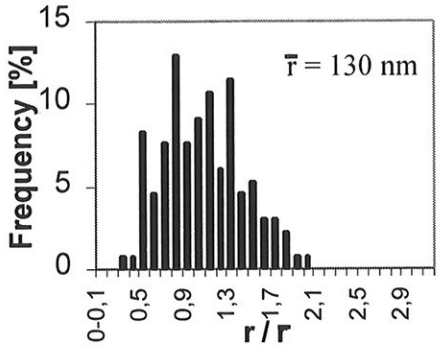

c) 580 °C, 3000 min.

Figure V-17 The influence of annealing at 580 °C on particle size distribution. a)-c) Quasi-stationary distribution profiles,

As can be seen from Figures V-16 and V-17, the particle size distribution is approximately independent of time at both annealing temperatures used. Such distributions are referred to as quasi-stationary distribution. Lifshiz and Slyozov [1961] and Wagner [1961] (LWS) determined a mathematical expression for the quasi-stationary distribution. They did this for two different cases depending upon whether long-range diffusion through the lattice or short-range diffusion across the interface boundary is the rate limiting factor for the coarsening process. As can bee seen in Figure V-18 both these distributions are rather strongly right skewed. In addition, the peak of the experimental distribution curve is lower and broader than the theoretical one. As opposed to the function determined theoretically, left skewed distributions are most often found in nature and also in this investigation. Several assumptions are made in the LSW-theory which limit its applicability.

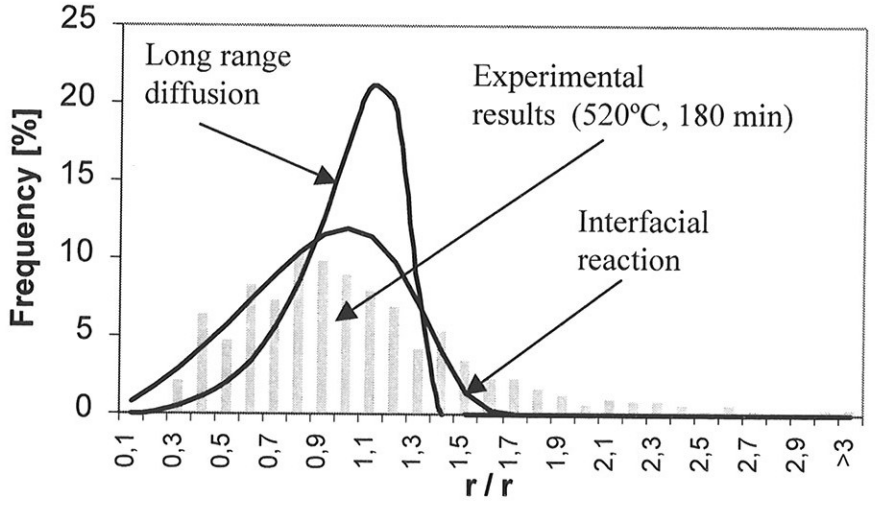

Figure V-18 Comparison of an experimental size distribution and the LSW distribution functions.

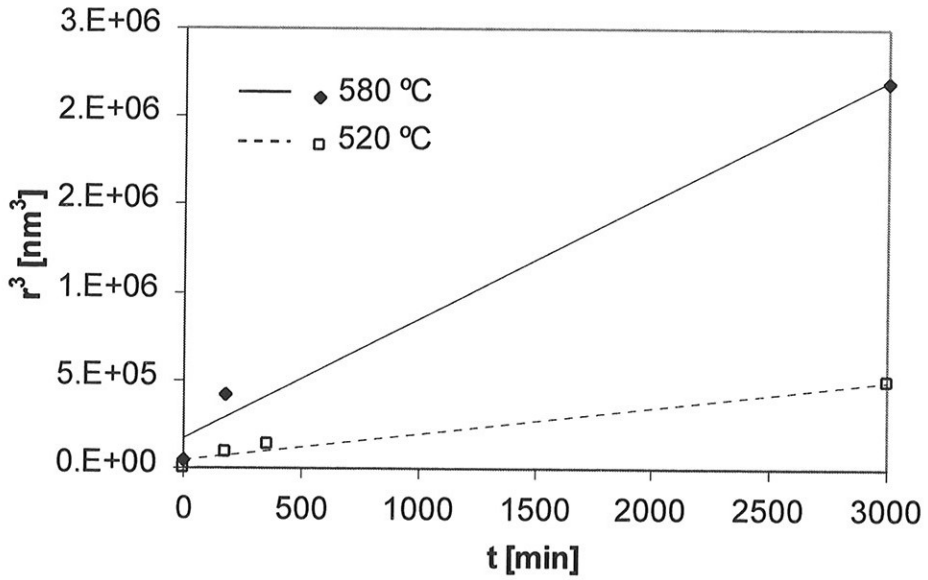

Figure V-19 Variation of the (mean particles radius)^3 as a function of time for α-Al(MnFe)Si dispersoids in alloy C.

The theoretical relationship between the mean particle radius and the coarsening time was by developed by Lifshiz and Slyozov [1961] and Wagner [1961] As described in Part I, the rate of coarsening depending on whether long-range diffusion through the lattice (equation I-14) or short-

range diffusion across the interface boundary (equation I-15) are the rate controlling factor for the coarsening process. The following relationships were obtained in these two cases:

Equation I-14: $$\bar{r}^3 - \bar{r}_0^3 = kt$$

Equation I-15: $$\bar{r}^2 - \bar{r}_0^2 = k_1 t$$

The variation of the $\bar{r}^3$ and $\bar{r}^2$ with time is presented in Figures V-19 and V-20 respectively. Even though the number of experimental data are small, the agreement with equation I-14 is clearly better than with equation I-15. Hence, long-range diffusion through the lattice is probably the rate controlling factor for the coarsening process.

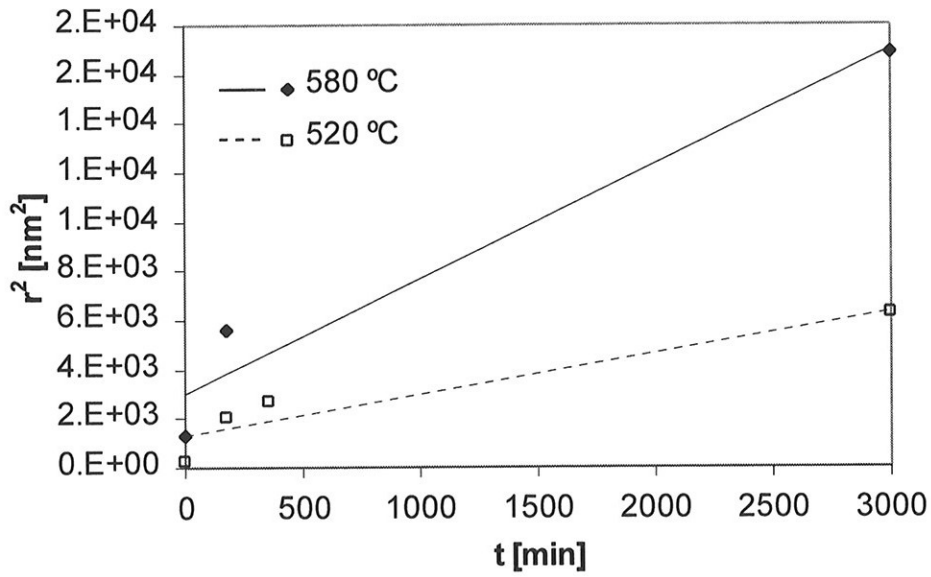

Figure V-20 Variation of the (mean particles radius)^2 as a function of time for α-Al(MnFe)Si dispersoids in alloy C.

2.2.4 Dispersoid density

As described above dispersoid coarsening is a process where the number of particles per unit volume of the system decreases with time at elevated temperatures. Table V-3 shows that the dispersoid density δ decreases considerably during annealing and this decrease increases with increasing

temperatures. The coarsening of alloy C (0.5 wt.% Mn) is especially fast and the density decreases from 570 dispersoids per μm^3 at the start of the annealing (520 °C) to only 7 after 3000 min. annealing. The coarsening process starts during the heating and probably before the temperature has reached 520 °C. During the short heating period (heating rate = 3 K/min) from 520 °C to 580 °C the dispersoid density decreases from 570 dispersoids per μm^3 to 50. In alloy D, which contains only Cr as a dispersoid-forming element, there are few dispersoids at the start of the annealing. Due to a slow coarsening rate the dispersoid density is larger in alloy D than in alloy C after annealing for 3000 min. After heating to 520 °C or 550 °C all the dispersoids containing Cr had not precipitated. Even after 30 min. annealing at these temperatures the nucleation and growth process was not finished. The coarsening process starts after about 60-180 min. and 30-60 min. annealing

Table V-3. Dispersoid density δ [number/μm^3] as a function of annealing time and temperature

Temp→	520 °C			550 °C			580 °C		
Alloy→ Time[min]	C	D	E	C	D	E	C	D	E
0	570	--	770	188	--	394	50	20	131
10	350	--	451	109	--	150	27	16	61
30	121	--	252	44	--	97	12.5	14	35
60	70	30	168	36	24	70	7.4	11	29
180	42	32	81	18	11	36	4.5	8.6	13
360	24	23	69	11	10	25	2.8	5	10
600	15	20	46	4.4	8.3	18	2.7	3.8	8.7
1200	7.7	15	33	2.5	5.5	13	1.5	2.8	4.6
3000	6.8	10	19	1.9	3.7	7	1.5	2	3

at 520 °C and 550 °C, respectively. In alloy E, which contains both Cr and Mn, the dispersoid density is larger than in both alloy C and D after the same heat treatments.

In alloy C the dispersoids are of the α-Al(MnFe)Si type while in alloy D the dispersoids are of the α-Al(CrFe)Si type. Since the Mn and Cr have lower diffusion rates than the other elements in the dispersoids (Fe and Si), diffusion of Mn and Cr are rate limiting in the coarsening process. Consequently, the difference in the rate of coarsening between alloys C and D at a given temperature is due to the difference in the diffusion rate of Mn and Cr. In alloy E both Cr and Mn are present in the α-Al(MnCrFe)Si dispersoids. Since the rate of diffusion of Cr in Al is lower than Mn in Al, the diffusion of Cr will probably be rate limiting for the coarsening reaction in alloy E.

In order to investigate the coarsening process a relationship between the dispersoid density δ and the mean radius of the dispersoids $\bar{r}$ is required. Some assumptions have to be made. The volume fraction of the dispersoids f_v is constant during the annealing, and is given by the following equation:

$$f_v = \delta \frac{4}{3} \pi \int_0^\infty r^3 f(r,t) dr \qquad \text{(V-8)}$$

where *f(r,t)* is the particle size distribution. Here the dispersoids are assumed to be spherical. The particle size distribution can be expressed as a function of the scaled particles radius $r/\bar{r}$. As seen in Figures V-16 and V-17 this type of distribution is approximately independent of annealing time. The distribution is thus a quasi-stationary. Under these conditions one obtains:

$$f_v = \delta \frac{4}{3} \pi \bar{r}^3 \int_0^\infty (r/\bar{r})^3 \bar{r} f(r,t) \frac{dr}{\bar{r}}$$

$$r/\bar{r} = \varphi$$

$$f_v = \delta \frac{4}{3} \pi \bar{r}^3 \int_0^\infty \varphi^3 f(\varphi) d\varphi$$

$$\int_0^\infty \varphi^3 f(\varphi) d\varphi = K_1$$

the following equation is obtained:

$$f_v = \delta \frac{4}{3} \pi \bar{r}^3 K_1 \qquad \text{(V-9)}$$

It is also assumed that long-range diffusion through the lattice is the rate controlling factor for the coarsening process. Thus, equation I-14 will be used in discussion of this problem. Substituting equation V-9 into equation I-14 gives:

$$\frac{1}{\delta} = K_2 (\bar{r}_0^3 + Kt) \qquad \text{(V-10)}$$

where

$$K_2 = \frac{4\pi K_1}{3 f_v}$$

and the constant K is described in Part I.

The inverse of the dispersoid density $1/\delta$ as a function of annealing time t in alloy C is presented in Figure V-21. The rate of coarsening is strongly temperature-dependent. As seen from equation V-10 the rate of the coarsening is dependent on the value of K. K contains the diffusion coefficient D. The relationship between D and the temperature T is given in equation I-16 and shows that D increases considerably with temperature. If the assumptions made in equation V-10 are valid, a linear variation of $1/\delta$ with t should be obtained. The experimental results for alloy C did not obey such a relationship (Figure V-21). Figures V-22 and V-23 show $1/\delta$ as a function of annealing time t in alloys D and E respectively. The same trend as that observed in alloy C was observed in these alloys. The rate of coarsening is strongly temperature-dependent and a linear variation of $1/\delta$ with t is not obtained.

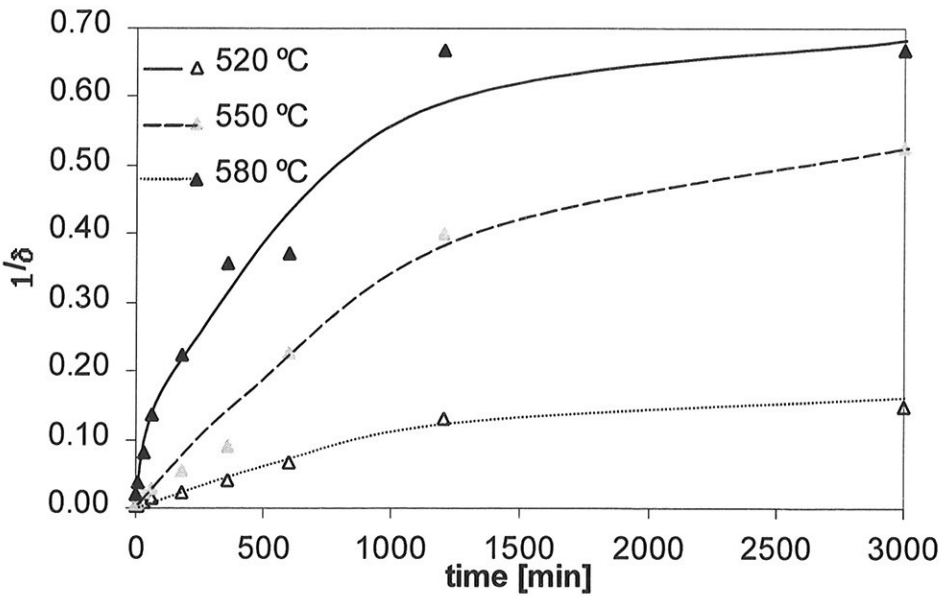

Figure V-21 *Variation of $1/\delta$ as a function of time for α-Al(MnFe)Si dispersoids in alloy C.*

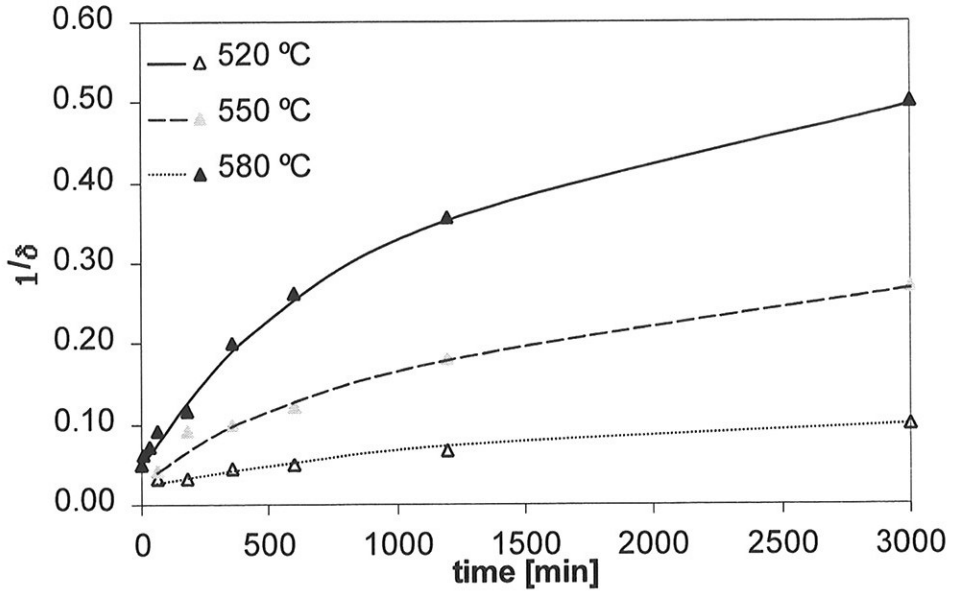

Figure V-22 Variation of 1/δ as a function of time for α-Al(CrFe)Si dispersoids in alloy D

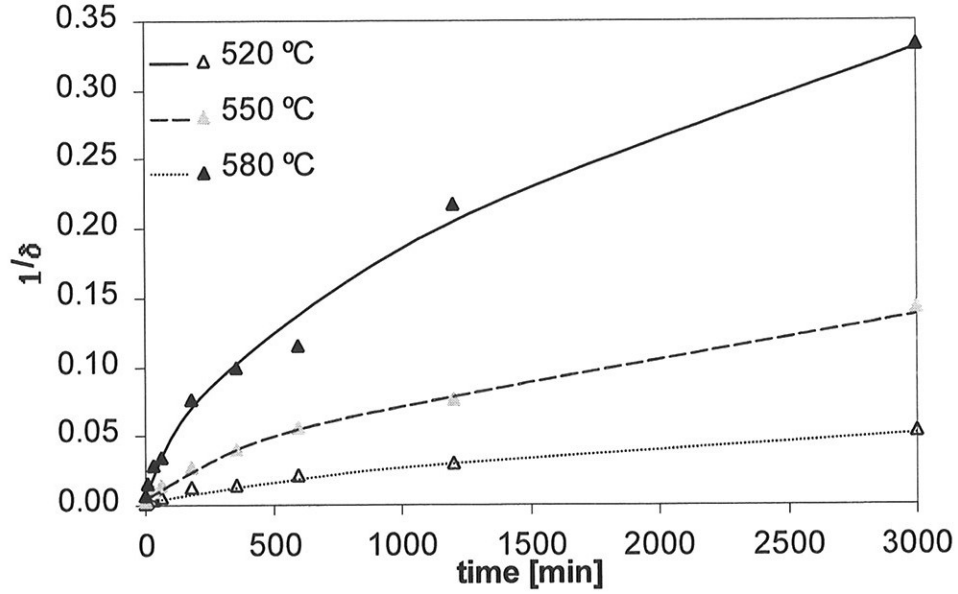

Figure V-23 Variation of 1/δ as a function of time for α-Al(MnCrFe)Si dispersoids in alloy E

Since the rate of coarsening is considerably lower at 520 °C than at 580 °C the variation in the measured values is also lower at 520 °C than at 580 °C. Thus, when the data are presented in the same diagram, the density measurements fit better with the equation V-10 at 520 °C than at 580 °C. In order to compare how the results diverge from equation V-10 at all temperatures, the δ_0/δ ratio as a function of time was presented (Figure V-24). δ_0 is the dispersoids density at the start of the annealing. As seen in Figure V-24 the coarsening has the same trend independent of the annealing temperature. However, if we choose a segment of the data within a short interval the agreement between the data and equation V-10 is very good. (V-25). The length of this interval is typical for a commercial homogenisation process. Hence, it will be acceptable for industrial application to use equation V-10 in order to predict the coarsening of the dispersoids.

As discussed above, the rate of the coarsening is dependent on the value of the constant K in equation V-10. The value of K varies between the alloys As described in Part I K is given by:

$$K = \frac{8}{9}\frac{D\gamma V_m C_{eq}}{RT}$$

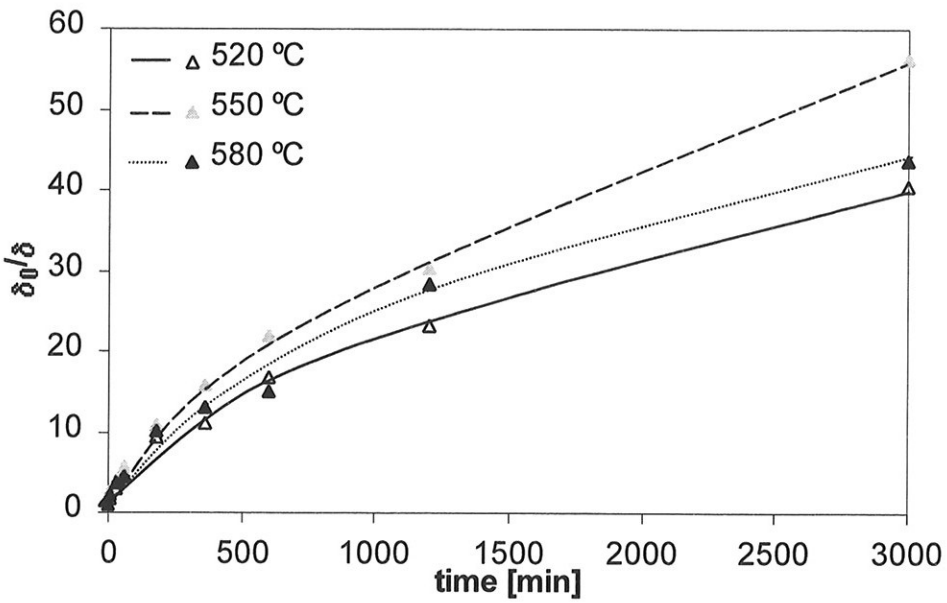

Figure V-24 Variation of δ_0/δ as a function of time for α -Al(MnCrFe)Si dispersoids in alloy E.

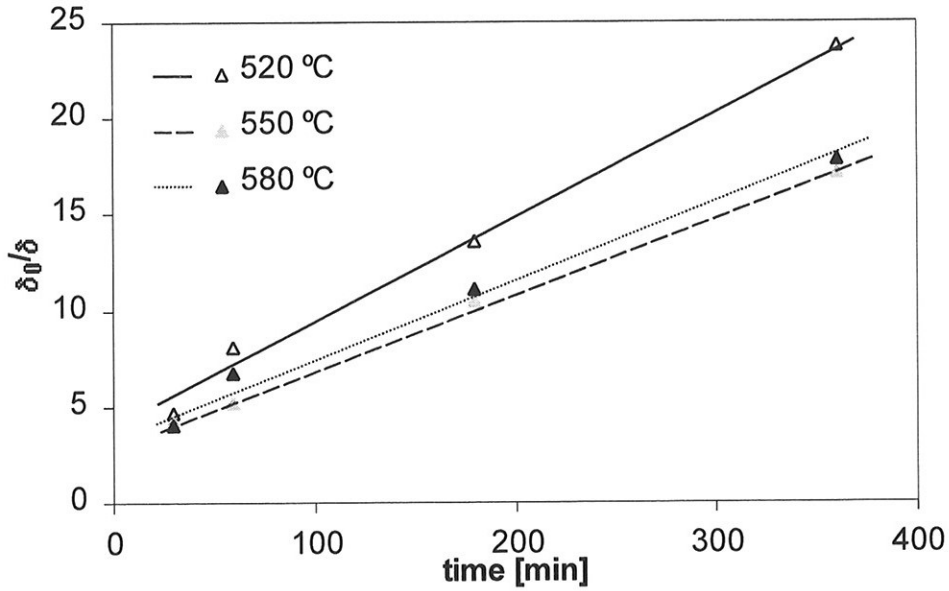

Figure V-25 Variation of δ_0/δ as a function of time for α-Al(MnFe)Si dispersoids in alloy C. The agreement between the experimental values and the equation of coarsening (V-9) is very good within a segment of the density measurements

The dispersoids in alloys C, D and E are α-Al(MnFe)Si-, α-Al(CrFe)Si- and α-Al(MnCrFe)Si dispersoids respectively. These phases have similar composition and structure. The interface energy γ and the molar volume of the phases V_m is thus probably also nearly of equal magnitude. As discussed above, diffusion of Mn is rate limiting for the coarsening process in alloy C while diffusion of Cr is rate limiting for the coarsening process in alloys D and E. As shown in Table I-2, the diffusion coefficient of Mn in Al is approximately 20 times faster than Cr in Al at same temperature. As can be seen in Figure V-26 the rate of coarsening is considerably faster in alloy C than in alloys D and E. The slope of the curves for alloys D and E is approximately the same. Even though equilibrium solid solubility C_{eq} also varies between the alloys the different slope is mainly due to different D.

Since the experimental data do not agree with equation V-10, the assumptions made for the coarsening process must be in error. A larger divergence is expected (and observed) if the short-range diffusion across the interface boundary (equation I-15) is suggested as the rate controlling factor for the coarsening process. Thus, the assumption of a constant volume fraction of the dispersoids during the coarsening is most likely not an acceptable assumption. A more detailed discussion of the discrepancy

between experimental results and equation V-10 is carried out later in chapter 2.3.

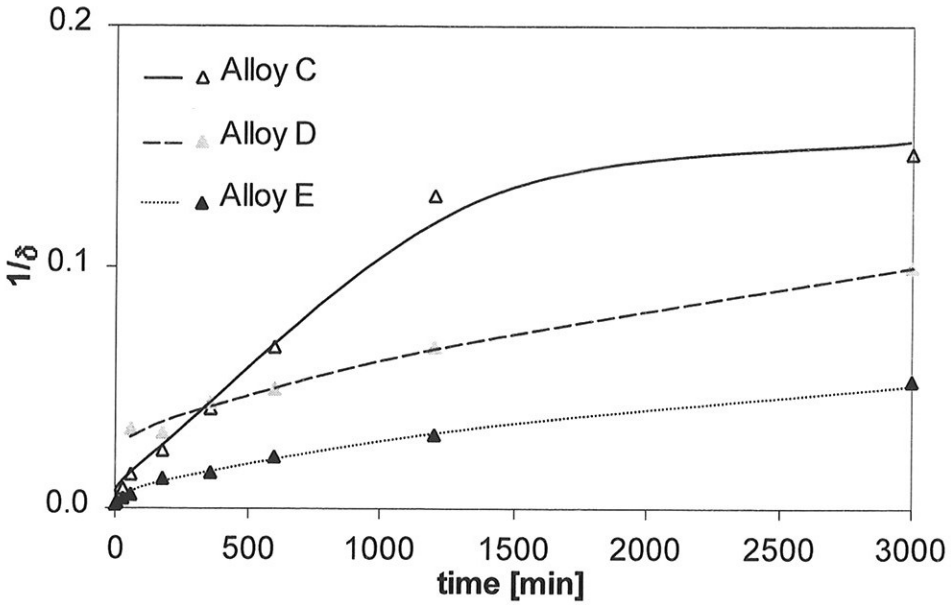

Figure V-26 Variation of 1/δ as a function of time for dispersoids. Annealing teperature is 520 °C.

Step-heat treatment

According to the Gibb-Thomson-equation, the solubility of a particle in a matrix is dependent on its size (radius). As seen in Figure I-4, the solubility decreases with increasing particle size. Thus, a small dispersoid may dissolve during heating, which results in a lower density of the dispersoids. The step-heating procedure may affect the survival of small dispersoids because the dispersoids have time to grow during the isothermal step of the annealing and thus be stable during the subsequent heating. In order to investigate this effect three heat treatment procedures were carried out on alloy C. The different procedures are shown in Figure V-27. All three heat treatments started with a heating rate of 3 K/min from room temperature. In heat treatment I and II the heating stopped at a temperature T_x, followed by annealing at this temperature for 60 min. Subsequently, the heat treatments continued with heating to 520 °C at a rate of 3 K/min. Heat treatment I was finished with annealing for 60 min. and water quenching and heat treatment II was finished with direct water quenching from 520 °C. In heat treatment III the heating stopped at 430 °C and the duration t_x at this temperature varied. After this up-quenching to 520 °C followed and continued with an annealing at this temperature for 60 min. The heat treatment was finished with quenching in water. All the TEM foils

used in this investigation were prepared in a standard way described previously in this part.

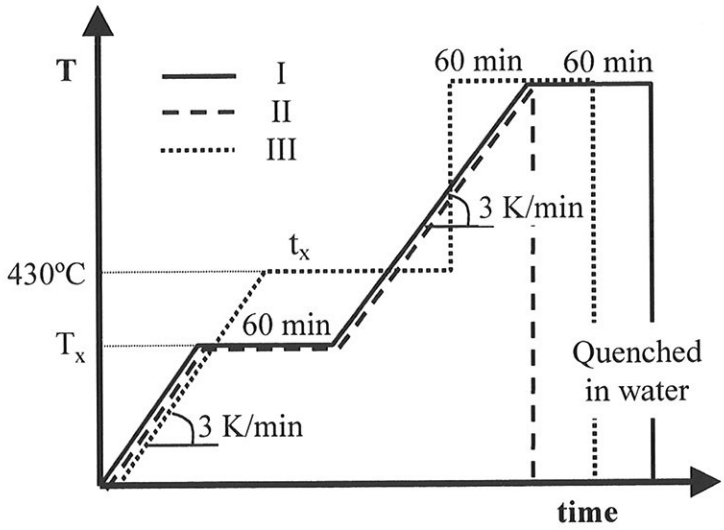

Figure V-27 The outline of three addition heat treatments in alloy C.
I = heating (3 K/min) - 60 min. at Tx - heating (3 K/min) - 60 min. at 520 °C - quenched in water.
II = heating (3 K/min) - 60 min. at Tx - heating (3 K/min) - 0 min. at 520 °C - quenched in water.
III = heating (3 K/min) - X min. at 430 °C - up-quenched - 60 min. at 520 °C - quenched in water.

After heat treatment I, the dispersoid density varied between 65 and 95 dispersoids per μm^3 (Figure V-28). No particular dependence of the dispersoids density on T_x was observed. The apparent spread in density is probably due to inaccuracy in the measurements. It is possible that the dispersoid density is different at the start of the annealing but because the rate of coarsening is high, this difference will be insignificant after 60 min. annealing. To resolve this question, heat treatment II was carried out. Heat treatment I and II are similar except for the final 60 min. annealing at 520 °C carried out for heat treatment I but not for heat treatment II. After heat treatment II the dispersoid density varied between 505 and 545 dispersoids per μm^3 (Figure V-29), and as heat treatment I no particular dependence of dispersoid density with T_x is observed. In order to investigate the effect of the duration of t_x (430 °C) on the dispersoid density, heat treatment III was carried out. The values for dispersoid density are at the same level as the density in treatment I and no clear trend was observable in this case (Figure V-30). The results show that none of the three step-heat treatment procedures

affect the dispersoid density. As described previously, the measurements of the density were carried out approx. 5 μm away from the interdendritic regions. Additional investigations (se Part IV) indicated that a different heating procedure does not affect the dispersoid density in the vicinity of the interdendritic regions, but the investigations showed that the variation in heat treatment can affect the distribution of dispersoids considerably. Thus even though the step-heat treatments not affect the dispersoid density in the measured areas it is possible that the treatments affect the distribution of the dispersoids.

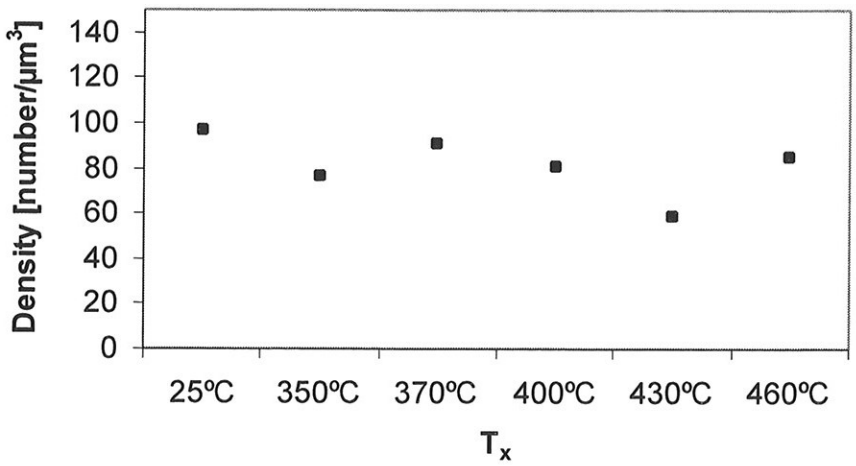

Figure V-28 Variation in dispersoids density after heat treatment I.

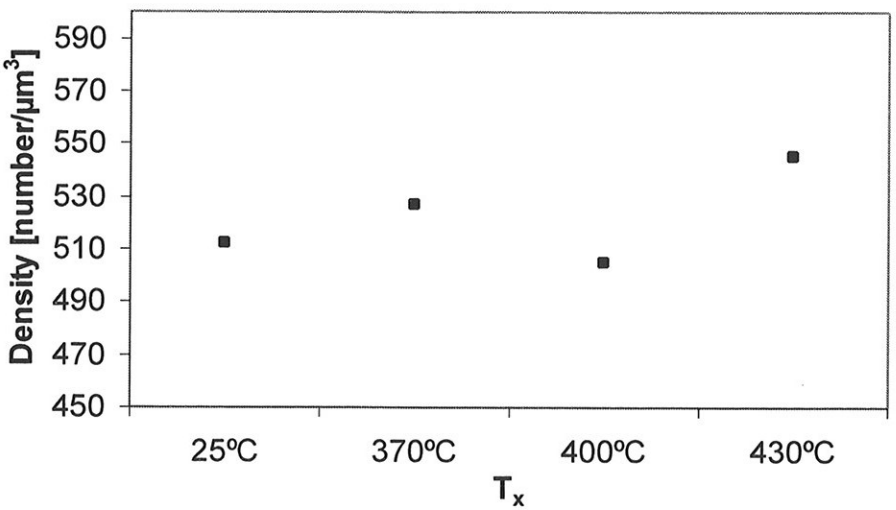

Figure V-29 Variation in dispersoids density after heat treatment II.

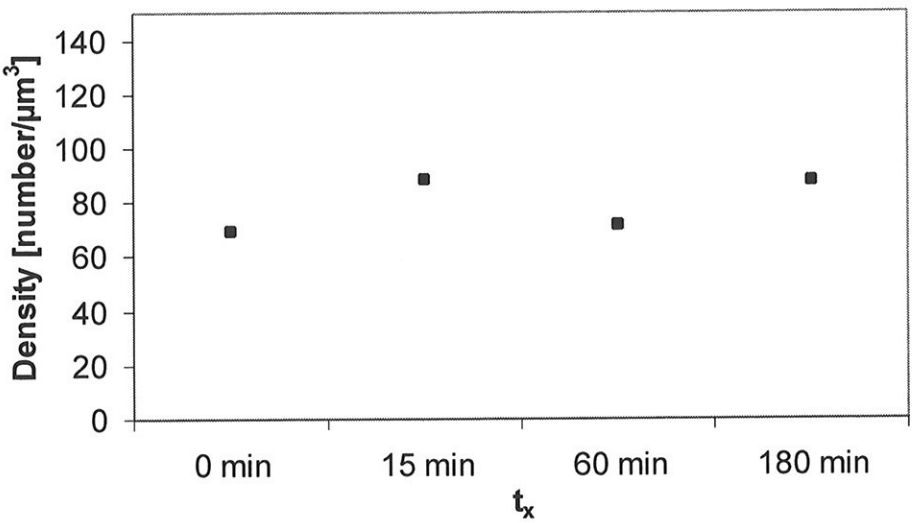

Figure V-30 Variation in dispersoids density after heat treatment III.

2.2.5 Variation in the composition of the α-Al(MnFe)Si and the α-Al(MnCrFe)Si particles during annealing.

When a small particle is embedded in a matrix, the matrix will necessarily be contribute to the measurements of the chemical composition. The apparent composition of the particle will be between the particle composition and the matrix composition. The variation of Fe/Mn-, Fe/(Mn+Cr)- and Mn/Cr ratio (weight %) of the dispersoids during annealing were investigated. The concentration of the Al-matrix does not, apart from the some effect of absorption, influence these ratios. Thus, the measured values of the concentration of the Al-matrix were excluded and only the ratio between the values of Fe, Mn, Si (and Cr) were used. (% Fe + % Mn + % Si (+% Cr)) = 100).

Figures V-31 and V-32 show the variation of the Fe/Mn ratio during heat treatment at 520 °C and 580 °C of alloy C. At the start of the annealing the primary particles (P) is rich in Fe while the dispersoids, which have just nucleated (D/M), have a high Mn content. During growth of the primary particles and the dispersoids their chemical composition approach each other. After 3000 min. annealing at 580 °C there was still a difference in the Fe/Mn ratio between the dispersoids and the primary particles which indicates that equilibrium is not established. The analysis from the dispersoids in the

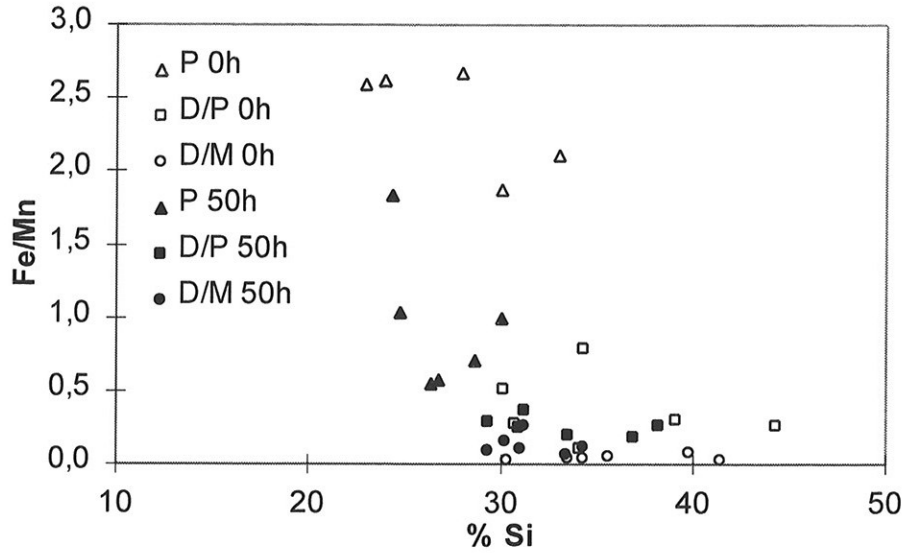

Figure V-31 The diagram shows how the Fe/Mn ratio in the primary particles (P), the dispersoids in the interior of the grain (D/M) and the dispersoids in the vicinity of the primary particles (D/P) in alloy C changes during annealing at 520 °C.

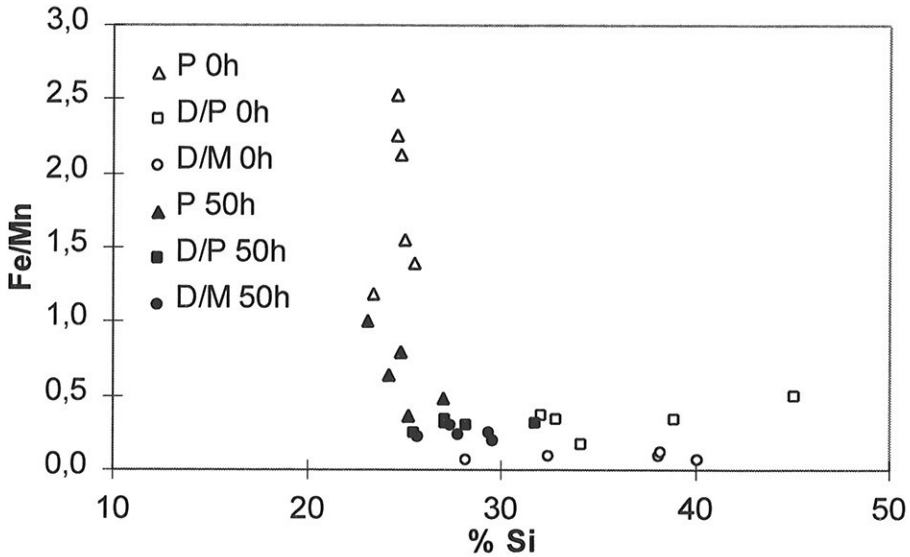

Figure V-32 The diagram shows how the Fe/Mn ratio in the primary particles (P), the dispersoids in the interior of the grain (D/M) and the dispersoids in the vicinity of the primary particles (D/P) in alloy C changes during the annealing at 580 °C.

vicinity of the primary particles (character D/P) shows an Fe/Mn ratio between the primary particles and the dispersoids.

Figure V-33 shows how the Fe/(Mn+Cr) ratio changes in alloy E during annealing at 580 °C. As can be seen, the Fe/(Mn+Cr) ratio varied with the Si concentration in the same manner as the Fe/Mn ration in alloy C. After extensive annealing the primary particles and the dispersoids approached each other in composition, but equilibrium was not established.

It is not easy to predict the content of Cr and Mn in the primary particles. But it is expected that the precipitated dispersoids contain considerably more Mn than Cr. The rate-limiting factor for the precipitation of the dispersoids is most likely the diffusion of Mn and Cr. Since Mn diffuses faster in Al than Cr does at the same temperature, the dispersoids are nearly "pure" α-Al(MnFe)Si dispersoids without Cr. As described in Part III, this precipitation occurs at approximately 350-400 °C. During additional heating to 580 °C and subsequently annealing at this temperature the dispersoids absorb Cr. As can be seen in Figure V-34 both the primary particles and the dispersoids contain considerable more Mn than Cr in the beginning of the annealing. After extensive annealing the Mn/Cr ratio decreases, but still more Mn than Cr is present, especially in the primary particles.

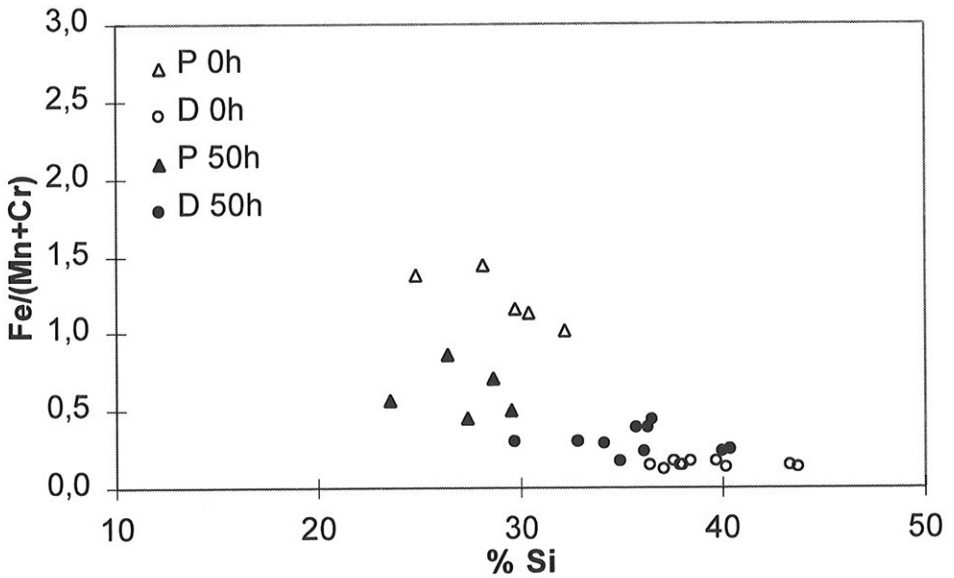

Figure V-33 The diagram shows how the Fe/(Mn+Cr) ratio in the primary particles (P), and the dispersoids (D) in alloy E changes during annealing at 580 °C.

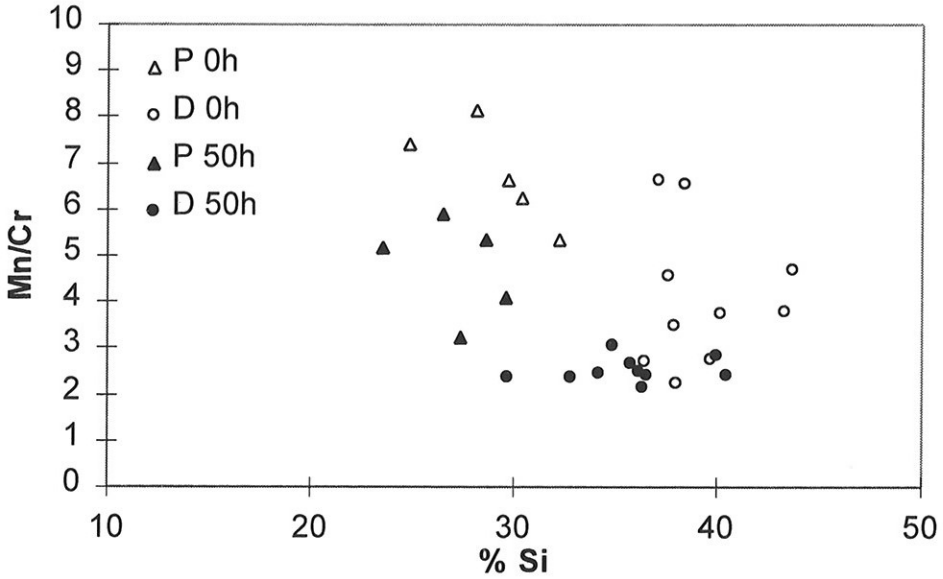

Figure V-34 The diagram shows how the Mn/Cr ratio in the primary particles (r P), and the dispersoids (D) in alloy E changes during annealing at 580 °C.

2.3 Coarsening of the dispersoids

The assumption of constant volume fraction of the dispersoids is probably not entirely correct. The reason why equation V-10 is not found to be valid is most likely due to the variation of the volume fraction with annealing time. The measurements by the Butanol method of the concentration of Mn and Si in solid solution in alloy C (Table V-2) support this conclusion. The Mn and Si in solid solution decrease during annealing which indicates that precipitation is going on.

As described above (chapter 2.2.5) an exchange of Mn and Fe between the primary particles and the dispersoids occurs during annealing. The primary particles absorb Mn while the dispersoids absorb Fe. Due to this exchange, the annealing time has to be extremely long to establish equilibrium. The concentration of Mn in solid solution decreases during annealing while the concentration of Fe in solid solution is probably constant. Thus, Fe, which is absorbed in the dispersoids, has to come from the primary particles while Mn, which is absorbed in the primary particles, may come from the dispersoids or the solid solution. If the areas with dispersoids are considered as one system and Mn leaves this system the system becomes more diluted. In order to investigate if a dilution occurs, the volume fraction

V_d of the dispersoids was calculated. The mean volume of one dispersoid is given by the following equation:

$$V_d = \frac{4\pi}{3} \cdot \frac{1}{n} \sum r_n^3 \qquad \text{(V-11)}$$

By using the data from the measurements of the particle size distribution in alloy C after annealing at 580°C, the mean volume of one dispersoid was determined. Equation V-11 was multiplied with the dispersoid density in order to obtain the volume fraction. At the start of the annealing, the volume fraction was 1.6 % and increased to 1.9 % after 3000 min. This volume fraction is probably too high. As described above, the measurements of size and density of the dispersoids were carried out approximately 5 μm from the primary particles. In these areas the dispersoid density is high compared to the density in the middle of the dendrites. The DDZ in the vicinity of the primary particles also results in a lower total volume fraction than the measured one. In addition, the calculation of the volume of the dispersoids was based upon the assumption that all the dispersoids were spherical. Several dispersoids were found to be needle-shaped which in most cases result in a larger calculated volume than the real one (see equation V-1). Even if the individual measurements of the volume fraction of dispersoids may have a rather large spread, the ratio between the measurements is most likely reasonably correct. Consequently, the decrease of Mn in solid solution results in precipitation of dispersoids. Whether some of the decrease of Mn in solid solution results in an increase of the amount of primary particles is difficult to determine.

However, if we assume that the volume fraction of dispersoids is constant, some Mn (and Si) has to leave the system and add it to the primary particles. In this case a modified coarsening equation can be derived. The equilibrium solubility C_{eq} is included in the constant K (equation V-10). If the C_{eq} decreases during annealing then K will also decrease. Thus equation V-10 can be express as following:

$$\frac{1}{\delta} = K_2(\bar{r}_0^3 + K'C(t) \cdot t) \qquad \text{(V-12)}$$

where K' is a constant and $C(t)$ is C_{eq} as a function of time. As discussed in chapter 2.2.1, the concentration of alloying elements in solid solution decreases during annealing. Both the electrical resistivity measurements and the chemical analysis of the matrix supported this. Mn is the rate limiting element (low diffusion rate in Al) for the coarsening of α-Al(MnFe)Si

dispersoids. Thus, when the coarsening process in alloy C is treated the Mn concentration in solid solution is equal to C_{eq}. According to Table V-2, the concentration of Mn in solid solution in alloy C decreases from 0.165 wt.% to

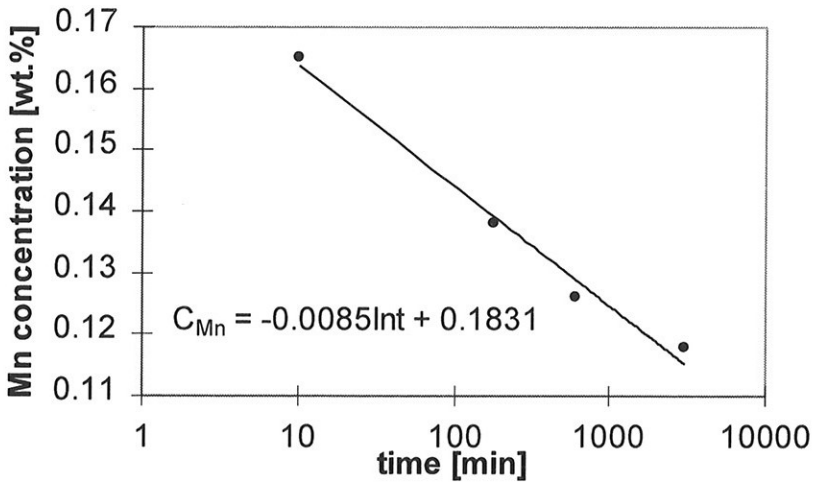

Figure V-35 The decrease of Mn concentration in solid solution with increasing annealing time.

0.118 wt.% during annealing when the material is annealed at 580 °C for 3000 min. The data from the measurements of the Mn concentration in solid solution are plotted in a semi-logarithmic diagram (Figure V-35). As can be seen the Mn concentration decreases with a constant slope during annealing. This slope can be expressed by the following equation:

$$C_{Mn} = -0.0085 \ln t + 0.1831 \qquad \text{(V-13)}$$

Since the diffusion of Mn is the rate limiting during coarsening in this case, C_{Mn} is equal to C(t):

$$C(t) = -0.0085 \ln t + 0.1813 \qquad \text{(V-14)}$$

Substituting Equation V-10 into Equation. V-8 gives:

$$\frac{1}{\delta} = K_2(\bar{r}_0^3 + K'(-0{,}0085 \ln t + 0{,}1831) \cdot t) \qquad \text{(V-15)}$$

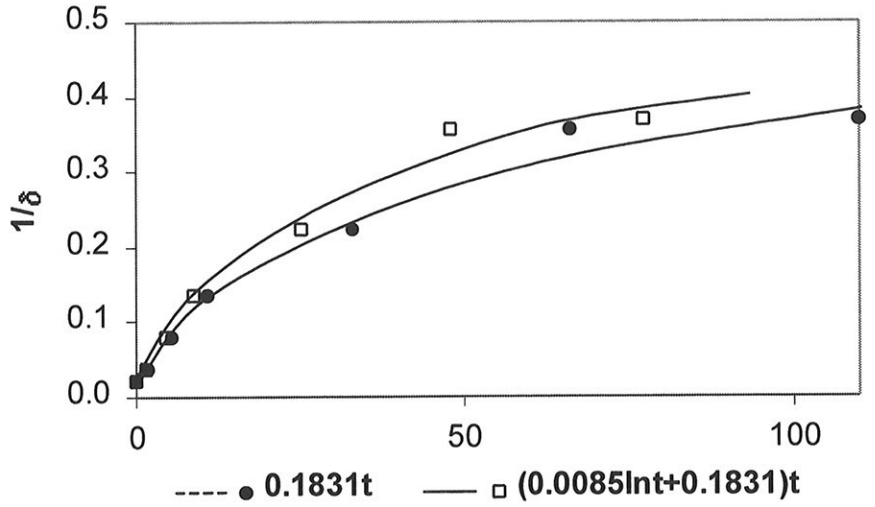

Figure V-36 *Variation of $1/\delta$ as a function of 0.1831t or (0.0085lnt+0.1831)t for alloy C annealed at 580 °C. In order to compare the original coarsening equation (V-10) with the modified coarsening equation (V-14) there are two x-axes, one for each equation.*

Compared with the original coarsening equation V-10 some improvements have been obtained (Figure V-36) by using equation V-15, but no linear variation of $1/\delta$ with t is obtained. The improvement by using equation V-15 was small. Hence, the decrease in Mn concentration during annealing can account for only a part of the difference between the experimental and the calculated behaviour.

In the theoretical description of the coarsening process only diffusion between the particles are taken into account. In the present case also diffusion of Mn and Fe between the primary particles and the dispersoids takes place. This process will affect the diffusion between the dispersoids. Several factors affect this coarsening process.

2.4 Summary

The changes of the microstructure of alloys C, D and E during continuous annealing summarised qualitatively in the following.

Alloy C (0.5 wt.% Mn)

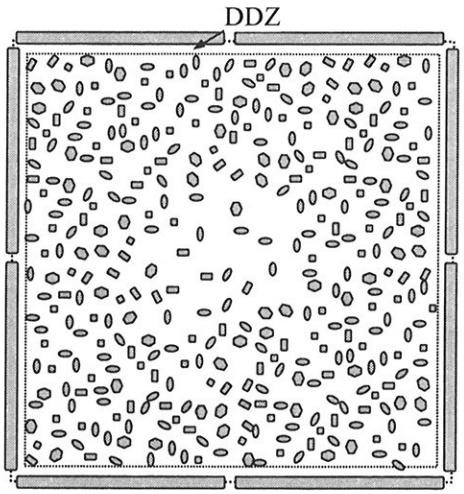

Figure V-37 Typical microstructure in alloy C at the start of annealing

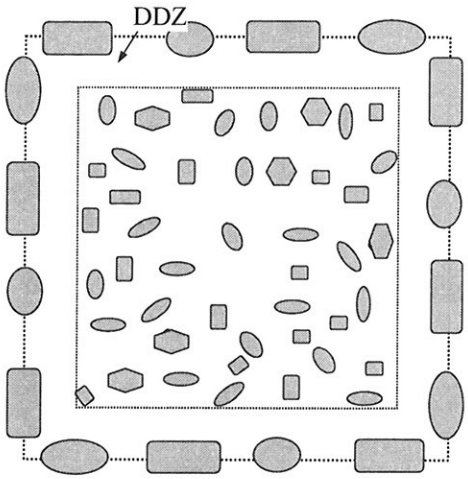

Figure V-38 Typical microstructure in alloy C after extensive annealing

Typical microstructure at the start of the annealing. (Figure V-37)

- Elongated or platelike primary α-Al(MnFe)Si particles are located at the grain boundaries and between the dendrites. These particles are rich in Fe.
- A large number of small α-Al(MnFe)Si dispersoids are present. These dispersoids are rich in Mn.
- Microsegregation during solidification results in a nonuniform distribution of the main alloying elements Mg and Si in solid solution. This results in a nonuniform distribution of dispersoids within the dendrites.
- The presence of dispersoid depleted zones DDZ are mainly due to the solidification path.

Typical microstructure after extensive annealing at high temperature. (Figure V-38)

- The primary particles break up into a necklace structure followed by spherodizing.
- As can be seen from Figure V-39 the compositions of the primary α-Al(MnFe)Si particles and the α-Al(MnFe)Si dispersoids approach each other.
- The DDZ has grown considerably. The primary particles grow at the expense of the neighbouring dispersoids.
- The dispersoid density has decreased considerably.
- The concentration of Mn in solid solution has decreased.

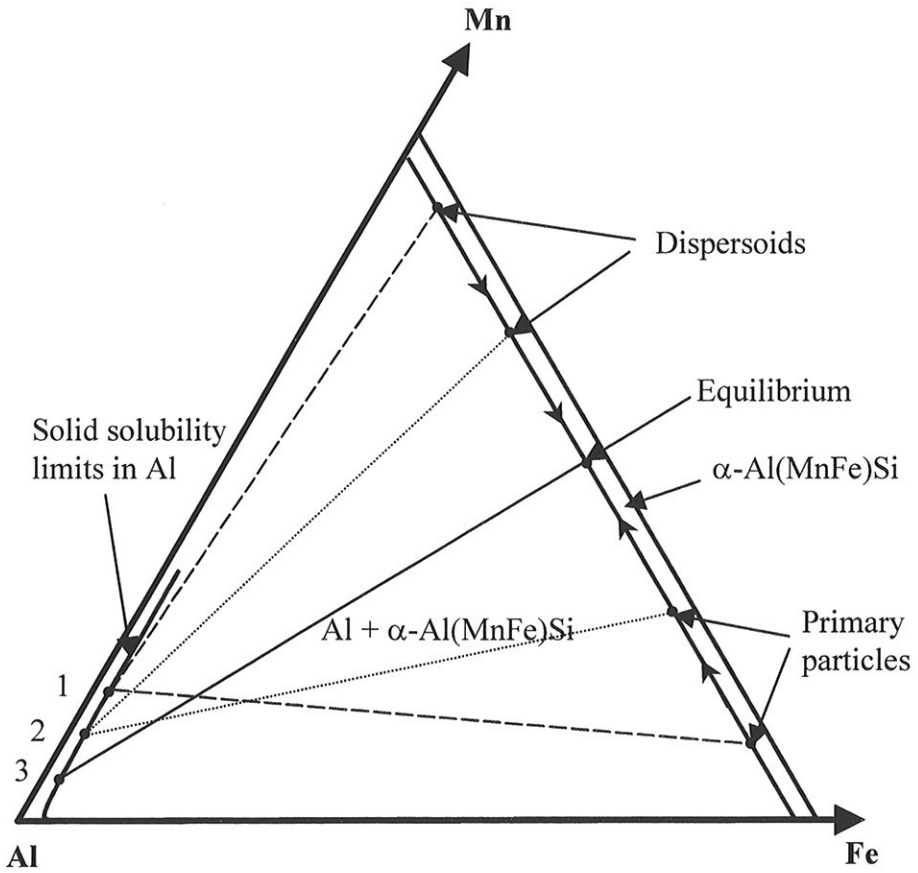

Figure V-39 A sketch of an isothermal section at approx. 580 °C of the Al-Mn-Fe-Si phase diagram. The concentration of Si is constant. The sketch shows the change of the concentration of Mn in solid solution during annealing. Point 1 shows the amount of Mn in solid solution at the beginning of annealing. The Mn-rich α-Al(MnFe)Si dispersoids exist together with the Fe-rich primary α-Al(MnFe)Si particles. During annealing the concentration of Mn in solid solution decreases to point 2. At this point the composition of the dispersoids and the primary particles have approached each other. After long annealing the system established equilibrium where the dispersoids and the primary particles have the same composition as indicated in point 3.

Alloy D (0.15 wt.% Cr)

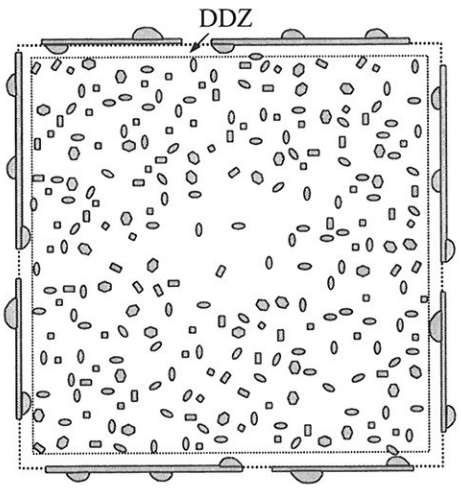

Figure V-40 Typical microstructure in alloy D at the start of annealing

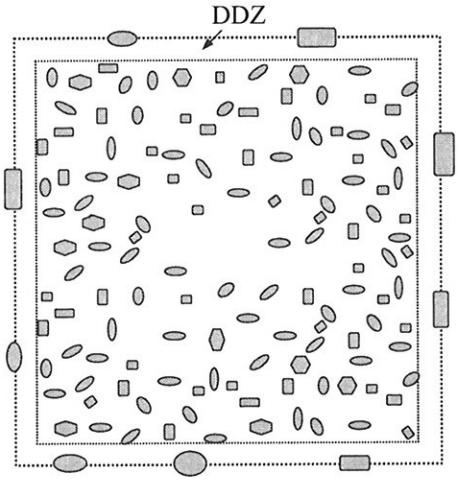

Figure V-41 Typical microstructure in alloy D after extensive annealing

Typical microstructure at the start of the annealing. (Figure V-40)

- Elongated or platelike β-AlFeSi particles are located at the grain boundaries and between the dendrites. Some small α-Al(CrFe)Si particles of various shapes are also present in between the dendrites.
- During heating to the annealing temperature small α-Al(CrFe)Si particles nucleate on the surface of the β-AlFeSi particles.
- The dispersoid density is low compared with the density in alloy C.
- Microsegregation during solidification results in a nonuniform distribution of the main alloying elements Mg and Si in solid solution. This results in a nonuniform distribution of dispersoids within the dendrites.
- The presence of dispersoid depleted zones, DDZ, are mainly due to the solidification path.

Typical microstructure after extensive annealing at high temperature. (Figure V-41)

- All the primary β-AlFeSi particles have dissolved. A necklace structure of α-Al(CrFe)Si particles which nucleated on the surface of the β-AlFeSi particles are present.
- The DDZ has grown, but the width of the DDZ is smaller than in alloy C.
- The dispersoid density has decreased somewhat, but the density is higher than in alloy C

Alloy E (0.5 wt.% Mn + 0.15 wt.% Cr)

- Only primary α-Al(MnCrFe)Si particles are present and during annealing these particles change in a way that is rather similar to the changes of the primary α-Al(MnFe)Si particles in alloy C.
- After all heat treatment procedures the dispersoids density is higher than both those in alloy C and alloy D.
- At the start of the annealing, the α-Al(MnCrFe)Si dispersoids are rich in Mn, while the primary α-Al(MnCrFe)Si particles are rich in Fe. During annealing the compositions of the primary particles and the dispersoids approach each other. In addition both the primary particles and the dispersoids absorb Cr.
- The width of DDZ is larger than in alloy D, but smaller than in alloy C.

References (Part I, Part II and Part V)

Alexander W. B., Slifkin L. M., Phys.Rev., B1 (1970), pp. 3274.

Altenpohl D., Aluminium und Aluminiumlegerungen, (1965),

Bäckerud L., Król E., Tamminen J., Solidification Characteristics of Aluminium Alloys, (1986),

Bardal A., Lie K., to be published in Materials Characterisation (1999).

Becker R., ann. Phys., 32 (1948), pp. 128.

Becker R., Döring W., Ann. Phys., 24 (1935). pp. 719.

Conte, A., Sanders T. H., The 5th int. conf. on Aluminium alloys, (1996), pp. 119.

Copper M., Acta Cryst., 23 (1967), pp.1106.

Donnadieu P.. et.al., The 4th int. conf. on Aluminium alloys, (1992), pp. 668.

Dons A. L., Z. Metallkde., 76 (1985), pp. 170.

Dons A.L., Scand. J. Met., 13 (1984^1), pp. 137.

Dons A.L., Z. Metallkde., 75 (1984^2), 170.

Dons A. L.,. Jensen E. K, Langsrud Y., Trømborg E., Brusethaug S., Metall. Mater. Trans. A, 30 (1999), pp. 2135

Dorward R.C., Conf. on Advances in Production and Fabrication of Light Metals and Metals Composite, (1992), pp. 351.

Egerton R. F., Electron Energy Loss Spectroscopy in the Electron Microscope, (1986), pp. 291.

Fujikawa S. -I., Hirano K. -I., Fukushima Y., Met. Trans., 9A (1978), pp.1811.

Hatch J.E., Aluminium Properties and Physical Metallurgy, (1984), pp. 205.

Hirasawa H., Scripta Met., 9 (1975), pp. 955.

Hornbogen E., Nucleation, Edited by A. C. Zettlemoyer, (1969), pp.309.

Kolby P., Sigli C., Simensen C. J., The 4th int. conf. on Aluminium alloys, (1994), pp. 508.

Kovacs-Csetenyi E., Cdurbakova T., Bardos Deak P., Ungar T., Mat. Sci. Forum, 13/14 (1987^1), pp. 491.

Kovacs-Csetenyi E., Griger A., Cdurbakova T., Ungar T., 8th Int. Light Metals Concress, (1987^2), pp. 599.

Lim C-Y., Shercliff H.R., Title: Quench sensitivity of Aluminium Alloy 6082, (technical report, University of Cambridge), (1993).

Lifshiz I. M., Slyozov V. V., J. Physics Chem. Solid, 19 (1961), pp. 35.

Lohne O., Dons A.L., Scand. J. Met, 12 (1983), pp. 34.

Mantl S., Petry W., Schroeder K., Phys. Rev., vol: 27 No: 9 (1983), pp 5313.

Mehrer H., Diffusion in Solid Metals and Alloys, (1992).

Merchant H. D., Crane J., Chia E. H., Homogenization and Annealing of Aluminium and Copper Alloys, (1988), pp. 183.

Modolfo L. F., Aluminium alloys: structure and properties, (1976), pp.787.

Mulazimoglu M.H., Zaluska A., Gruzleski J.E., Pray F., Met. Trans. A, 27A, (1996), pp. 929.

Munson D., J. Inst. Metals., 95 (1967), pp. 217.

Musulin I., Celliers O.C., Materials Processing and Performance (Conference Australia), 1991), pp. 71.

Nes E. Z. Metallkde., 63 (1972), pp. 248.

Phillips H.W.L., Annotated equilibrium diagrams of some aluminium alloys, (1959).

Phragmen G., J. Inst. Metals, 77 (1950), pp. 489.

Ping L., Dr thesis, KTH (1987).

Porter D. A. and Easterling K.E, Phase Transformation in Metal and Alloys, (1981).

Reiso O., Hydro Aluminium A/S, Sunndalsøra, private communications.

Reiso O., Dr thesis, NTH, (1992).

Robinson K., Acta Cryst. 6 (1953), pp. 854.

Rømming C., Hanssen V., Gjønnes J., Acta Cryst, B50 (1994), pp. 307.

Simensen C. J., Fartum P., Andersen A., Fresenius Z. Anal. Chem., 319 (1984) pp. 286.

Smithells METALS reference Book Sixth Editon (1983), pp 13.

Størkersen N. J., Høier R., Lohne O., STF34 A80032, (1980).

Trømborg E., Dr thesis NTH, (1994).

Turnull D., Fisher J. C., J. Chem. Phys., 17 (1949), pp. 71.

Vollmer M., Weber A., Z. Physik. Chem., 119 (1925), pp. 277.

Wagner C., Z. Elektrochem., 651961, pp. 581.

Westengen H, O. Reiso, L. Auran, Aluminium, 56 (1980), pp.768.

Westengen H., Z. Metallkde., 73 (1982), pp. 360.

Zajac S., Hutchinson B., Johansson A., Gullman L. O., Mat. Sci. and Tech., 10 (1994). Pp. 323.